ON THE PATHWAY OF WHOLE BLOOD ANALYSIS BY PORTABLE ATR-IR AND CHEMOMETRICS

A Thesis Submitted to
the Graduate School of Engineering and Sciences of
İzmir Institute of Technology
in Partial Fulfillment of the Requirements for the Degree of

MASTER OF SCIENCE

in Chemistry

by
Mert KOÇ

December 2017
İZMİR

We approve the thesis of **Mert KOÇ**

Examining Committee Members:

Asst. Prof. Dr. Engin KARABUDAK
Department of Chemistry, İzmir Institute of Technology

Assoc. Prof. Dr. Engin ÖZÇİVİCİ
Department of Biotechnology and Bioengineering, İzmir Institute of Technology

Asst. Prof. Dr. Betül ÖZTÜRK
Department of Culinary Arts and Management, İzmir University of Economics

26 December 2017

Asst. Prof. Dr. Engin KARABUDAK
Supervisor, Department of Chemistry,
İzmir Institute of Technology

Prof. Dr. Ahmet Emin EROĞLU
Head of the Department of Chemistry

Prof. Dr. Aysun SOFUOĞLU
Dean of the Graduate School of
Engineering and Sciences

ACKNOWLEDGEMENTS

There are a lot of person without whom it would not have been possible to complete this master thesis and to whom I am grateful.

To my supervisor, Asst. Prof. Dr. Engin KARABUDAK, for his full support, expert guidance, understanding and encouragement over the three years. His in-depth knowledge and patience made it possible to complete this thesis and I cannot image this study could not be finished without his endless help. He helped me become a better researcher. I'm extremely grateful to him.

Besides my advisor, I would like to thank to rest of my thesis committee: Assoc. Prof. Dr. Engin ÖZÇİVİCİ and Asst. Prof. Dr. Betül ÖZTÜRK.

My deceased grandfather Mehmet Koc, I owe my thanks to all the time. He was a village institute graduate teacher. He had a researcher character. He had learned to make radio with limited resources. After his retirement, his teaching love did not fade away. He graduated from college to become a teacher again. Because of his illness, he left the teaching again and left us early. I had a chance to get to know him for only a few years, but his learning and teaching passion inspired me throughout my life. Today I thank my hero for the contributions to me.

I would like to thank my family Gülcan and Ayhan KOÇ who supported me throughout my education life. They were always by my side and respected my preferences.

To my darling, Papatya İRİZ, she was always by my side. She supported me when I felt bad. In this difficult thesis process, I can deal with difficulties thanks to your love.

To members of Karabudak Research Group, İpek HARMANLI, Özge Sevin KESKİN, Uğur SOĞUKKUYU, Emre Yusuf GÖL, Mehmet KIVANÇ, and Ahmet AYTEKİN for their help, great patience and motivation at all times. They are always with me when I feel desperate and they are always there for me when I need them.

Finally, I thank to Ebru TEKİN, Yasemin BİLGİ, Gün Deniz AKKOÇ, Ayten Ekin MEŞE, Hülya SAMANCIOĞLU and Tunç ARAS for their help. When I needed them, they always helped me.

This work was supported by the Scientific and Technological Research Council of Turkey (TÜBİTAK), Grant No: 115E038.

ABSTRACT

ON THE PATHWAY OF WHOLE BLOOD ANALYSIS BY PORTABLE ATR-IR AND CHEMOMETRICS

Currently, the number of patients per state hospital in Turkey is too high. Doctors need point of care(PoC) tests like blood analysis, to diagnose his/her patients. Patients is firstly examined by a doctor. If the doctor needs blood analysis, then patient gives blood to blood laboratory. After a certain time, the results are given to the patient and he/she meets with the doctor again to show the results. This causes too much time loss. In addition, these analyses are not performed in some small healthcare centers and cause extra time loss, which is another major problem in the health care system. Electrochemical, spectrophotometric and enzymatic analysis methods are mostly used for blood analysis. The sum of glucose, urea, triglycerides, cholesterol, albumin and total protein tests cost for 7TL. Blood samples are taken separately about 2-5ml volume for each test and preliminary procedures are required. On the other hand, ATR-IR spectrometry is a technique that does not require preliminary sample preparation, less sample volume, cheap and results in shorter time. Studies have been carried out in the literature which have shown positive results on glucose, urea, triglycerides, cholesterol, albumin and total protein in blood, plasma and serum using ATR technique. The six components in blood have importance in the diagnosis of a disease at the patient. The aim of this thesis is a preliminary study to determine the glucose, urea, triglyceride, cholesterol, albumin and total protein concentrations in 1 minute, 1 μl of blood, using disposable crystals and less than 1 dollar in the doctor's room by direct analysis of the blood using ATR-IR spectrometry and using chemometrics algorithms to predict them from the spectral data.

ÖZET

PORTATİF ATR-IR VE KEMOMETRİ İLE TAM KAN ANALİZİ YAPMA ÇALIŞMASI

Günümüzde, Türkiyede devlet hastanesi başına düşen hasta sayısı çok yüksektir. doktorların yaptıkları hasta başı testlerin(point of care) başında kan tahlili gelmektedir. Kan tahlili için hasta önce ilgili doktora muayene olmak zorunda. Sonra doktorun yönelndirmesiyle laboratuvara kan vermekte ve tekrardan kan sonuçlarını doktora göstermek zorundadır. Bu da fazlasıyla zaman kaybına sebebiyet vermektedir. Ayrıca bazı sağlık ocaklarında bu tahliller yapılmamakta ve ekstra zaman kaybına neden olmakta ve sağlık sisteminde önemli bir sorun olarak karşımıza çıkmaktadır. Kan analizi için çoğunlukla elektrokimyasal, spektrofotometrik ve enzimatik analiz yöntemleri kullanılmaktadır. Glikoz, üre, trigliseritler, kolesterol, albumin ve toplam protein testlerinin toplamı 7TL'ye mal olmaktadır. Analizlerde kullanılacak olan kan örnekleri her test için ayrı ayrı 2-5ml arası alınmaktadır ve ön hazırlık işlemleri uygulamak gerekir. Öteyandan ATR-IR spektrosmetresi tekniği ise ön örnek hazırlığı gerektirmeyen, az hacimde, daha ucuz ve kısa sürede sonuç veren bir tekniktir. Literatürde daha önce ATR tekniği kullanarak kan, plazma ve serumda glikoz, üre, trigliseritler, kolesterol, albumin ve toplam proteinin tayini üzerine olumlu sonuçlar veren çalışmalar yapılmıştır. Kandaki altı bileşen hasta başı testlerde hastaya teşhis koymada büyük önem taşımaktadır. Bu tezin amacı, ATR-IR spektrometresi tekniği kullanarak kanın direk analizin edilmesi ve analizden elde edilen verileri kemometrik algoritmalardan yararlanarak glikoz, üre, trigliserit, kolesterol, albumin ve toplam protein değerlerinin 1 dakikada, 1µl kanın kullan at kristallerle ölçülüp 1 doların altında doktorun odasında saptanması için bir ön çalışmadır.

TABLE OF CONTENTS

LIST OF FIGURES

Figure **Page**

LIST OF TABLES

Table **Page**

CHAPTER 1

HISTORY OF SPECTROSCOPY AND MODERN MICROMACHINED DISPOSABLE SI ATR-IR

1.1. History of Spectroscopy

1.1.1. Theory of Light and Matter

Light has fascinated human kind for centuries. In the history of science, the systematic study of light started with Galileo (1564–1642), who used lenses to observe space. Then, Newton (1643–1727) understood light as a color spectrum. Maxwell (1831–1879), in turn, clarified that light included both magnetic and electric fields. Einstein (1879–1955) conceptualized the idea that light exists as particles. Finally, Feynman (1918–1988) developed electrodynamic diagrams. Figure 1.1. presents the scientists who contributed to the light theory we know today.

Figure 1.1. Scientists that developed light and wave theories: (a) Galileo 1564–1642, (b) Newton 1643– 1727, (c) Maxwell 1831–1879, (d) Einstein 1879–1955, and (e) Feynman 1918–1988.

1.1.1.1. The Duality of Light as Particle and Wave

Through the ages, many experiments tried to discern the nature of light. Galileo and other scientists made futile attempts to measure its speed. Then, Newton explained light's behavior with the idea that light was made of particles. His famous prism experiments divided light into a color spectrum (Figure 1.2). He passed a beam from a light source through a prism to separate light into six colors. Figure 2 shows Newton's prism experiment.[1-2]

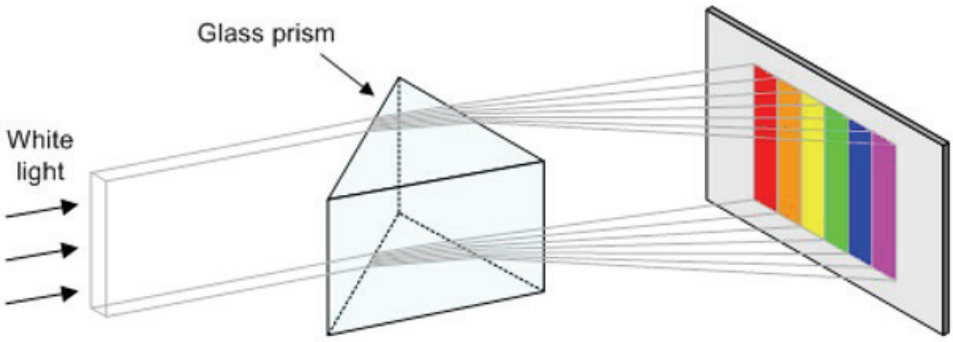

Figure 1.2. Newton's experiment for splitting white light into a spectrum.

On the other hand, Maxwell defined light as an electromagnetic wave. Maxwell's equations (Equation (1.1)) describe electromagnetism by combining electricity, magnetism, and their propagation speed (see Figure 3). Then, Einstein used the photoelectric effect to observe that light consists of energy packages called photons, whose energy depends on the frequency of light.[1-3]

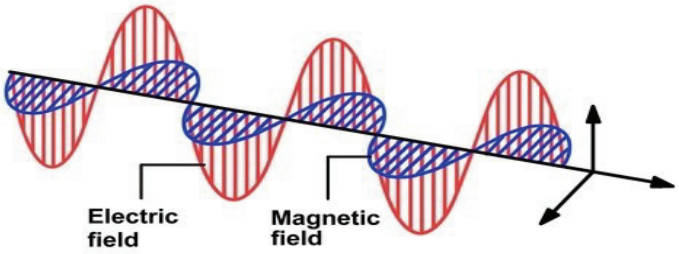

Figure 1.3. Electromagnetic wave.

However, a paradox emerged concerning why light has wave properties in addition to photon properties. The debates on this paradox resulted in several experiments showing that light has both wave and particle properties.[1-3]

$$\left(\mathbf{c^2\nabla^2 - \frac{\partial^2}{\partial t^2}}\right)\mathbf{E = 0} \qquad (1.1)$$

$$\left(\mathbf{c^2\nabla^2 - \frac{\partial^2}{\partial t^2}}\right)\mathbf{B = 0}$$

where

$$\mathbf{c = \frac{1}{\sqrt{\mu_0 \varepsilon_0}}}$$

Equation (1.1) is the electromagnetic wave equation, where c is the speed of light, $\boldsymbol{\nabla}$ is the Laplace operator, t is the time, E is the magnetic field, and B is the magnetic flux density.

Due to emission and absorption properties, light manifests particle-like behavior. The energy carried by light waves is packaged in discreet bundles called photons or quanta.[1-2]

1.1.1.2. Particle and Wave Duality of Matter?

From as far back as the ancient Greeks and Romans, philosophers have tried to define matter. According to classical physics, matter is a particle with a definite position and velocity. Atoms are composed of neutrons and protons in the nuclei and electrons in the orbitals. This theory was sufficient for heavy and slow matter with small particle wavelength. However, classical physics could not explain why electrons whose direction continuously changes do not emit electromagnetic waves and do not collapse into the nucleus. Quantum physics explained this phenomenon with the wave function of matter. Electrons remain in their orbitals and do not collapse into the protons thanks to their wave function, described by the Schrödinger equation. This wave function helps describe particles with very small mass and rapid velocity.[1-2]

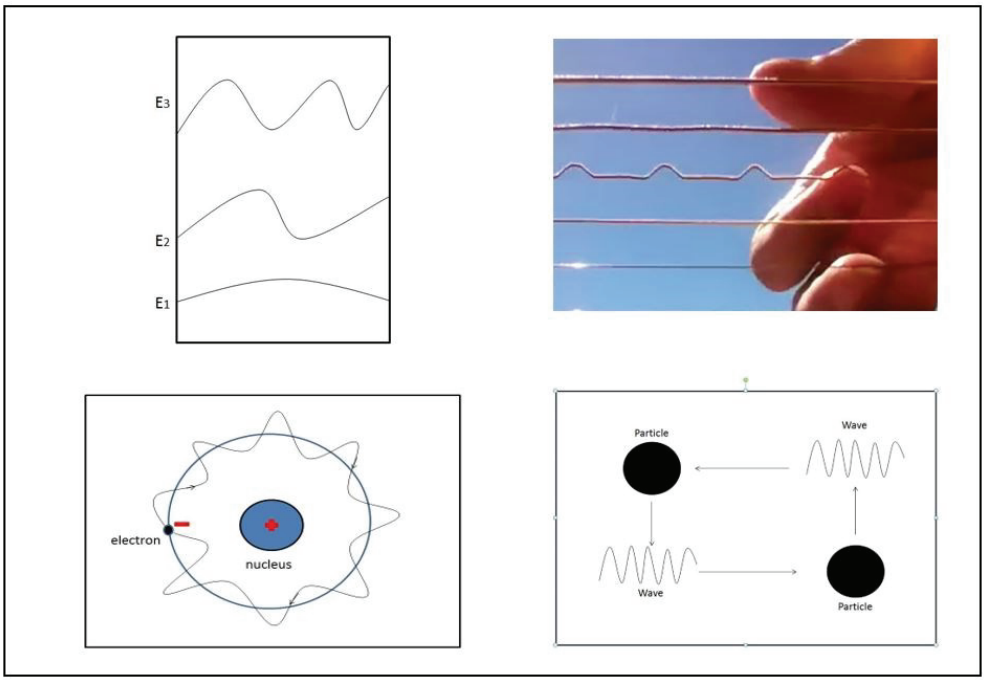

Figure 1.4. Particle–wave duality.

According to quantum physics, light, like matter, has both wave and particle properties (Figure 1.4). The only difference is that matter has mass, but light does not. Schrodinger's equation (Equation (1.2)) describes the electron's wave function, which classical physics could not:[2-3]

$$H\psi = E\psi$$

$$i\hbar\frac{\partial\Psi}{\partial t} = \hat{H}\psi \tag{1.2}$$

$$\left(-\frac{\hbar^2}{2m}\nabla^2 + V\right)\psi = \imath\hbar\frac{\partial\psi}{\partial t}$$

Equation (1.2) is the Schrodinger equation, where Ψ is the wave function, E is the energy of the state Ψ, H is the Hamiltonian operator, t is the time, $\hbar$ is Planck s constant, ∇ is the Laplace operator, and m is the mass of particle.

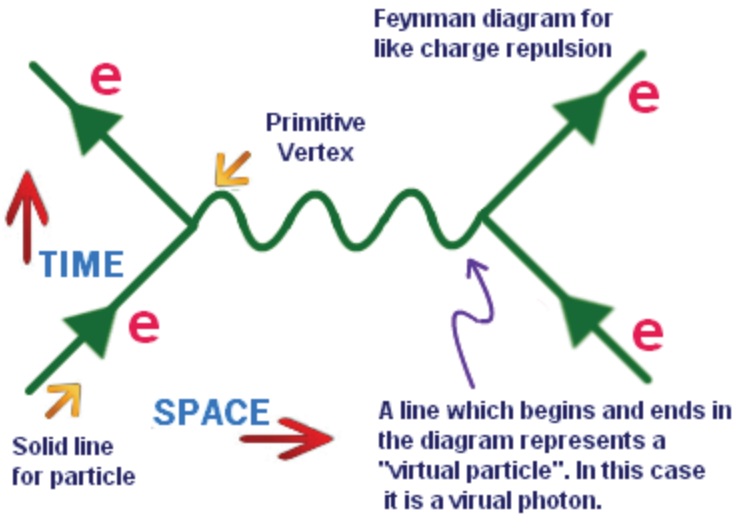

Figure 1.5. Feynman diagram.

In the early 1930s, physicists tried to develop a new mathematical model to identify radiation and absorption of charged particles. Their theories proved insufficient, providing only discursive or infinite results against strong physical questions. Feynman was attracted by the problem of a stable QED theory in the late 1940s. The problem called for complex mathematical equations. However, Feynman followed a different path from his colleagues. He developed a quantum electrodynamics diagram (Figure 1.5) that illustrates what happens when subatomic particles interact with each other. Nowadays, it is commonly used as a tool to visualize complex calculations in physics in a simplified way. The diagram in Figure 1.5 shows that as two electrons move through space and evolve in time, they interact and exchange a photon. The magnitude of the force can be calculated by using Feynman calculus.

1.1.2. Theory of Light and Matter Interactions: Spectroscopy Theory

In short, spectroscopy is the study of interactions between light and matter. When electromagnetic radiation hits and interacts with a sample (Figure 1.6), absorption, emission, reflection, and transmission can be observed.

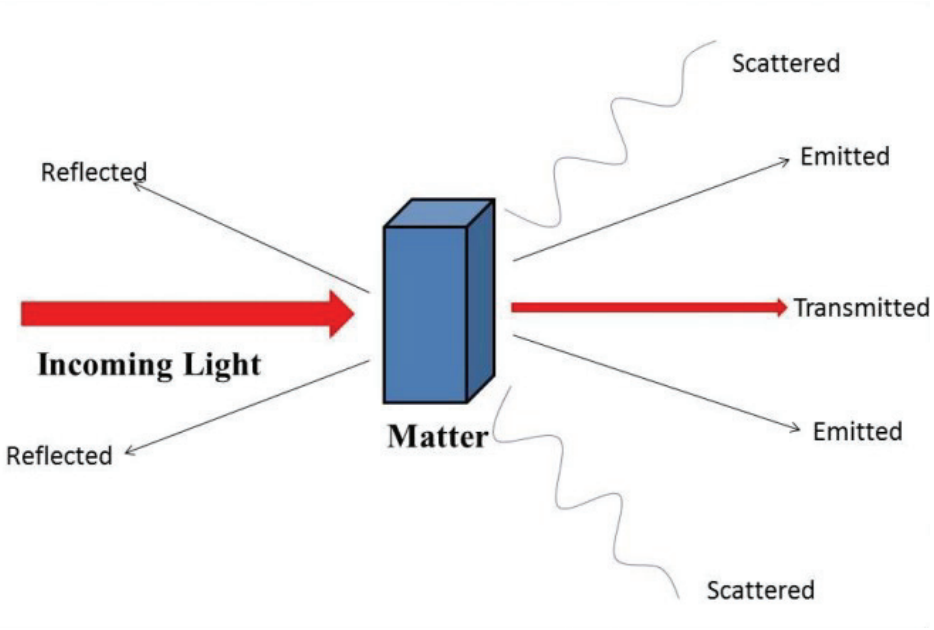

Figure 1.6. Light and matter interaction.

When radiation interacts with a sample, the electrons interact with light and are excited to a higher energy state from a lower energy state, and absorption is observed. Emission is observed if the excited electrons emit photons while relaxing to a lower energy state. Reflection can occur depending on physical specifications of the sample surface, and medium difference is the most com-mon and effective reason for this deflection. If the sample is transparent in the specified wavelength of the light, it will pass through the sample and transmission will be observed.[4-5]

When a photon strikes the outer layer of an atom, it is absorbed by an electron only if the amount of energy it carries is exactly equal to energy differences between high and low quantum energy levels. The energy carried from the light also affects the electrons of an atom in different ways that are explained by the Jablonski diagram. Different spectroscopic techniques analyze in principle different photon and electron interactions in molecules and atoms. So, spectroscopy gives valuable, sensitive, and specific information about atoms, orbitals, bonds, and matter.[3-6]

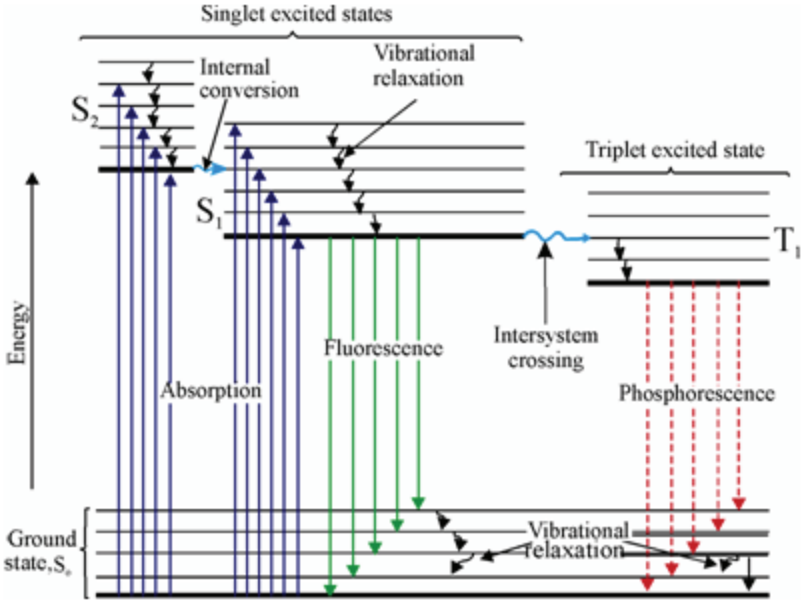

Figure 1.7. Jablonski diagram.

Figure 1.7 shows that fluorescence occurs if the proton emission exists between states of the same spin state. See for example S_1->S_0, where S_0 is the ground state of a molecule and S_n refers to the nth excited single state. When the spin states of the first and the last energy levels are different, the emission is called phosphorescence. See for instance T_1->S_0, where T_n refers to nth excited triplet state. As shown in the diagram, this is indicated by a longer wavelength and therefore a shorter red line. The lifetimes of fluorescent states are relatively short ($1x10^{-5}$ to 10^{-8} seconds) compared to phosphorescence ($1x10^{-4}$ seconds to minutes or even hours), because fluorescence is statistically much more possible than phosphorescence for most molecules. In the diagram, photon emitters are shown as flat arrows, while wavy arrows refer to the non-radioactive process.

Internal conversion (IC), intersystem crossing (ISC), and vibrational relaxation are three non-radiant deactivation processes. The diagram shows examples of these three processes. IC occurs between energy states, which are in the same spin state. ISC occurs between different spin states. Vibrational relaxation occurs between vibrational states in the same energy state and spin. It happens quickly (<1 x 10^{-12} seconds).[1, 4-7]

1.1.2.1. Spectroscopy with Different Wavelength Regions

The electromagnetic spectrum (Figure 1.8) comprises all electromagnetic waves of various frequencies and wavelengths that come from light sources. The wavelengths and frequencies of the electromagnetic spectrum range from the nanometer to the meter scale. A very small range of wavelengths can be seen by the human eye, and are called visible light. They can appear in different colors depending on the wavelengths and frequencies of the light.[1, 3-4, 6]

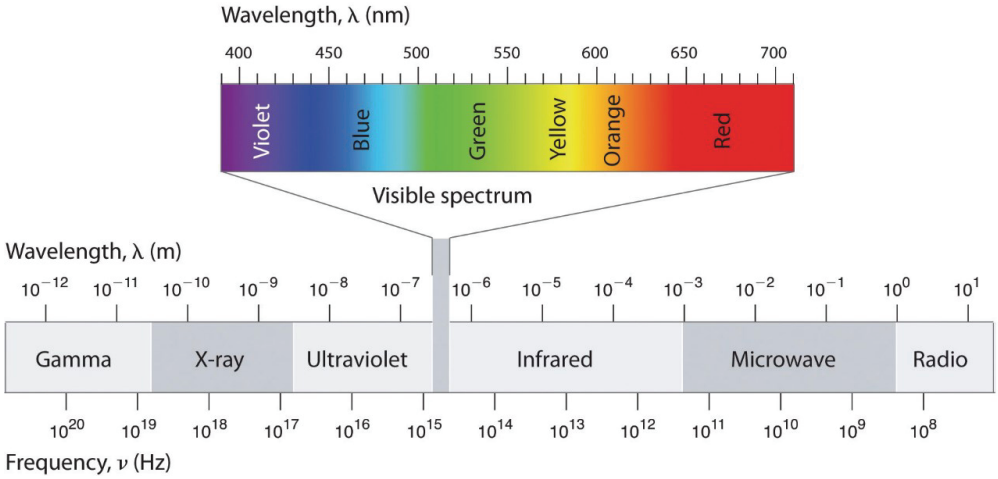

Figure 1.8. Electromagnetic spectrum.[8]

Spectrometers are used to analyze spectrums. A general block body diagram is shown in Figure 1.9 for spectrometers. In the following sections of this review, we will focus on ultraviolet–visible (UV–Vis), Raman, and infrared (IR) spectroscopies.

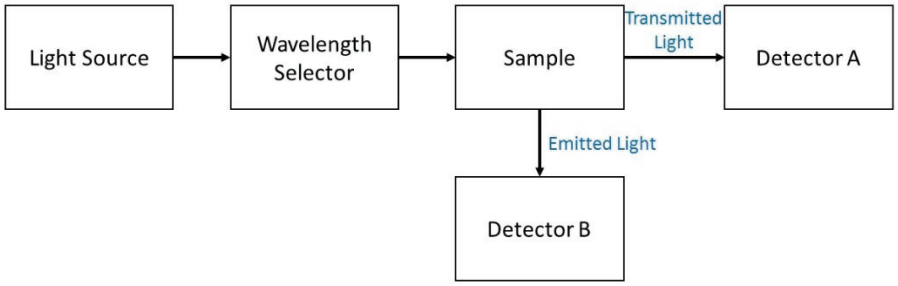

Figure 1.9. General block body diagram for spectrometer instruments.

1.1.2.2. Ultraviolet–Visible Spectroscopy

UV–Vis spectroscopy occurs in a narrow range of the electromagnetic spectrum, and consists of visible and ultraviolet light. The visible spectroscopy consists mainly of the molecules or matter that absorb visible light wavelengths and frequencies. The specific peaks can be seen by comparing with the standard of the matter and give sufficient information on the characterization of a matter in a mixed solution.[4-6]

UV spectroscopy is based on the UV radiation absorption of a sample, occurring from the electron transition from lower electronic states to higher electronic states (Figure 10). There are four types of transitions:

1. $\sigma \rightarrow \sigma^*$ transition
2. $n \rightarrow \sigma^*$ transition
3. $n \rightarrow \pi^*$ transition
4. $\pi \rightarrow \pi^*$ transition

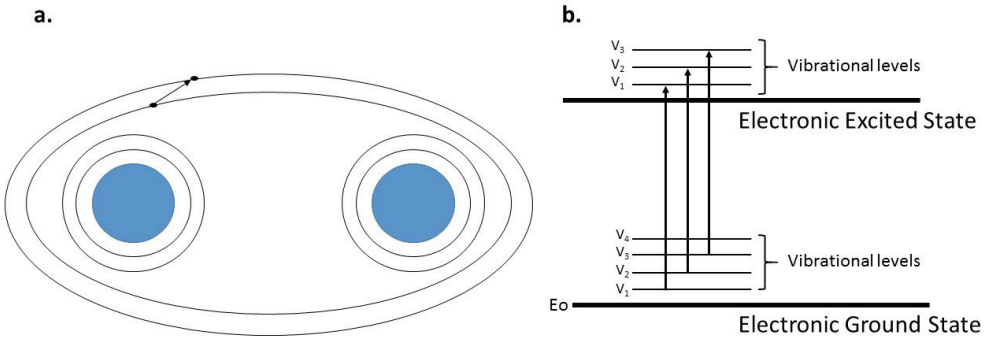

Figure 1.10. (a) Electron distribution changes on the outer shell. (b) UV spectroscopy transitions on the Jablonski diagram.

Here, s is a sigma bond, s is an anti-sigma bond, p is a pi bond, and p is an anti-pi bond. These describe molecular orbitals.

UV radiation has large energy, so these transitions can generate wavelengths of 380 nm to 0,6 nm and from $8x10^{14}$ Hz to $3x10^{17}$ Hz. UV radiation changes electron distribution of atoms or molecules. UV light especially affects microorganisms. The absorbed UV light damages DNA. That's why ultraviolet light is used in medicine or related fields for sterilization.[4-6]

1.1.2.3. Raman Spectroscopy

The Indian physicist C.V. Raman discovered that the small amount of light scattered by some molecules differs depending on the wavelength of the incoming beam, and that the wavelength shifts change according to the chemical structure of the scattering molecules (1928). In 1931, he won the Nobel Prize in physics for his discovery and systematic explanations. According to the theory, Raman scattering events are the result of vibration changes with the same type of quantized IR absorption. The wavelength "difference" between the incoming and scattered light falls to the mid-IR region. Raman scattering and IR absorption spectra of a particle are very similar. These two techniques are complementary to each other; an IR active group can be Raman inactive, or a Raman

active group can be IR inactive. If the molecule or the vibration mode of a molecule has a dipole moment, then theoretically it can be detected by IR spectroscopy; on the other hand, if the molecule or its vibrational modes has no dipole moment, it can theoretically be detected by Raman spectroscopy.[7, 9] Figure 1.11 shows raman transitions and a vibrating molecule.

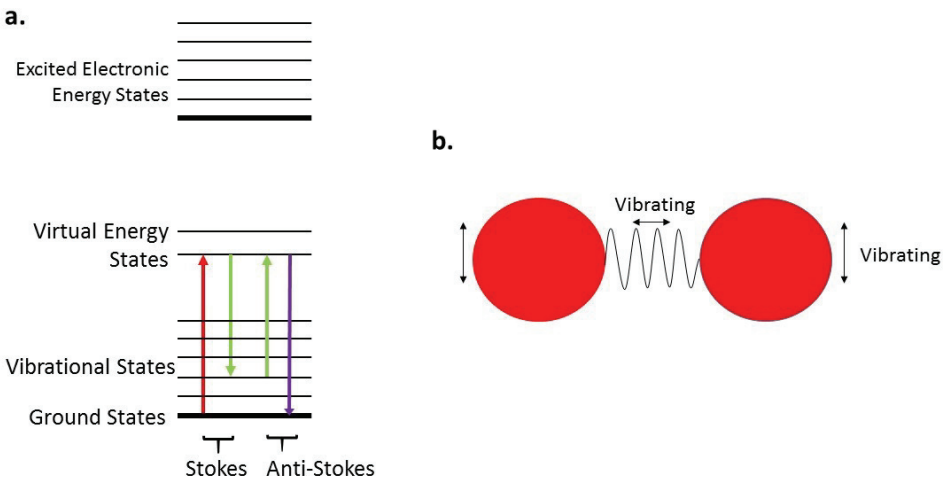

Figure 1.11. (a) Raman spectroscopy transitions on the Jablonski diagram. (b) Vibrating molecule.

Some of the advantages of Raman spectroscopy are that it is a non-destructive method, it is used to analyze low wavenumber regions, and it can be used to measure high-temperature-dependent studies. Preparation of the sample is remarkable since even water can be used as a solvent.[5] Moreover, Raman spectroscopy can be used with microscopic techniques to achieve better focusing. Small sample volumes can be used. Raman spectroscopy has the capability of light-fiber, which allows a larger separation of the sensing probe and the spectrometer.[10] It gives specific information about the molecular structure of biological samples without any labeling, in comparison to standard techniques such as optical micros-copy, fluorescence spectroscopy, and immunoassays. The groups of the molecules are especially important for their Raman active or IR active properties. Raman spectroscopy helps with bonds and molecules where dipole moment is absent or weak.[5, 7, 10]

1.1.2.4. IR Spectroscopy

IR spectroscopy is a well-known and routinely used technique also known as vibrational spectroscopy. Samples must have a molecular dipole moment in order to be studied by IR spectroscopy. Solid, liquid, or gas samples can be analyzed by IR spectroscopy. The molecules in the sample can be identified by determining the chemical structures according to the frequencies of the absorbed IR radiation. The absorbed IR radiation can be detected in the IR spectrum between the area of 12,800 and 200 cm^{-1}, which is divided into far-, mid-, and near-IR spectra. The most important region for identification is the mid-IR region, in which stretching, bending, vibrational, and rotational modes are observed (Figure 1.12).[4-6] Vibrational or rotational modes can be calculated theoretically using the formula:

$$Linear\ Molecules\ Modes = 3 * n - 5$$
$$Nonlinear\ Molecules\ Modes = 3 * n - 6 \quad (1.3)$$

Where n is the number of atoms in the molecule. Not all of these calculated modes can be seen in the IR spectrum because they must be IR active. IR active means the molecule should have dipole moment change.

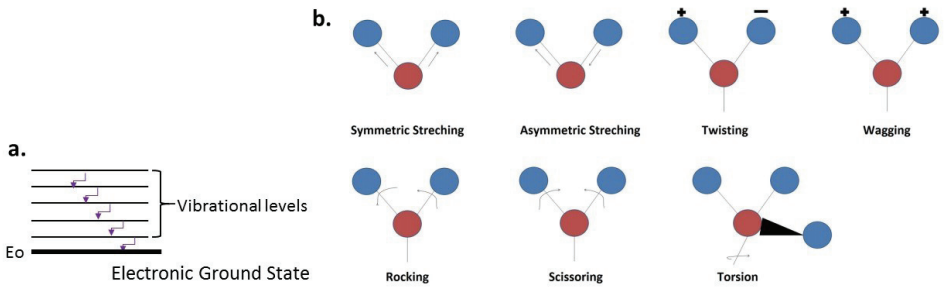

Figure 1.12. (a) IR spectroscopy transitions on the Jablonski diagram. (b) Vibrational modes.

1.1.2.4.1. Limitations of IR and Raman Spectroscopy

IR and Raman spectroscopy are widely used in the fields of drug development and drug testing in order to obtain knowledge of the molecular structure of a sample. The two methods give complementary knowledge about the molecule investigated. The biggest limitation of IR transmission spectroscopy is that strong IR absorption of water molecules prevents accurate usage of IR spectroscopy in aqueous solutions (Figure 1.13). Thus, in order to analyze aqueous solutions, attenuated total reflection (ATR) technique is used with IR spectroscopy.[6-8, 11]

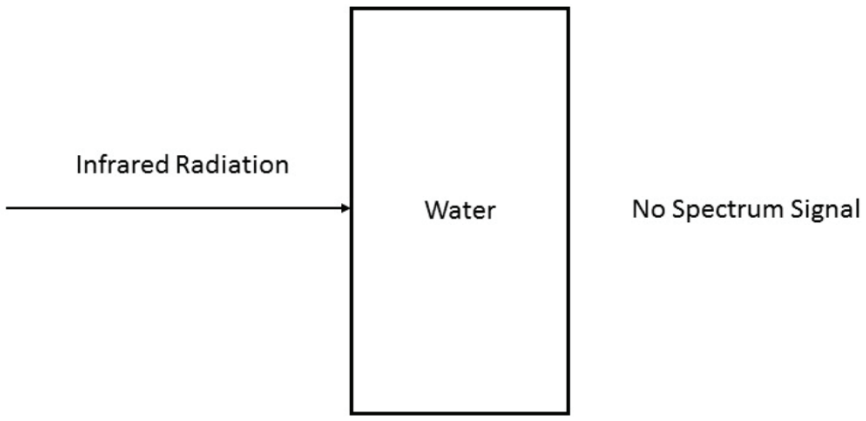

Figure 1.13. Main disadvantage of IR transmission spectroscopy. Strong IR absorption of water prevents use of IR transmission mode in aqueous solutions.

1.1.2.5. ATR-IR Spectroscopy

ATR-IR spectroscopy is a surface characterization technique that was developed nearly half a century ago.[12] The IR enters a stationary processed specific ATR crystal, which provides attenuated total reflectance of the IR beam inside the crystal. ATR-IR analysis works well with aqueous samples, and is, therefore, used in many fields of research.[4-6]

1.1.2.5.1. Principle of ATR-IR

ATR is used alongside IR spectroscopy to provide reflections of IR beams by using a highly refractive crystal that has an angle greater than the critical angle. This produces internal reflections at the surface of the crystal which is in contact with the sample. These internal reflections (Figure 1.14) form multiple evanescent waves that penetrate the sample. These evanescent waves enter the sample at a depth of 0.5–2 mm, which causes IR radiation and sample interaction, allowing us to record the ATR-IR spectrum of the sample.[11]

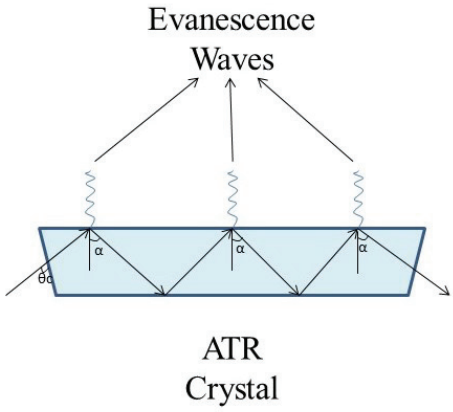

Figure 1.14. ATR crystal and evanescent waves.

Mid-IR beams are usually used for ATR-IR applications because of a special region called a fingerprint region. In comparison with other IR wavenumber regions, fingerprint regions are special because they contain molecule-specific molecular vibrations, so each peak corresponds to only one specific molecule.[4-6, 11]

The critical angle, total reflectance, internal reflection element (IRE), evanescent wave, and penetration depth are important terms in ATR-IR spectroscopy. The most important component of ATR-IR is a polished IRE on which the sample is placed. The light, which passes through the polished IRE, must be reflected and form evanescent waves to interact with the sample at the interface. This is ensured by the high refractive index material of the polished IRE and an incidence angle larger than the critical angle. The attenuation occurs during the interaction of evanescent waves with the sample, and the reflected light is collected by a detector.[5, 12-14]

The materials commonly used for ATR crystals are Ge, ZnSe, or diamond. In general, Ge or ZnSe are used as the raw materials, but they are expensive and usually fixed on the setup in IR spectroscopy. In addition, analyses that require high temperature or highly acidic and basic solutions are harmful to these crystals.[5, 12-14] Among the three common crystal materials, diamond is the least practical because of its high cost and limited surface area, despite being stable and the most robust. ZnSe is the most affordable material, but can only be used in the pH range of 5–9.[5, 11-14] Today, an emerging alternative IRE is disposable silicon (Si) IRE, which has various advantages that we will discuss in later sections.[5, 12-14]

1.1.2.5.2. Advantages of ATR-IR

There are three main advantages of the ATR-IR technique in comparison to IR transmission spectroscopy. First, samples can be measured at aqueous solutions, which are not suitable for IR transmission spectroscopy, since large peaks of water prevent accurate measurement in IR transmission spectroscopy.[5, 9-10, 12-15] Second, it is easier to prepare a sample for both liquid and solid materials when compared to IR transmission spectroscopy.[15] Third, ATR-IR is suitable to analyze samples' surfaces if it is required for the samples and we can change the penetration depth of evanescent wave by changing the reflection angle.[9]

1.1.2.5.3. Application of ATR-IR

ATR-IR is the one of the most important techniques for surface analysis, in which surface absorption, surface thickness, and surface interactions between chemicals and molecules can be determined. In particular, the fingerprint regions give more specific and reliable information about molecules in ATR-IR. As a result, drug–protein interactions and redox reactions can be investigated. Coating thickness and smoothness can be determined.[9-10, 12-14, 16-29]

One of the most important applications of ATR-IR is the measurement of body fluids, which give possibility of easier sample preparation, working with low volume and non-destructive measurement on sample. At crime scenes, samples of body fluids such as blood, saliva, semen, or vaginal fluid are collected for forensic analyses (30). However,

samples may be too limited to analyze repetitively. Developed techniques such as proteomics or mRNA analyses are not yet suitable for general use. ATR-IR spectroscopy also has the capability to determine the dissimilarity between biologic molecules such as proteins and their phosphates, sugars by using the finger print region. Moreover, small amounts of sampling are enough for repeat analyses.[17, 21-22, 25, 30]

1.1.2.5.4. Disadvantages of ATR-IR

Sensitivity problem of ATR-IR: ATR-IR works by using evanescent waves, so its sensitivity is not as good as that of the transmission technique. In the transmission technique, light directly passes through the sample, and the detector gathers what comes after sample–light interaction. On the other hand, in the evanescent wave technique, light is projected onto the sample surface and evanescent waves occur in the interface between sample and IRE; hence, light does not pass through the sample, and thus the transmission technique is more sensitive than the evanescent wave technique.

Surface sensitivity: The evanescent wave technique only analyzes a few microns of the sample's surface. The transmission technique allows us to analyze the whole sample (both bulk and surface), but the range of evanescent waves is limitedly adjustable. Some situations require depth to get information about a sample. The ATR is a surface limited technique, so if the sample is not homogeneous in the size of the penetration depth of evanescence wave, we can only get signal from the surface. So, ATR-IR spectroscopy might give different signals compared to the IR transmission technique. This must be taken into consideration when experiments are carried out.

Availability of ATR-IR crystal: Crystals of ATR-IR are not easy to produce and relatively expensive, although they can be used repeatedly. Advanced techniques are needed to produce commercially available crystals, and these processes are costly. Also, they tend to be fragile. In addition, during ATR-IR analysis, the crystal may be damaged if care is not taken. Because the ATR-IR is a surface-sensitive technique, the damaged crystal usually reduces sensitivity.

As explained before, it is necessary to carefully clean the crystal before every single measurement. So, it is not practical to use new crystal for each sample measurement. This may cause sample to sample contamination. In some fields like biomedical applications, cleaning the crystal again and again is not possible, because of

the requirement of hygiene. Also, high-temperature processes can damage the crystal, if high-temperature measurement is required in any field.

1.2. Modern Micromachined Disposable Si ATR-IR

1.2.1. Micromachined ATR-IR

The science of altering and examining fluids in micron-sized channels or micron-sized chamber is called microfluidics. It is usually practiced in the range of microliters (10^{-6}) and picoliters, and includes tens to hundreds of micrometer-sized channel networks. Microfluidics was applied to research chemical weapons at the Defense Advanced Research Projects Agency (DARPA) of the US Department of Defense starting in the 70s.[31] With the progress of molecular biology in the 80s, scientists decided to investigate a novel analysis method, since determination of genomes and proteins involved extended steps. In the beginning, a single micro-device was generated for the microfluidic chip. However, the major expectation was to perform multiple analyses with the single tool in microfluidics. Also, the analysis was of lower cost. Additionally, when the microfluid chip connected with nanochannels, it allowed the transportation of liquid and the other devices. For instance, gas chromatography, high-performance liquid chromatography, and capillary electrophoresis can be synchronized with the microfluidic chip so that separation can occur in the nanochannels of the microfluidic chip.[31]

In addition, microfluidics has become more popular in chemical synthesis. The major advantages of microfluidics include extended experiment time, being faster, and using small quantities of solvents. Using microfluidics is environment friendly due to the small amount of toxic compounds and waste produced. The management of heat of the reaction and mixing product has an important role in synthesis chemistry and microfluid technology supports to keep these parameters under control. Also, formation of by-products is lower than that in macro-scale experiments. This has advantages in quantum dot synthesis. Since the range of quantum dots is desirable in chemistry, the efficiency of reactions is improved. So, the combination of microfluidics technique with the synthesis of quantum dots appears promising.[31]

Microfluidics is an important field that can be used in various other applications in order to minimize the experimental space, which is also known as lab-on-chip.

Microfluidics has various advantages on various applications, but on the other hand, it is very difficult to detect chemicals in-situ inside the microfluidics channels. Because microfluidics channels have closed geometry, so many of the analytical techniques cannot analyze the chemicals online inside the microchannels. This is why micromachined Si ATR-IR is developed as a novel analytical tool for analyzing the liquids inside micro/nanofluidics in-situ.[12-14]

1.2.1.1. Polished IRE-Coupled Microfluidics

Since light travels at different speeds inside different materials, the refractive index of the material is especially important in the field of ATR-IR. Due to the high refractive index of ATR-IR IRE, incoming IR light creates total reflectance inside the IRE material. Therefore, there is no intensity loss during these reflections. For this reason, the type of IRE material used in ATR-IR setups is very important.[13]

As mentioned before, IRE material must have a high refractive index and transparency in order to accurately measure wavelengths. In addition, it must be a mechanically processed material to allow formation of a specific shape to determine the appropriate angle of incidence. This is especially important in order to arrange the penetration depth of the evanescent wave. Commercial IREs called polished IREs are produced by mechanical polishing to achieve this specific shape.[13] The polished IRE must have a very smooth surface on its reflection side.

The major drawbacks of commercial IREs are their production costs. As an alternative to commercial IREs, μSi-IREs are produced as well-developed microfabrication products.[12] In fact, μSi-IREs can work in the fingerprint region, while commercial IREs cannot. In addition, the disadvantage of Si-IRE (that the working spectral range is limited to a cut-off value below 1,500 cm^{-1}) is removed by producing μSi-IRE.[13]

1.2.1.2. μSi-ATR-IR-Coupled Micro/Nanofluidics

The first Si-ATR-IR microfluidics system in the literature was presented in 2004.[32] Anisotropic KOH-etching of a Si wafer is a certain method to generate optically smooth surfaces with a Si wafer. It was performed instead of polishing wafers. This demonstrated

that μSi-IREs can instantly occur from a 100 mm Si wafer. Anodic bonding was used to bond the wafer with micromachined channels on top of these Si-IREs. The top surface and connections occurred with PDMS material, as shown in Figure 1.15.[12-14]

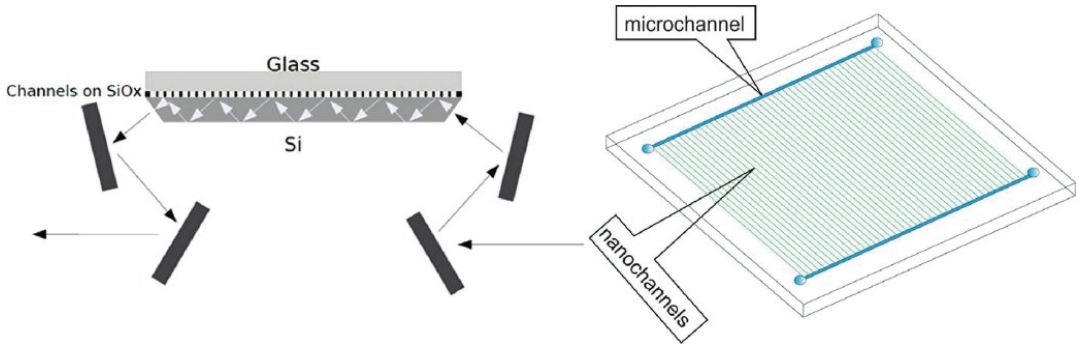

Figure 1.15. Micromachined Si-ATR IR systems[13]

The whole system was put into a commercial FTIR spectrometer without fabrication of any special optical setup. Fabricated IREs (Figure 1.16) were produced with a length of 1 cm so that the probe could measure the fingerprint region. This allowed the examination of a wavenumber as low as 800 cm^{-1}. The study proved for the first time that Si-ATR-IR could examine the chemical reactions in the channels of microfluidic chips[13-15].

Figure 1.16. Refractivity of (a) KOH-etched Si wafer. (b) Piece of Si wafer.[13]

1.2.1.3. Disposable ATR-IR Crystals and Their Importance in Chemical Analysis

It is a well-known fact that IR spectrometers are expensive and massive instruments, although technology is improving day by day. One of the reasons is that ATR-IR crystals are neither easily produced nor disposable. The crystals are made of Ge, ZnSe, or diamond. Generally, if a crystal is placed into the spectrometer system, it will not be replaced until it is broken or contaminated. Because of their price, crystals must be used carefully.

However, a new promising development allows the production of easily replaceable crystals made from a Si wafer. Si wafers are relatively cheap materials compared with Ge, ZnSe, and diamond. Karabudak et al.[12] successfully fabricated disposable Si IREs. In disposable IRE fabrication, a dicer is used in place of the time-consuming KOH-etching process. This allows a huge number of disposable Si IREs to be produced quickly and cost effectively. Therefore, one-time use Si IREs (disposable Si IREs) can be produced. These disposable Si IREs can have a significant effect on different fields in which ATR-IR is used. They eliminate the need to clean ATR-IR crystals every time, so the sample can be kept with the crystal as long as needed.[12] These crystals will be an advantage in the field of biomedical research, where high hygienic conditions are required. Also, highly explosive, highly acidic, and highly basic experiments can be performed. Another important feature is ease of use. When the amount of sample to be examined is small, it can easily be stored on the crystal for reuse. Then, this crystal can be analyzed without any of the problems of other devices, such as scanning electron microscopes (SEMs). It even stood up to a temperature test in the oven up to 1,414ºC.

1.2.1.4. Miniaturizing of ATR-IR Spectrometers

Many instrumentation companies are trying to make smaller IR spectrometers. Smaller versions of IR spectrometers are announced every year. A review of handheld IR spectrometers was published by O'Brien et al.[33] Companies such as Pyreos and Hamamatsu are producing handheld spectrometers. However, the poor spectral quality and high cost of these instruments prohibit their use. Nevertheless, it is most probable that these systems will become more common in analytical labs in the near future if

technological developments allow the manufacturing of smaller IR spectrometers with better quality and low cost. Additionally, there have been academic trials to unite whole ATR-IR systems into a single embedded chip, as shown in Figure 1.15.[13-14] In these systems, the whole light source and detector are accrued into the same Si wafer. However, they have two major disadvantages. First, these systems do not work as efficiently as commercial IR spectrometers, since the embedded light source and detector are not as efficient as commercial ones. For instance, the embedded light source is not as accurate or intense as commercial light sources. This minimizes the quality of the spectra that are observed. In addition, embedded detectors cannot detect all wavelengths at once. Some specific wave ranges are chosen and the whole system works in these wavelengths. Another drawback is that the manufacturing process of these devices is time consuming, expensive, and complex. The manufacturing process requires clean room facilities, which adds to the cost of the device. Device cost is not a scientific issue; however, it is important to general use of the analytical technique. In brief, technologically, it is possible to integrate a light source and detector into a single Si wafer. However, with current technology, the system efficiency is too low and the cost is too high. If the cost of microfabrication is reduced and the quality of an embedded light source/detector is improved, these kinds of systems can have an important role in the field.[13-14]

The company Pyreos started to fabricate hand-held mid-IR spectrometers. Portable Pyreos ATR is a small size ATR spectrometer with the dimensions 165 x 74 x 35 mm. ZnSe crystal has been used as an ATR crystal with a surface area of 17 x 27 mm. The ATR can scan a 1818 – 909 cm^{-1} range. The company has also been developing kits, one of which was purchased by our laboratory. (Figure 1.17) These systems can analyze samples using mid IR radiation including fingerprint region. The sample can be easily placed on an ATR-IR crystal, and spectrum can be taken in a second. In addition, it is a small, lightweight, battery powered, low power consumption device that can analyse liquids, solids, and slurries. Figure.17 shows the basic working process of Pyreos ATR and a Pyreos ATR model. The ATR can be easily cleaned, which allows fast and reproducible analysis. Pyreos ATR is used with SphinxSuite Software combined with powerful and easy to use chemometric analysis software.[34]

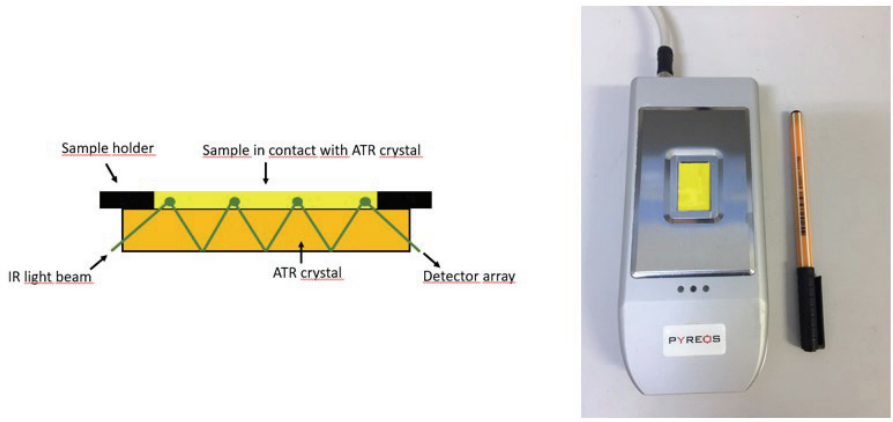

Figure 1.17. Basic scheme of Pyreos ATR and Pyreos PY0715-ATR. [34]

Meanwhile, micro-spectrometers are being improved by other companies. Hamamatsu has developed a finger-tip size, ultra-compact spectrometer head. The device is integrated with micro-electromechanical systems (MEMS) and image sensor technologies. It can be used with printers and a handheld color monitoring device. It can also be and combined with mobile devices if a suitable application is used. The device has a 340 to 780 nm spectral response range with 15 nm spectral resolution. Its weight is only 5g, and its dimensions are 20.1*12.5*10.1mm. (Figure 1.18).[35]

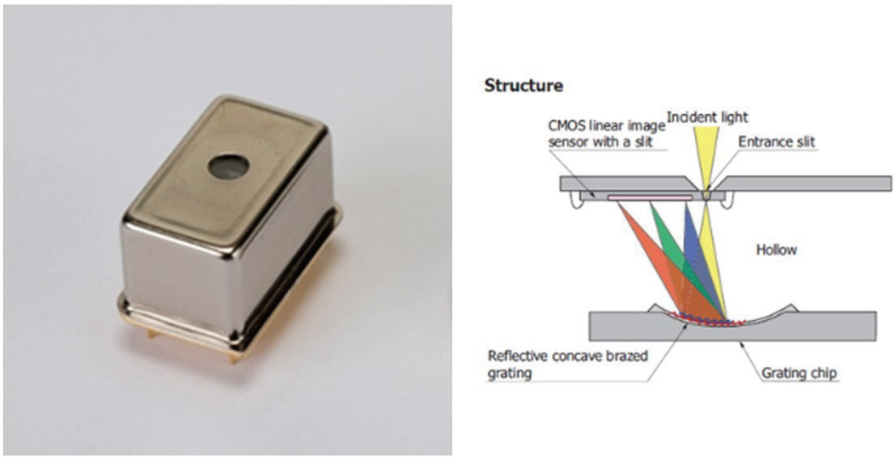

Figure 1.18. Basic scheme of finger-tip size spectrometer head.[35]

1.2.1.5. Future Perspectives and Emerging Applications of ATR-IR Technology

Micro-machined ATR-IR is suitable for research on high-pressure catalytic reactions. A high-pressure micro-machined ATR-IR can be developed in the future. Reaction mechanisms at 600 bar might be analyzed. Such technology would be valuable to the petroleum refining processes, for example. An Illustrative drawing is shown in Figure 1.19. Ultra-high-pressure micromachined Si ATR-IR may play an important role in such research.

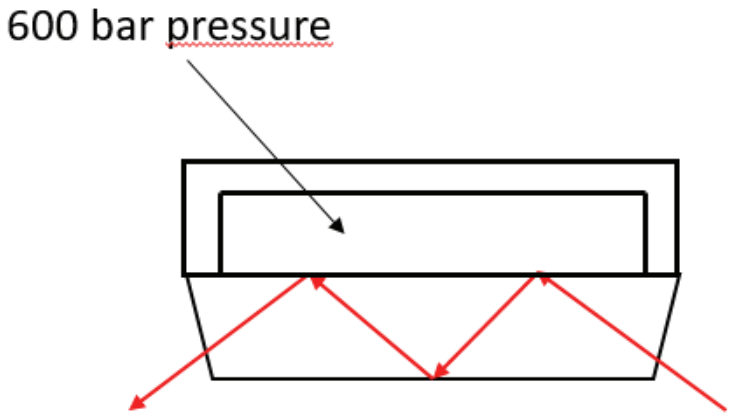

Figure 1.19. High-pressure microfluidics ATR-crystal system.

Another application might be biomedical research and biomedical device fabrication. Dis-posable ATR crystals are useful for biomedical analysis (Figure 1.20), because disposable ATR crystals ensure superior hygienic conditions; a new crystal can be used for each sample. In addition, if disposable ATR crystals are employed, biomedical researchers may reuse samples, since IR spectroscopy is a non-destructive analysis. In this way, properties of the same sample can be measured by another analysis method. This is a significant improvement for biomedical research. Also, chemical reactions in confined spaces and confinement effects of molecules might be researched. Moreover, safety issues surrounding the study of explosive, highly toxic, and highly expansive reactions can be solved.

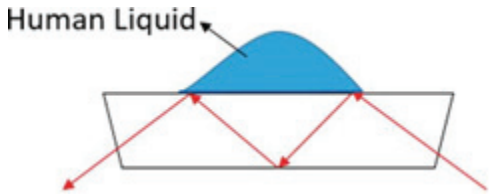

Figure 1.20. Biomedical applications with disposable Si ATR-IR.

In forensic science, samples are gathered from crime scenes. The samples might be too limited for multiple analyses, so tests should be done carefully and samples should be preserved as much as possible. Disposable ATR-IR crystals allow the use of the same sample in more than one analysis since it is non-destructive. The samples can be preserved with dis-posable crystals so that a new analysis can be done or previous analysis can be repeated. Also, using handheld ATR-IR spectrometers, forensic scientists can analyze these samples at the crime scene.[25]

1.3. Conclusion

Since the beginning of history, scientists have tried to explain what light is and how it can be used. In the 17th century, Newton discovered that white light was composed of a spectrum of different colors, and with prisms it was possible to divide it into its components. Although Newton himself described this phenomenon in different terms, this meant that white light contained a range of wavelengths. A few centuries later, quantum physics was developed, and scientists like Schrodinger, Feynman, de Broglie, and Einstein claimed that light had both particle and wave properties. This information precipitated improvements in spectrometric methods, such as UV–Vis, Raman and IR. IR spectroscopy is one of the most important and useful analytical methods in chemistry. Using IR radiation, IR active molecules can be detected easily, and samples can be reused since IR spectroscopy is a non-destructive method. Another advantage is that to perform the analysis, only a small portion of the sample is needed. However, it is not very accurate for aqueous solutions due to high absorptivity of water molecules in the IR region. Signals produced by water molecules hide or distort signals of other molecules. ATR-IR has solved this problem, so that we can take IR spectra accurately and precisely for aqueous solutions.

Currently, more ATR-IR spectroscopy techniques are being developed each day. For example, ATR crystals are being integrated with disposable Si-wafer crystals. These crystals can be changed easily without advanced technical tools. Therefore, they are cheaper than commercial disposable ATR crystals. Moreover, the crystals can be designed as microfluidic chips that allow analysis with even less sample. This may be especially advantageous to forensic scientists, who often must deal with limited samples. Disposable ATR crystals combined with miniature ATR-IR spectrometers allow easy transportation and analysis in many environments for forensic scientists and medical doctors, so that they can analyze body liquids immediately. Another way to improve this method may be to develop high-pressure miniature ATR-IR spectrometers for study of high-pressure reactions. It is difficult, expensive, and dangerous to install high-pressure test equipment in large quantities. mSi-ATR-IR would allow high-pressure material to be tested in very small volumes. This would be useful when studying explosive, highly toxic, and highly expansive reactions, or even yet untested reactions.

1.4. Motivation of My Thesis

Currently, the number of patients per state hospital in Turkey is too high. Doctors need point of care(PoC) tests like blood analysis, to diagnose his/her patients. Patients is firstly examined by a doctor. If the doctor needs blood analysis, then patient gives blood to blood laboratory. After a certain time, the results are given to the patient and he/she meets with the doctor again to show the results. This causes too much time loss. In addition, these analyses are not performed in some small healthcare centers and cause extra time loss, which is another major problem in the health care system. Electrochemical, spectrophotometric and enzymatic analysis methods are mostly used for blood analysis. The sum of glucose, urea, triglycerides, cholesterol, albumin and total protein tests cost for 7TL. Blood samples are taken separately about 2-5ml volume for each test and preliminary procedures are required. Moreover, the devices used in these analyses have high prices and are not produced in Turkey. On the other hand, ATR-IR spectrometry is a technique that does not require preliminary sample preparation, less sample volume, cheap and results in shorter time. Studies have been carried out in the literature which have shown positive results on glucose, urea, triglycerides, cholesterol, albumin and total protein in blood, plasma and serum using ATR technique. The six

components in blood have importance in the diagnosis of a disease at the patient. The aim of this thesis is a preliminary study to determine the glucose, urea, triglyceride, cholesterol, albumin and total protein concentrations in 1 minute, 1 μl of blood, using disposable crystals and less than 1 dollar in the doctor's room by direct analysis of the blood using ATR-IR spectrometry and using chemometrics algorithms to predict them from the spectral data.

CHAPTER 2

DETECTION SPECIES WITH PORTABLE PYREOS ATR

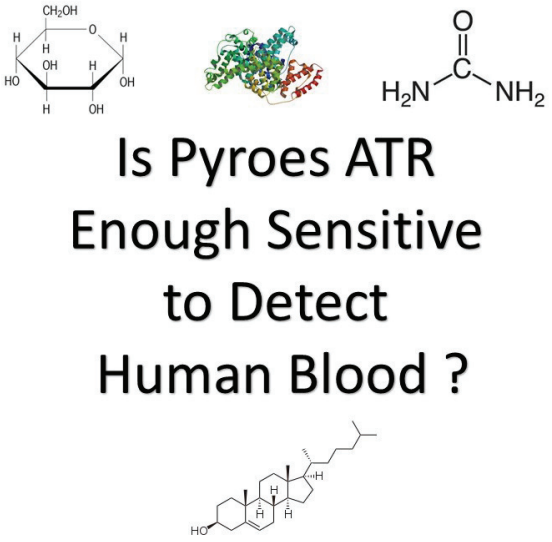

2.1. Introduction

Nowadays, advanced analysis equipment have high technology. Various companies continue to develop these devices. However, these advanced devices are often large in size and are not suitable for transport to different locations for each measurement. In the field of IR spectroscopy devices; there were only portable devices running in the NIR area. In recent years, the portable ATR device developed by the Pyreos firm was developed and marketed. At this point, this device allowed the measurements to be made at the desired location and brought new excitement to the research. In this direction, we aim to develop a new blood measuring device using the Pyreos portable ATR.

The purpose of this chapter was to measure the glucose and urea aqueous solutions; which were prepared according to the value range in the human serum, by using Pyroes ATR and Perkin Elmer(PE) Spectrum II UATR. From these measurements; our aim was to view the signals of this molecules accurately using the Pyreos device, and to determine the limit of detection(LOD) for both the devices. Sample concentrations were

prepared according to amount in the human serum. We assume that if the sensitivity is sufficient to detect the molecules at the samples, the device will be accepted for the using in analysis of the real blood samples.

In the chapter, we are using portable Pyreos ATR-IR PY712 model. If we basically introduce Pyreos PY712, a ZnSe crystal is attached on the device. There is 17 x 27 mm ATR surface area which gives wide area to get information about samples. It scans wavenumbers area between 1818 – 909 cm^{-1} with electrically modulated MEMS emitter. Its operating environment is 0 - 60°C. It has 165 x 74 x 35 mm dimensions. Moreover, it has a battery that works 5 hours while continuous measurements occur up to 70 min. This means that a person can easily use wherever he/she wants. We will deeply examine the device following.

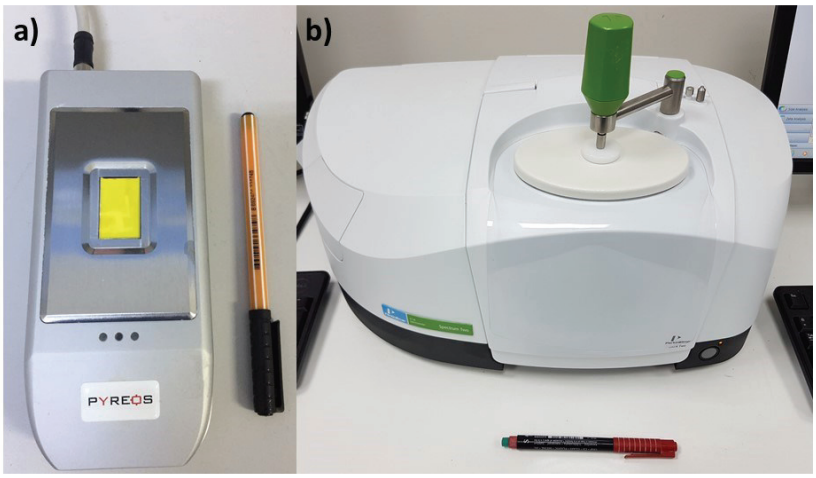

Figure 2.1. a) Pyreos ATR-IR PY712 b) Perkin Elmer Spectrum II UATR FTIR.

Figure 2.1. shows both devices that we used in the chapter. It is important to know the working mechanism of these devices in order to understand what is causing differences in their spectrum for same samples. For this reason, we firstly introduced the working mechanism of PE spectrum II UATR and Pyreos ATR-IR PY712.

Michelson interferometer optical system is used in PE spectrum II UATR. The system basically includes a IR light source, a beamsplitter, three mirrors(one moving, two

constant) and a detector. Figure 2.2 shows its optical diagram. In addition this, PE spectrum II UATR has ATR attachment.[36]

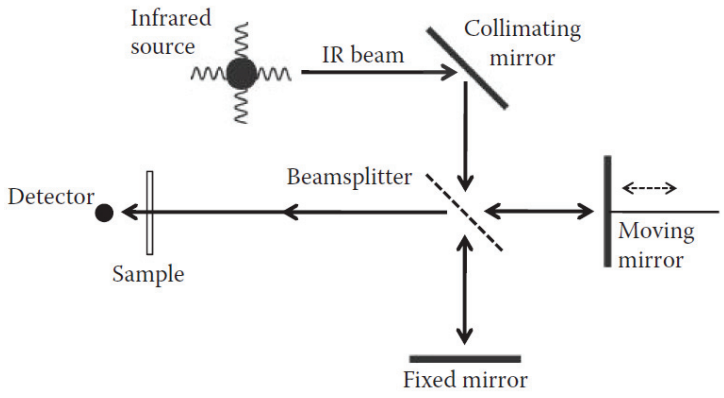

Figure 2.2. The Michelson interferometer optical diagram

Light source of the device is diode laser. The light includes all wavelength between known range. The generated light is guided to the beamsplitter by the collimating mirror. The beamsplitter is made of a thin germanium film between 2 pieces of KBr glass. KBr passes infrared light completely. The Germanium film passes a part of the infrared light, reflecting part of it. At this point a semi-transparent mirror is obtained. In this way, the light is divided into two pieces and goes to moving and fixed mirrors. The formation of light at different wavelengths occurs in the phase in which these two separated light recombine. In order to understand this phenomenon, it is necessary to understand the formation of constructive and destructive interferences and their effects on the wavelength of recombined light. Let's say A_1 is the reflected light from the fixed mirror, A_2 is the reflected light from the moving mirror and A_f is recombined light at the end of reflections. Equation 2.1 is the mathematical representation of A_f.[36]

$$A_f = A_1 + A_2 \tag{2.1}$$

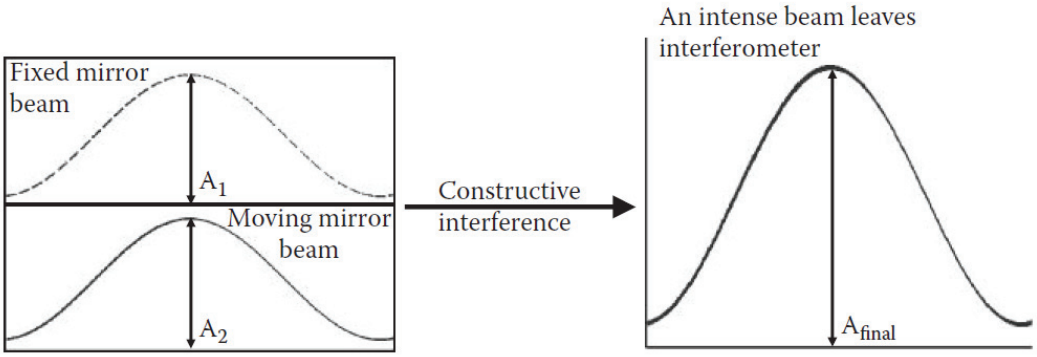

Figure 2.3. Constructive interference

According to this equation, a constructive interference (figure 2.3.) forms when A_f is bigger than A_1 and A_2. If A_f is less than either wave, alone, and even zero, a destructive wave (figure 2.4.) forms.

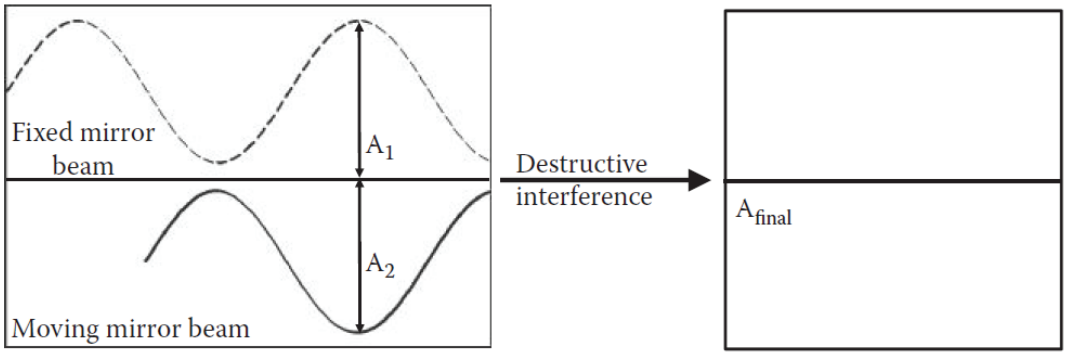

Figure 2.4. Destructive interference

The formation of these interferences is mathematically shown in equation 2.2 and 2.3.

$$\delta_c = n\lambda \quad \text{for constructive interference} \tag{2.2}$$

$$\delta_d = (n+1/2)\lambda \quad \text{for destructive interference} \tag{2.3}$$

The final beams are shown at figure 2.5 when n is equal to zero.

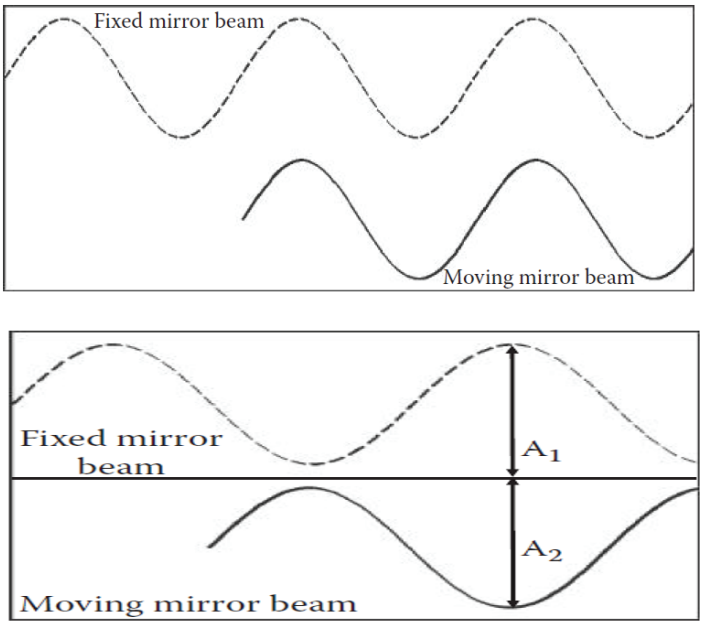

Figure 2.5. Final beams that come from mirrors (n=0)

Equation 2.4. shows the effect of the displacement of the moving mirror on the wave frequency. Thanks to this displacement, when the two lights are combined, the other wavelenghts have cancelled each other so that only one wavelength is produced.

$$F = (2\nu v)/c \tag{2.4}$$

where, F = Fourier Frequency of the interferogram in Hertz , ν = Frequency of the light wave in Hertz, v = Moving mirror velocity (assumed constant) in cm/sec, c = The speed of light in cm/sec. In the equation, if we use the W / ν conversion instead of c in this equation, we get the following equation:

$$F = 2\nu W \tag{2.5}$$

Equation 2.5 gives a direct relationship between the frequency of a light wave and the Fourier frequency of its corresponding interferogram. If we rearrange equation 2.5:

$$W = F/2v \tag{2.6.}$$

Equation 2.6 shows that for each different wavenumber of light a different frequency interferogram exists.

The moving mirror is moved back and forth once. This is called a scan and a scan between 650-4000cm^{-1} for the device. During the scanning, light passes through the ATR crystal and interreacts with sample. In the first chapter, we mentioned about the working dynamics of the ATR in broad terms, so we did not mention again. After that, the light finally reaches the detector. Detectors have to be protected from the environment in order to work well. Because of this reason, a IR window; that is made by the same material as the beamsplitter window, is placed in front of the detector. As a detector, $LiTaO_3$ wafer is used. In this case, the window is made of KBr. Moreover, noise level of the device is proportional to the area of the detector, so detectors have small areas, generally it is less than 1mm^2.

This material is a pyroelectric. Pyroelectricity is the ability of certain materials to generate an electrical potential when the temperature of material is changed. Equation 2.7. show how electrical potential changes when the temperature of material increases or decreases.

$$V = p\ t\ \Delta T/\varepsilon \tag{2.7}$$

where ε: electric permittivity of the material, p: pyroelectric coefficient, t: thickness of the material, ΔT: temperature change.

This electrical potential is measured by electrical contacts placed on the surface of the $LiTaO_3$ element. After that point, wave is turned to electrical signal. Signals are sent to computer and the computer applies Fourier transform to electrical signals to form a IR spectrum.

Pyreos ATR has a own unique design. In the previously mentioned PE spectrum II ATR device, the light is first separated into wavelengths by a beamsplitter and reaches the detector after being passed through the sample or ATR crystal. In this device, the light is first passed through the sample, and after that, it is separated into wavelengths by a filter and reaches the detector. I will explain them step by step. Light source of the device is electrically modulated MEMS emitter. It is a practical application of thin film transmitters. Applying an electric current, this thin film heats up and turns into a light source. The resulting light contains wave lengths between 5.5μm and 11μm and is

directed to the ZnSe crystal. After the light reflects through the crystal (9 reflections), it directly reaches the line array filter. The working mechanism of this filter is shown at figure 2.6.

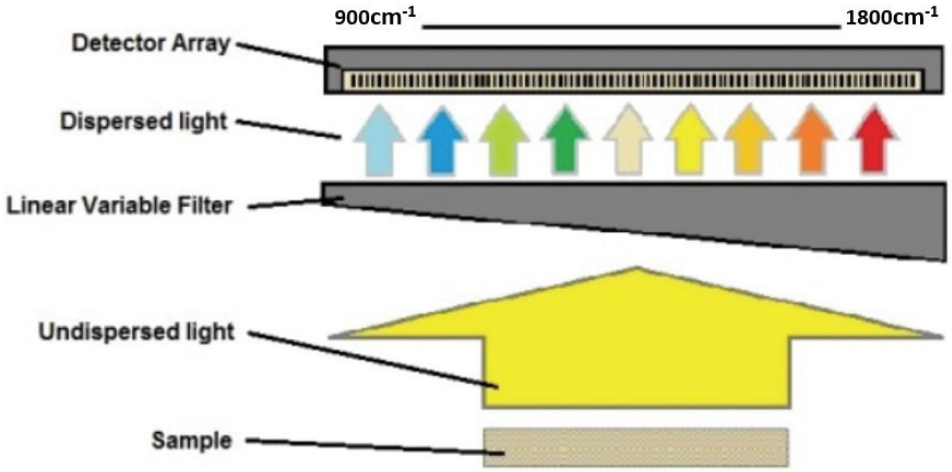

Figure 2.6. Working mechanism of linear array filter.

The incoming light is reflected in this filter that has a different thickness each point. In the previous paragraph we have shown the formation of constructive and destructive waves. The light is reflected in the filter as shown and merges with the other incoming light. Thus, different constructive and destructive waves are formed, and the light separates into wavelengths. Once the light is separated into wavelengths, then they reach the linear array sensor. This sensor is pyroelectric thin film sensor that is made of lead zirconium titanate(PZT) material. It is divided by 128-pixel, and each separated wavelength hits only onto one pixel. The electric currents are transferred; that vary according to the wavelengths of the light coming to each pixel, to computer and by using the Laplace transform, spectrum is get.

2.2. Experimental

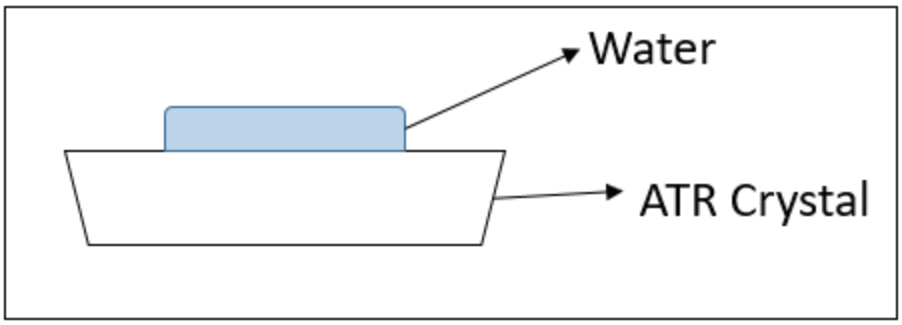

Figure 2.7. Basic ATR System.

The most important part is sensitivity of Pyreos ATR for the detect of glucose, urea, cholesterol, triglycerides, albumin and total protein in venous blood ranges. First, we decided to start with glucose and urea ATR measurements. The reason starting with glucose and urea is that, we had glucose and urea samples and they are soluble in water. The other components of human blood that we want to analyze, is insoluble or slightly soluble in water like cholesterol and triglycerides. Albumin and total proteins are soluble in water however these are more complex then glucose and urea.

Table 2.1. Parameters for human serum.

Concentrations	**mg/dl**	**mmol/L**
Glucose	70-99	3.9-5.5
Urea	7-20	2.5-7.1
Cholesterol	120-200	3.1-5.2
Triglycerides	35-150	0.4-1.7
Albumin	3500-5500	0.5303-0.8333
Total Protein	6600-8400	-

Glucose is found between 70-99mg/dl and urea is found between 7-20mg/dl as it is seen table 2.1. Ten glucose and urea samples were prepared between 0-16667 mg/dl in water. (Table 2.2.) At the first part of the measurement we used Pyreos ATR-IR PY715 and the second part of the measurement we used Perkin Elmer Spectrum Two UATR-IR.

Table 2.2. Concentrations of Glucose and Urea.

Sample	Glucose Concentration(mg/dl)	Urea Concentration(mg/dl)
0	0	0
1	32	32
2	65	65
3	130	130
4	260	260
5	521	521
6	1042	1042
7	2083	2083
8	4167	4167
9	8333	8333
10	16667	16667

2.2.1. Pyreos ATR-IR Measurements

Pyreos ATR was set for 200 scans between 1800-900cm^{-1} wavenumbers. Its resolution was 8cm^{-1} as default. Before we started measurements, water was measured as background. Firstly, we measured 25 water samples. After glucose and urea samples were measured in an order. At last we measured 25 samples again. After each measurement, the ATR crystal was cleaned with ethanol and wiped with microfiber cloth. Collected data were plotted separately.

2.2.2. Perkin Elmer Spectrum Two UATR-IR

PE ATR was set for 16 scans, 4cm^{-1} resolution and between 4000-650cm^{-1} wavenumbers. Water was measured as background, before measurements were analyzed. Firstly, we measured 20 water samples. After glucose and urea samples were measured in an order. After each measurement, the ATR crystal was cleaned with isopropyl alcohol and wiped with paper napkin. Collected data were plotted separately.

2.3. Discussion

In the chapter we wanted to determine limit of detections(LODs) of commercial Pyreos ATR-IR 712 spectrometer for glucose, urea, cholesterol, triglycerides, albumin, and total protein. Also, to make a comparison we used Perkin Elmer Spectrum II UATR-FTIR spectrometer. At the beginning, we thought to start with glucose and urea would be better, because these molecules had been simpler molecules than the others and they could be solved in water and also urea had the lowest concentration level in the others component. If we could detect lower urea concentration, we might detect the others too. Hence, we prepared eleven samples from 0 to 16667mg/dl for glucose and eleven samples from 0 to 16667mg/dl and measured them with both instruments. Before glucose measurements and after urea measurements we analyzed twenty-five water samples with Pyreos ATR, and before glucose measurements we analyzed twenty water samples with PE ATR.

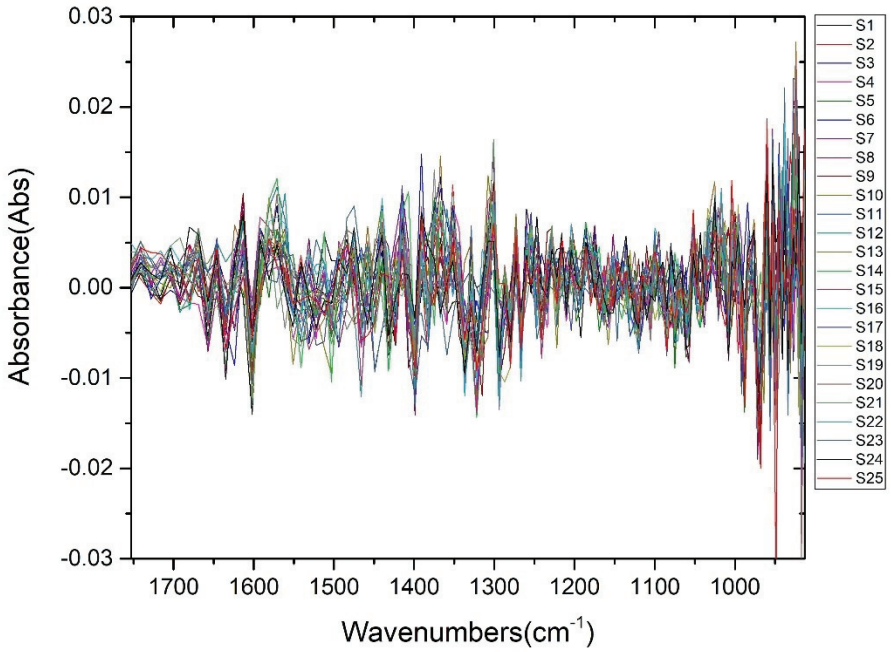

Figure 2.8. After measurement of samples, spectrum of water samples (S1-S25 from same water source) at water background with Pyreos ATR-IR PY715 spectrometer in order to see the noise levels.

Figure 2.8. shows twenty-five water sample measurements. We used the measurement to detect standard deviation of Pyreos ATR for later. Before the glucose measurements had 25 water spectra with air background. However, S1, S2, S3 and S4 samples were separated from the others. This led to systematic error of the device. We had started the measurements, shortly after we switched on the device so we though that the device needed time to work efficiently. We could say that according to figure 2.8., twenty-five data were together at the graph. We used figure 2.8. to calculate standard deviations for glucose maximum absorbance peak and urea absorbance peak.

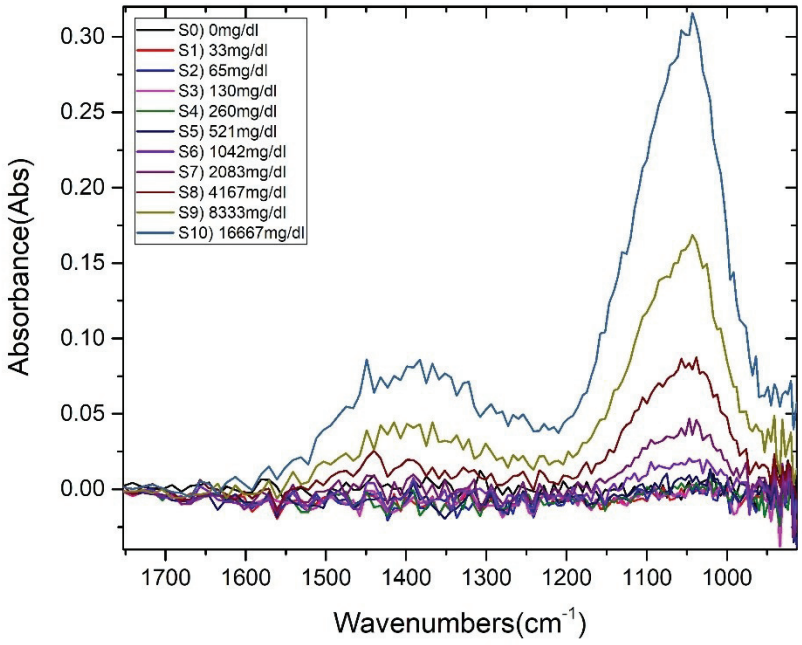

Figure 2.9. Glucose samples(S0-S10) spectrum which measured with Pyreos ATR-IR PY715 spectrometer at water background.

Figure 2.9. shows glucose absorbance spectrums. As it can be seen, first six data look like water spectrum. Glucose peaks are hard to see. Noise level is preventing to separate glucose peaks. However, the highest peak was 1043cm^{-1} at the highest concentration so we chose this peak to get a calibration curve and also we used this peak in data of figure 2.8. to calculate standard deviation at 1043cm^{-1}. Standard deviation was calculated as %0.00273. Limit of detection is three times of standard deviation at %99.9 confidence level, so this was 0.00819.

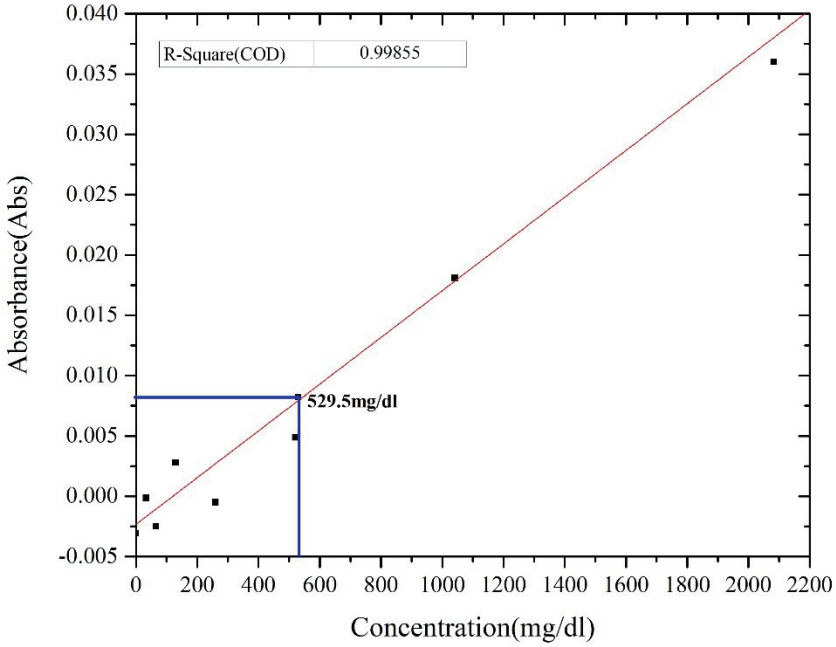

Figure 2.10. Calibration curve of Glucose which taken from Pyreos ATR (Maximum absorbance peak at 1043cm^{-1})

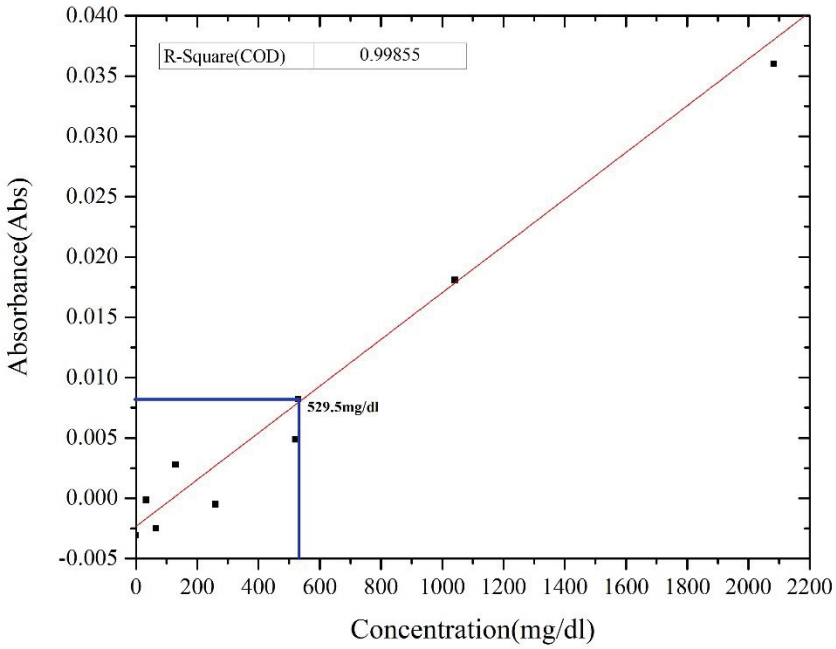

Figure 2.11. Zoomed in calibration curve of Glucose which taken from Pyreos ATR.

We plotted calibration curve from maximum absorbance peaks of glucose (Figure 2.10. and 2.11.) and we added a border at 0.00819 as starting point of limit of detection for glucose at Pyreos ATR. 0.00819 corresponded to 529.5mg/dl which is too high level that we needed to detect from human serum. (Table 2.1) According to LOD of glucose, we cannot detect lower than 529.5mg/dl.

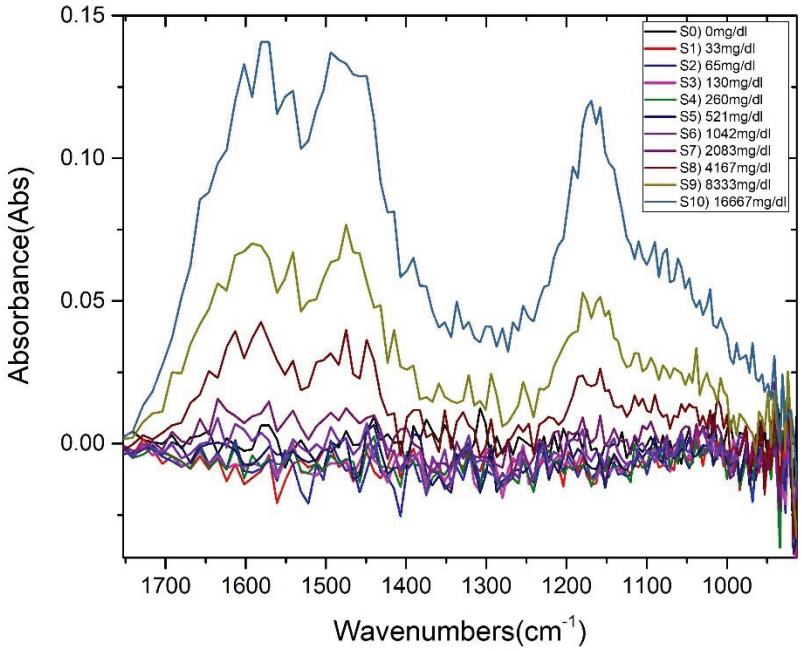

Figure 2.12. Urea samples(S1-S10) spectrum which measured with Pyreos ATR-IR PY715 spectrometer at water background.

Figure 2.12. shows urea absorbance spectrums. As it can be seen, first seven data look like water spectrum. Urea peaks are hard to see too in the graph. We could say again that noise level was preventing to separate urea peaks. The highest peak was 1571cm^{-1} at the highest urea concentration and so we chose the peak to evaluate a calibration curve and also we used for this peak in data of figure 2.9. to calculate standard deviation at 1571cm^{-1}. Standard deviation was calculated as % 0.00327. Three times of standard deviation at %99.9 confidence level was 0.00981.

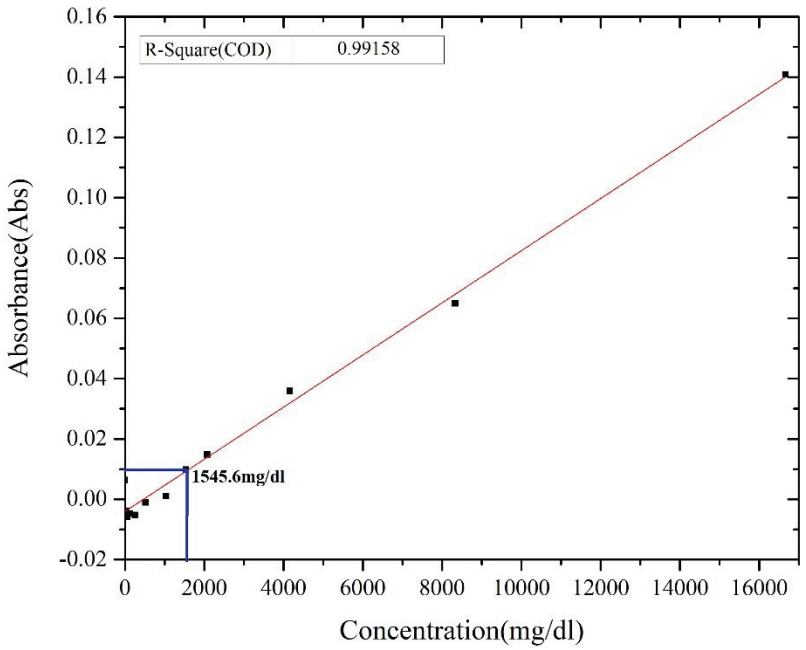

Figure 2.13. Calibration curve of Urea which taken from Pyreos ATR. (Maximum absorbance peak at 1043cm^{-1})

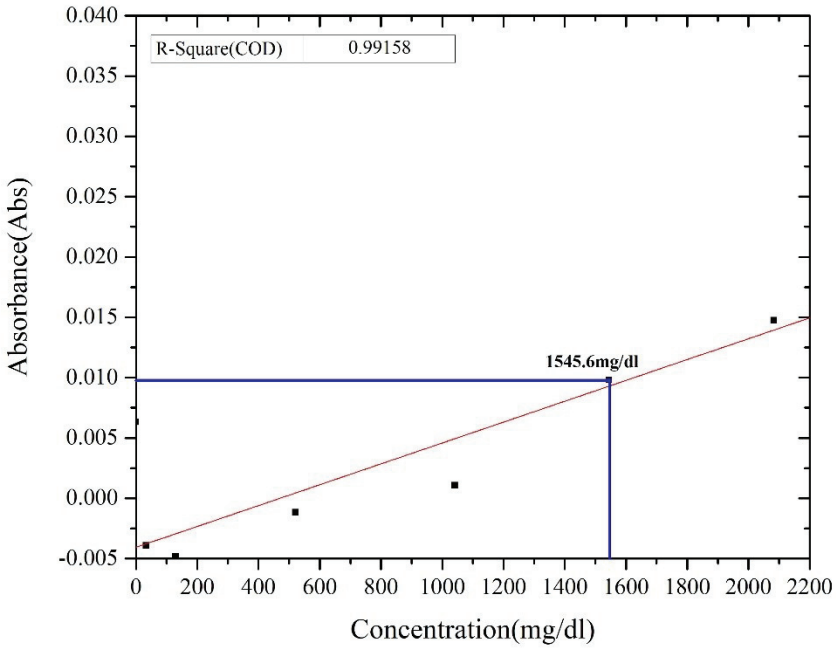

Figure 2.14. Zoomed in calibration curve of Urea which taken from Pyreos ATR.

We plotted calibration curve from maximum absorbance peaks of urea (Figure 2.13. and 2.14.) and we added a border at 0.00981 as starting point of limit of detection for urea at Pyreos ATR. 0.00981 corresponded to 1545.6mg/dl which we needed to detect minimum level from human that was 7mg/dl. (Table 2.1) According to LOD of urea, we cannot detect lower than 1545.6mg/dl. It is even much more higher than glucose detection limit.

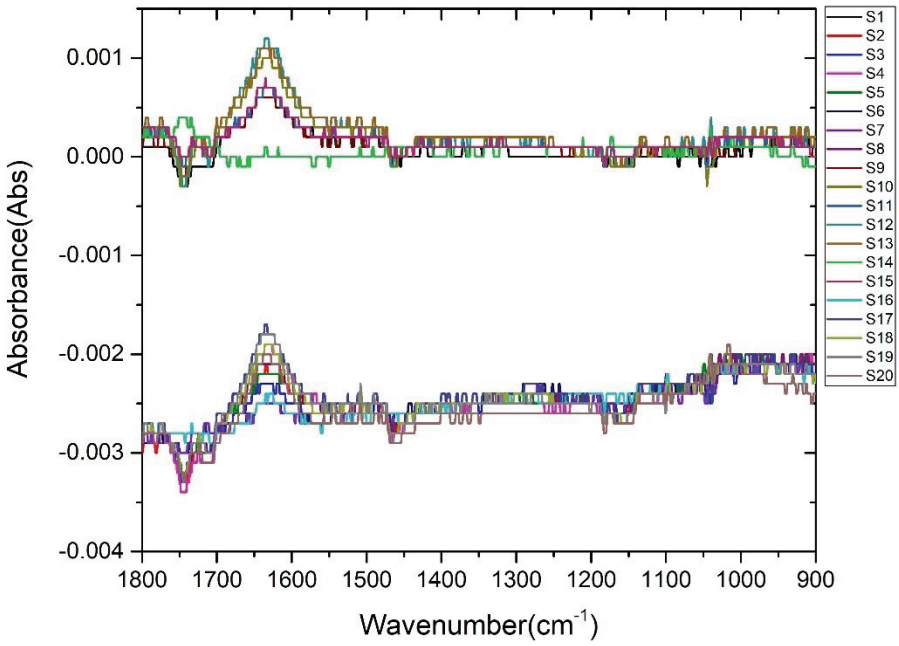

Figure 2.15. Water samples (S1-S20) spectrum which measured with Perkin Elmer Spectrum Two UATR-IR spectrometer at water background in order to see the noise levels.

After these plotting and calculations, we plotted data of Perkin Elmer Spectrum Two UATR. Figure 2.15. shows spectrum of water samples. It was clear, there was a huge spectrum shifts because of the systematic errors.

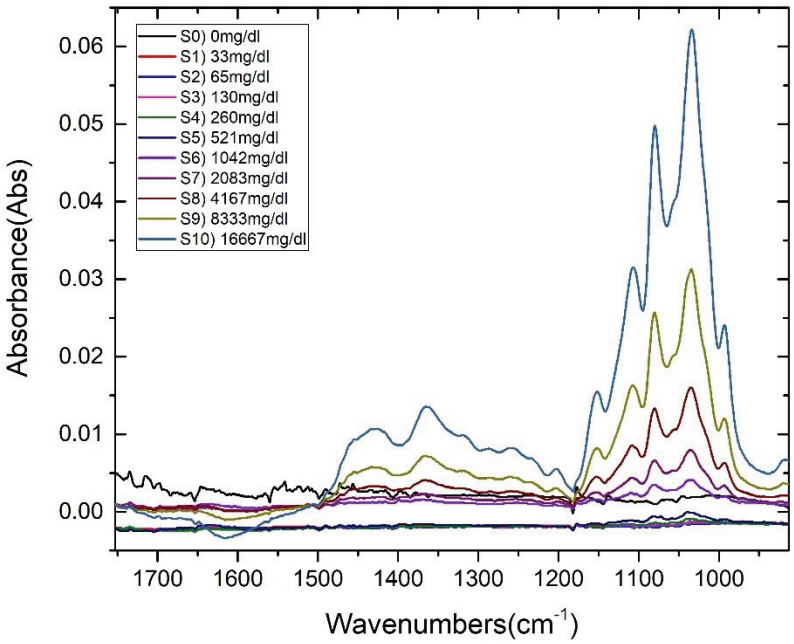

Figure 2.16. Glucose samples(S0-S10) spectrum which measured with Perkin Elmer Spectrum Two UATR-IR spectrometer

Figure 2.16. shows glucose absorbance spectrums. Spectrum of S0 was looked like water spectrum like in figure 2.15. and at first six data, we could not see peak changes clearly because of noise and also as it could be seen, there were spectrum jumps because of the systematic errors. The highest peak was 1034cm^{-1} at the highest concentration so we chose this peak to get a calibration curve. This was 1043cm^{-1} at Pyreos spectrometer. There was a peak shift for glucose. The reason might be systematic errors. We expected to see same absorbance peak for same samples. Data of figure 2.15. was used for this peak to calculate standard deviation at 1034cm^{-1}. Standard deviation was calculated as %0.00113. Three times of standard deviation was 0.00339 at %99.9 confidence level.

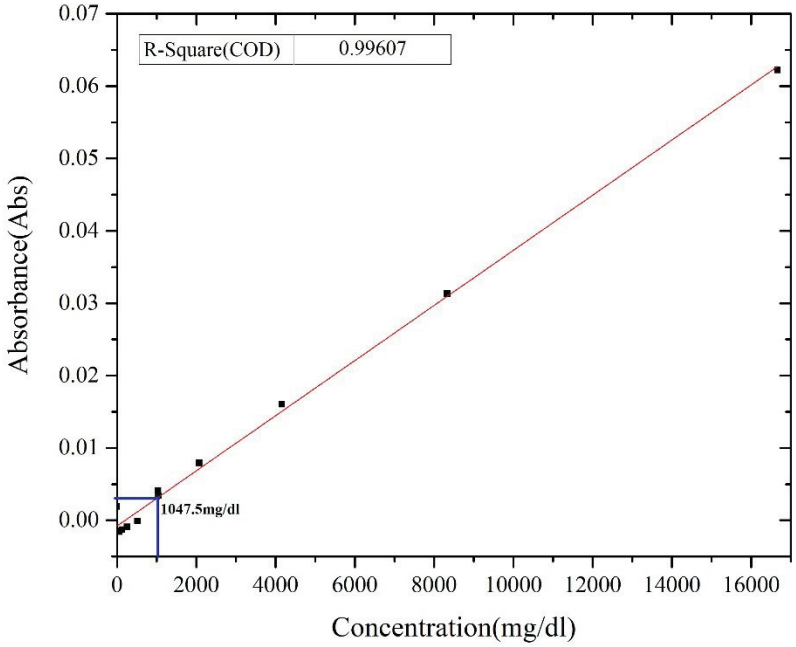

Figure 2.17. Calibration curve of Glucose which taken from Perkin Elmer Spectrum Two UATR-IR. (Maximum absorbance peak at 1034cm^{-1})

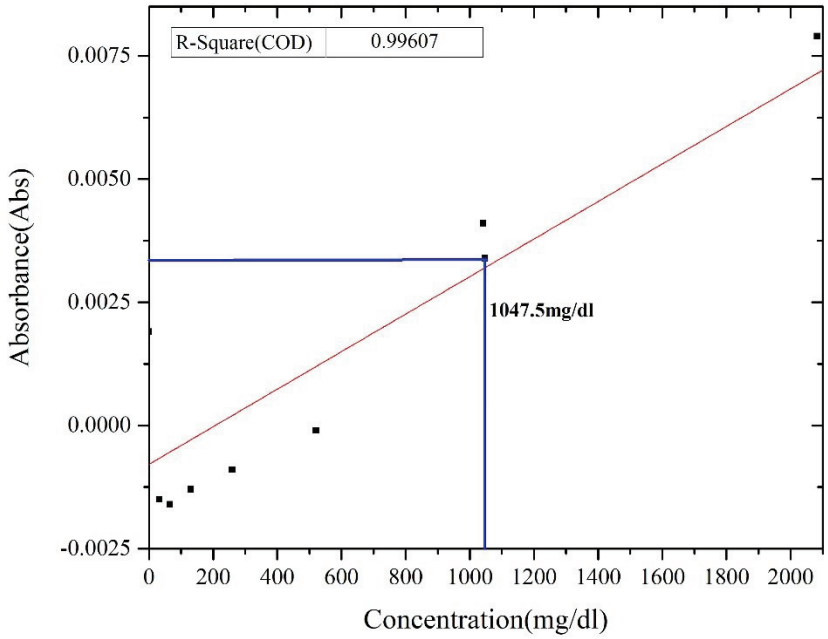

Figure 2.18. Zoomed in calibration curve of Glucose which taken from Perkin Elmer Spectrum Two UATR-IR.

We plotted calibration curve from maximum absorbance peaks of glucose (Figure 2.17. and 2.18.) and we added a border at 0.00339 as starting point of limit of detection for glucose at Perkin Elmer Spectrum Two. 0.00339 corresponded to 1047.5mg/dl which is too high level too again that we needed to detect from human serum. (Table 2.1) According to LOD of glucose, we cannot detect lower than 1047.5mg/dl.

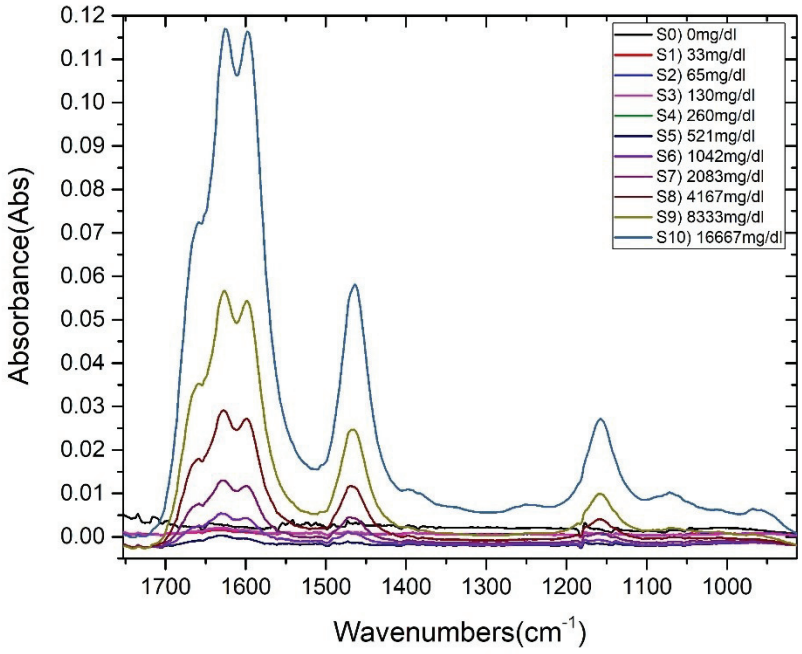

Figure 2.19. Urea samples(S0-S10) spectrum which measured with Perkin Elmer Spectrum Two UATR-IR spectrometer.

Figure 2.19. shows urea absorbance spectrums. Spectrum of S0 was looked like water spectrum like in figure 2.15. again. We could not see peak changes clearly because of noise and also as it could be seen, there were spectrum jumps because of the systematic errors for first six data. The highest peak was 1676cm^{-1} at the highest concentration so we chose this peak to get a calibration curve. This was 1571cm^{-1} at Pyreos spectrometer. This peak shift was bigger than Pyreos ATR for urea. We assumed the reason might be systematic errors. We expected to see same absorbance peak for same samples again, as we mentioned before. Data of figure 2.15. was used for this peak to calculate standard deviation at 1676cm^{-1}. Standard deviation was calculated as %0.00145. Three times of standard deviation was 0.00435 at %99.9 confidence level.

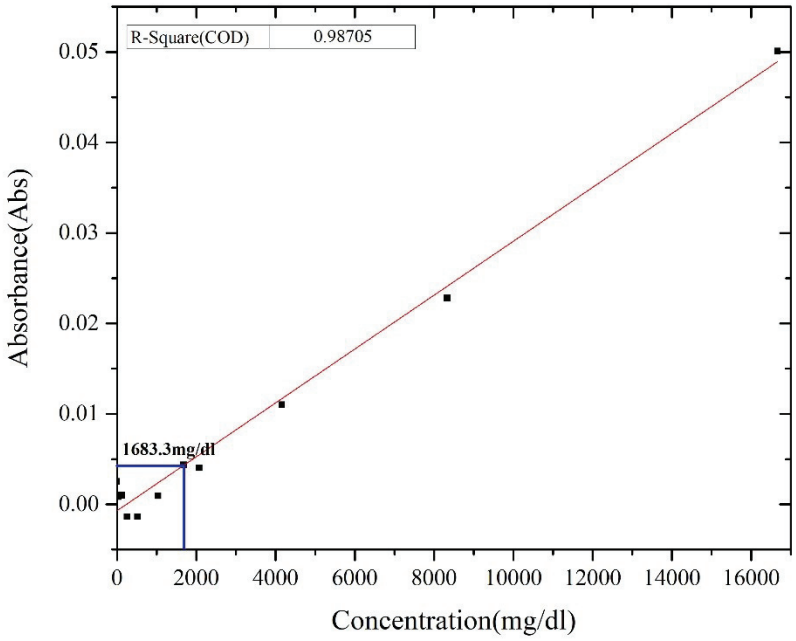

Figure 2.20. Calibration curve of Urea which taken from Perkin Elmer Spectrum Two. (Maximum absorbance peak at 1676cm^{-1})

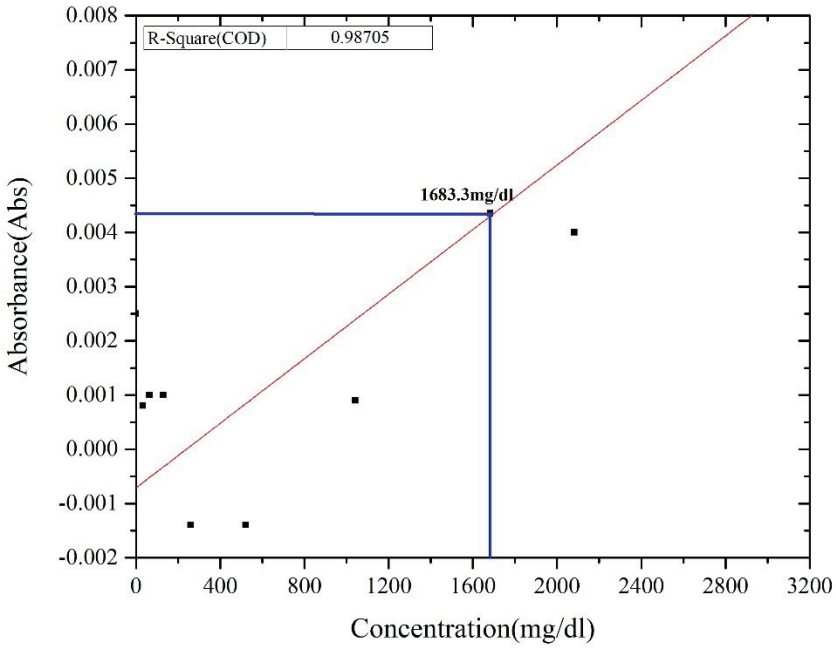

Figure 2.21. Zoomed in calibration curve of Urea which taken from Perkin Elmer Spectrum Two.

We plotted calibration curve from maximum absorbance peaks of urea (Figure 2.20. and 2.21.) and we added a border at 0.00435 as starting point of limit of detection for urea at Perkin Elmer Spectrum Two. 0.00435 corresponded to 1683.3mg/dl which is again too high that we needed to detect from human serum. (Table 2.1) According to LOD of glucose, we cannot detect lower than 1683.3mg/dl.

In addition, there were baseline shifts at PE spectrum II UATR measurements. To solve the problem, we did additional studies. For water measurements, we repeated measurements with 25, 32 and 36scans at 8cm^{-1} resolution. All measurements were made by taking water background before each sample measurement.

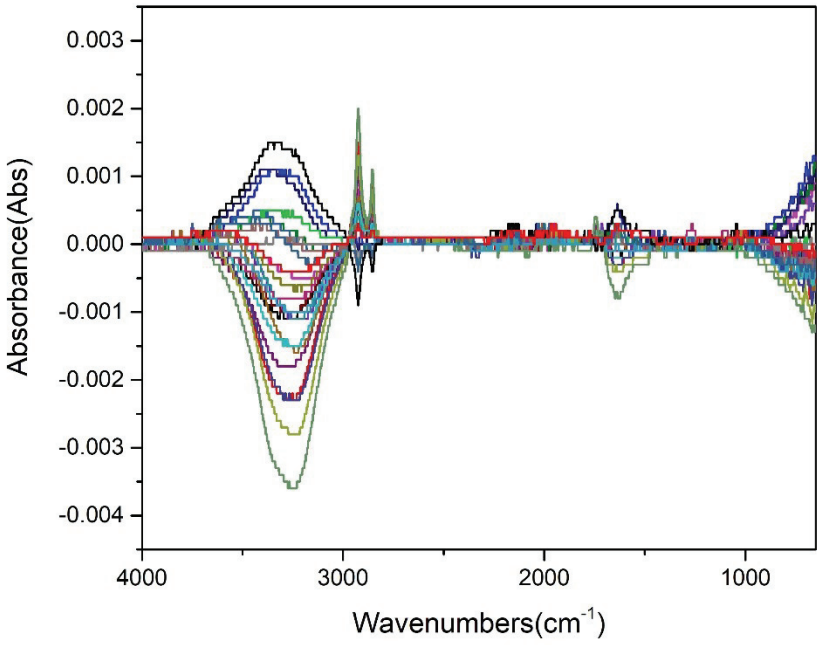

Figure 2.22. 25 water absorption spectra with PE spectrum II UATR that is set 25 scans between 4000-650cm^{-1} at 8cm^{-1} resolution.

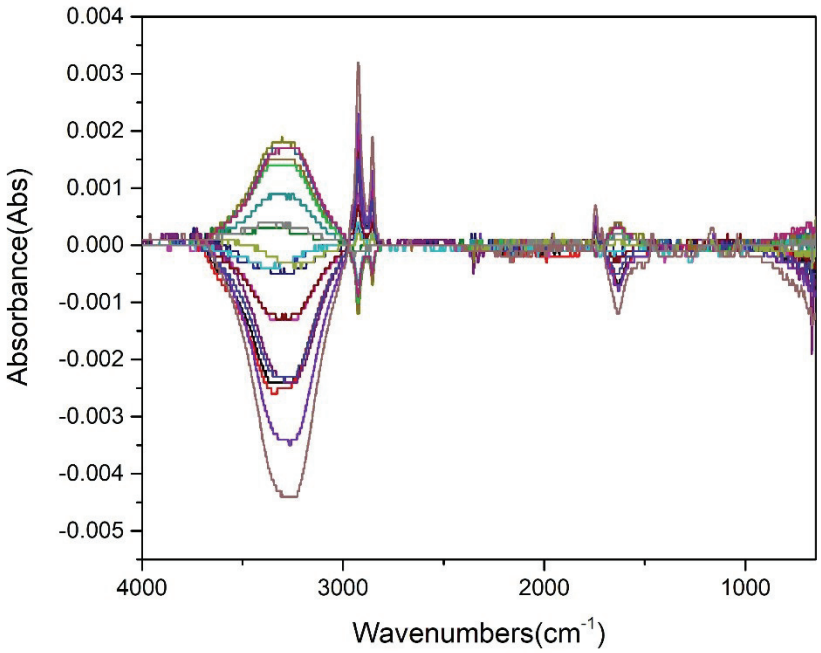

Figure 2.23 25 water absorption spectra with PE spectrum II UATR that is set 32 scans between 4000-650cm^{-1} at 8cm^{-1} resolution.

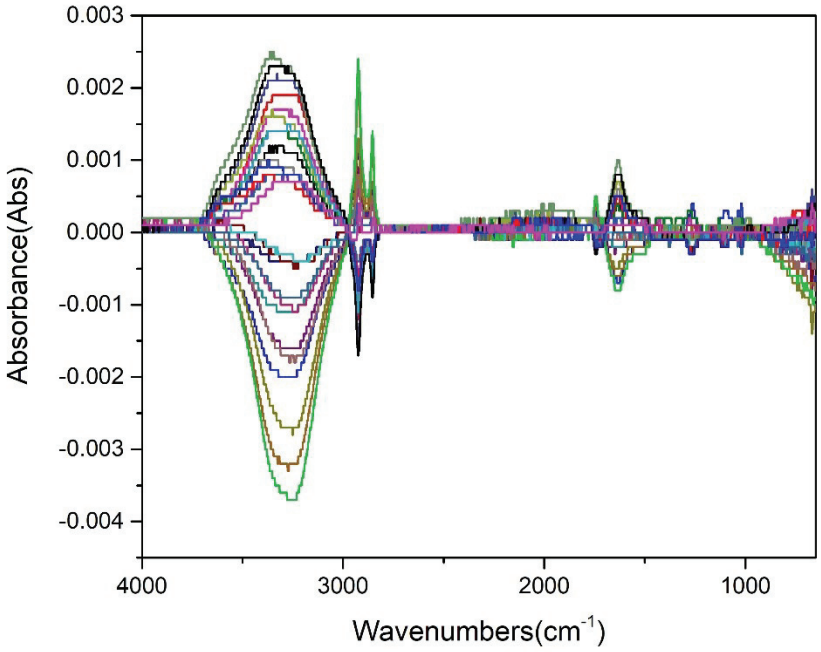

Figure 2.24. 25 water absorption spectra with PE spectrum II UATR that is set 36 scans between 4000-650cm^{-1} at 8cm^{-1} resolution.

As can be seen from the figures, baseline shifts no longer exists. The solution was that, while a measurement was starting, the one had to watch carefully the live spectrum screen on the computer. If he/she saw any shift from the 0 line or he/she had any doubt about shift or personal error, the measurement had to be stopped and a new background measurement had to be done. According to my experiences, after 4 or 5 measurements, the spectrometer needed a new background. Also while sample loading on the crystal, the one should care the air bubbles in the sample and should wait a few second (5 sec. suggested) before the measurement starts.

2.4. Conclusion

As a summary, we can analyze and detect glucose and urea sample at Pyreos ATR-IR 715 spectrometer. However, it is not enough to detect lower concentration. In this part we will summarize why Pyreos is not enough to detect. Table 2.3. shows summary of the important results.

Table 2.3. Summary of The Results (Abs: Absorbance).

The Maximum Abs. Peak Wavenumber(cm^{-1})	Glucose	Urea
Pyroes	1043	1571
Perkin E.	1034	1676
The Maximum Abs. Height At The Highest Concentration	**Glucose**	**Urea**
Pyroes	0.3159	0.1408
Perkin E.	0.0622	0.0501
%Stdev	**Glucose**	**Urea**
Pyroes	0.00327	0.00273
Perkin E.	0.00145	0.00113
LOD	**Glucose(mg/dl)**	**Urea(mg/dl)**
Pyroes	529.5	1546.6
Perkin E.	1047.5	1683.3

If we started to examine with maximum absorbance peaks, we can see peak shifts for both glucose and urea. One of the reasons is these devices have different resolutions and scans that $8cm^{-1}$ resolution and 300 are for Pyreos, and $4cm^{-1}$ resolution and 16 scans are for Perkin Elmer. Resolution and scan difference might cause the peak shifts. Furthermore, the devices apply different mathematical transformation to the signals they receive. Laplace transformation is applied by the PY device. Pyroelectric circuits are

usually Laplace transformed.[37] So Pyreos company might use because of the design of the device. On the other hand, Fourier transformation is applied by the PE device. Fourier transformation is version of the Laplace transformation that is a specialized version of the system of sinusoidal waves. Fourier transformation work better in these systems.

Secondly, there is a relationship between height of maximum absorbance peaks and standard deviations. We related standard deviation to noise. If noise level is high but height of absorbance peaks is low or around the noise level, it can prevent the peaks to be seen. However, sometimes noise level might be high, and height of absorbance peaks are also higher than noise level. In this case, peaks can be observed. According to table 2.3., when we compared the peak heights and the standard deviations, standard deviation of Pyreos ATR is 2.25552 times higher for glucose and 2.41593 times higher for urea than Perkin Elmer ATR and Pyreos ATR has 5.0788 times higher absorbtion peak for glucose and 2.8104 times higher absorbtion peak for urea than Perkin Elmer ATR. We can say that despite Pyreos ATR has higher noise level than Perkin Elmer ATR, it is more sensitive because of having high absorbance peaks.

Another result is that, we need more sensitive ATR spectrometer than these commercial devices. Pyreos ATR detects 529.5mg/dl for glucose and 1546.6 for urea while Perkin Elmer ATR detects 1047.5mg/dl for glucose and 1683.3 for urea. These numbers are too much higher than needed values that are 70mg/dl for lower glucose concentration and 7mg/dl for lower urea concentration. We should increase sensitivity or lower the noise level 7.6 times.

Also, we observed baseline shifts at spectrum. To solve this, we repeated the measurements for only water measurements. The measurements were performed at 25, 32 and 36 scans with a new water background measurement before the water sample measurement started. Signal to noise ratio is directly proportional of the root square of the number of scans. Although the number of scans was increased, baseline shift was observed in some measurements that were not recorded. This situation showed us that the baseline shift may not be related to the number of scans. The reason might be water vapor and CO_2 gas in the air. Generally, spectrometers are sealed to prevent ingress of air. In advance spectrometers, there is air purging system that using N_2. However, PE spectrum II UATR spectrometer has not an air purging system. The spectrometer was sealed with plastic rubber and air intake was tried to be reduced. Water vapor might cover a side of the KBr window and time to time it might be shifted to another side on the window

surface. We did not know when the technical service last calibrated the device so the problem may be solved by re-calibration of the device.

CHAPTER 3

COMPARISON OF BIOLOGICAL METHODS AND MULTIVARIATE CALIBRATION METHODS FOR DETECTION OF ARTIFICIAL SERUM SAMPLE CONCENTRATION

In this chapter, information about literature review, the definition and topics of chemometrics, univariate calibration, multivariate calibration methods such as classical least squares, inverse least squares, principal component regression and partial least squares, and their mathematical algorithms, which are frequently used in the analysis of complex mixtures in analytical studies are presented. Our aim in this chapter, was to prepare artificial serum samples which included glucose, triglycerides, cholesterol, albumin and total protein components and to analyze these samples by ATR FTIR spectrometer and employing PLS model by using Minitab 16 statistical software.

3.1. Literature Review

In recent years, there have been a lot of studies about determining concentrations of glucose, urea, cholesterol, triglycerides, albumin and total protein components in whole blood, plasma and serum samples in Europe and many other countries. There are different techniques to determine these components such as raman spectroscopy, diffuse reflectance FTIR, transmission FTIR and ATR FTIR. These studies received support from chemometric data analysis as univariate analysis and multivariate analysis like partial least squares (PLS) and its combinations with hybrid spectra space(HSE) and artificial neural network(ANN); and principle component analysis (PCA). Such techniques compared with chemometric methods give more precise and accurate results, according to these studies. PCR is the most commonly used method for this purpose.

Janatsch, Kruse-Jarres et al.[38] studied about to determine concentrations of glucose, urea, uric acid, triglycerides, total cholesterol, and total protein in human blood plasma. PE 1800 and Bruker IFS113V spectrometers equipped with DTGS detector and

ZnSe ATR crystal; were used for analysis of human blood plasma and reference spectra. The samples were measured without any preperation and drying process. They used PLS (partial least square) calibration method as a multivariate calibration method. The plasma spectra was taken between 750-1750cm^{-1} with 0.9% aqueous NaCl solution background and the specra was used in the PLS algorithm. According to PLS prediction results, root mean square error of predictions were 2.1g/L for total protein, 22mg/dl for glucose, 33mg/dl for triglycerides, 31mg/dl for cholesterol and 4.4mg/dl for urea. Another study was performed by Stohr, Bhandare et al.[39] PE 1710 ATR FTIR spectrometer equipped with DTGS detector and ZnSe ATR crystal; was used for determination of albumin, ethanol, cholesterol, lactic acid and urea in phosphate buffered saline(PBS) solution in the wavenumber range between 450-4000cm^{-1}. The samples were measured without any preperation and drying process. They built univariate and multivariate methods for the determinations of these components. Peak height and peak area methods were performed by using turbo pascal algorithms. PLS and PCR were performed by using using turbo pascal algorithms. RMSEPs of peak heights were calculated as 59.1mg/dl for albumin and 11.8mg/dl for cholesterol. RMSEPs of peak areas were calculated as 60.5mg/dl for albumin and 19.4mg/dl for cholesterol. RMSEPs of multivariate models were calculated as 51.5mg/dl for albumin and 7.9mg/dl for cholesterol by using PLS algorithm and 49.1mg/dl for albumin and 8.0mg/dl for cholesterol by using PCR algorithm. In the study of Bhandare, Mendelson et al.[40], PE 1750 ATR spectrometer equipped with DTGS detector and ZnSe ATR crystal, was used to determine glucose concentration in whole blood samples. The measurements were performed with 0.9% NaC1 aqueous solution and without any preperation and drying process, in the wavenumbers between 750-1500cm^{-1}. PCR, PLS and PLS-ANN methods were applied to spectral data by using Lab-Calc software and Neural Works Professional software. RMSEP values were found out as 24.0mg/dl, 21.5mg/dl and 15.6mg/dl for PCR, PLS and PLS-ANN respectively. Another Bhandare, Mendelson et al.[41] study was on glucose determination in PBS solution. Measurements were taken by using PE 1710 ATR spectrometer equipped with DTGS detector and ZnSe ATR crystal and with PBS solution background, in wavenumber range between 450-4000cm^{-1}. Univariate method was applied with based on peak area and peak height and RMSEPs were calculated as 47.3mg/dl, 40.1mg/dl and 42.0mg/dl for total area between 1180-950cm^{-1}, peak height at 1035cm^{-1} and peak height at 1079cm^{-1}, respectively. PCR, PLS and PC-ANN were applied and result of RMSEPs were 16.5mg/dl, 18.3mg/dl and 18.3mg/dl for PLS between 1425-930cm^{-1}, PCR 1425-930cm^{-}

[1] and PC-ANN 1425-930cm^{-1}, respectively. Heise, Marbach et al.[42] studied to determine concentrations of glucose, total protein, cholesterol, triglycerides, uric acid and urea in human blood plasma with directly analysing by using Bruker IFS66FT spectrometer equipped with MCT detector and ZnSe crystal. The measurements was taken in wavenumber range between 950-3100cm^{-1}. Multivariate model was built with using PLS algorithm and the algorithm was written in MATLAB. RMSEP results were 10.4mg/dl, 1.21g/L, 1.42mg/dl, 10.3mg/dl and 2.9mg/dl for glucose, total protein, cholesterol, triglycerides and urea, respectively. Heise and Bittner[43], in their study; directly analyzed transmission spectra of plasma in wavenumber range between 420-6800cm^{-1} with using Bruker IFS66FT equipped with InSb detector. Glucose, total protein, cholesterol, triglycerides and urea were determined by using PLS-regression vector choices(RVC) as a multivariate method. They splitted the spectrum into two range and then PLS-RVC was applied. According PLS-RVC results at 1.chosen range, RMSEP values were found 18.0mg/dl for glucose, 0.98g/L for total protein, 8.3mg/dl for cholesterol, 13.7mg/dl for triglycerides and 5.6mg/dl for urea and at 2.chosen range of RMSEP values were found 16.3mg/dl for glucose, 0.98g/L for total protein, 7.8mg/dl for cholesterol, 12.8mg/dl for triglycerides and 5.3mg/dl urea. Shen, Davies et al.[44] used Bruker IFS113V spectrometer equipped with MTC detector to determine concentration of glucose in whole blood in wavenumber range between 500-7000cm^{-1}. Without any sample preperation, whole blood samples were analyzed directly. A four-vector PLS model was employed for the determination of glucose concentration and RMSEP was calculated as 10.63mg/dl. In the study of Perez-Guaita, Ventura-Gayete et al.[45], concentrations of glucose, creatinine, cholesterol, triglycerides, high-density lipoprotein(HDL), low-density lipoprotein (LDL), urea and uric acid were determined in human blood serum by using Bruker Tenson27 ATR spectrometer equipped with DLaTGS detector and ZnSe ATR crystal; and PLS model without sample preperation. The measurements were performed in wavenumber range between 600-4000cm^{-1}. Matlab was used for PLS, PCR and MANOVA(Multivariate analysis of variance methods). RMSEP values were evaluated for 17.8mg/dl, 26.3mg/dl, 43.9mg/dl and 10.6mg/dl for glucose, cholesterol, triglycerides and urea respectively. Another Perez-Guaita, Ventura-Gayete et al.[46] study, was directly the determination of concentrations of albumin, total globulin, γ-globulin, hemoglobin in whole blood and serum. They used Bruker Tenson27 ATR with DLaTGS detector and Bruker IFS66V ATR with MTC detector. The measurements were performed in wavenumber range between 600-4000cm^{-1}. Multivariate model was applied by using PLS

algorithm in Matlab. Also first derivation and vector normalization were applied. RMSEP of Albumin was calculated as 0.191g/dl by combining FD-PLS. Perez-Guaita, Kuligowski et al.[47] had studied about the determination of concentrations of glucose, total protein, urea and triglycerides in serum samples by combining IR spectrometry and multivariate methods. The samples were measured with air background, in wavenumber range between 600-4000cm^{-1} by using Bruker Tenson27 ATR spectrometer equipped with DTGS detector and ZnSe ATR crystal. Also water spectrum was measured and subtracted to each sample spectra. They developed a partial least squares regression(PLSR) model and three different locally weighted partial least squares regression(LW-PLSR) by using Matlab and PLS toolbox software PLSR model and LW-PLSRw was constructed by using the whole spectral range between 900 and 1750cm-1 , LW-PLSRa model was constructed by using analyte characteristic spectral regions and LW-PLSRm model was constructed by using analyte specific regions. RMSEPs were calculated as 24.7mg/dl, 22.2mg/dl, 19.7mg/dl and 17.1mg/dl for PLSR, LW-PLSRa, LW-PLSRw, and LW-PLSRm respectively for the determination of glucose in serum. For the determination of urea in serum, RMSEPs were calculated as 13.4mg/dl, 11.6mg/dl, 11.3mg/dl, and 9.5mg/dl for PLSR, LW-PLSRa, LW-PLSRw, and LW-PLSRm respectively. For the determination of proteins in serum, RMSEPs were calculated as 0.253g/dl, 0.243g/dl, 0.240g/dl, and 0.240g/dl for PLSR, LW-PLSRa, LW-PLSRw, and LW-PLSRm respectively. For the determination of triglycerides in serum, RMSEPs were calculated as 45.0mg/dl, 43.2mg/dl, 50.6mg/dl, and 40.1mg/dl for PLSR, LW-PLSRa, LW-PLSRw, and LW-PLSRm respectively. In the study of Jessen, Hoskuldsson et al.[48], glucose, triglycerides, urea, cholesterol, albumin and total protein in human plasma were determined by using FTIR which was Bruker Tensor 27 equipped with MTC detector, and PLS calibration model. Transmission spectra of samples were taken in wavenumber range between 950-3100cm^{-1}. According to PLS prediction results, RMSEP values were calculated as 4.14mg/dl, 0.88g/L, 4.25mg/dl, 5.31mg/dl, 0.49g/L and 25mg/dl for Glucose, total protein, cholesterol, triglycerides, albumin and urea. An interesting study was performed by Li, Li et al.[49] They used Bruker Alpha ATR spectrometer equipped with DTGS detector and ZnSe ATR crystal to analyse whole blood samples and developed a multivariate method based on combining interval PLS(iPLS) and hybrid space spectra. RMSEP values were found as 6.34mg/dl for glucose and 7.92mg/dl by using HSEiPLS model. Another interesting study was performed by Li, Lv et al.[50] with using HSEiPLS algorithm. Bruker Alpha ATR spectrometer equipped with DTGS

detector and ZnSe ATR crystal, was used to determine the concentrations of glucose and cholesterol in whole blood samples. Multivariate method was chosen as HSEiPLS combination. RMSEP results were calculated as 13.62mg/dl, 22.68mg/dl, 11.23mg/dl, 29.78mg/dl, 9.59mg/dl, 6.58mg/dl, 14.18mg/dl, 10.25mg/dl and 8.02mg/dl by using PLS-SPXY, PLS-0thD-SPXY, PLS-1stD-SPXY, PLS-2ndD-SPXY, PLS-C-SPXY, DSFPLS-C-SPXY, PLS-0thD-C-SPXY, PLS-1stD-C-SPXY and PLS-2ndD-C-SPXY model respectively, for glucose. For cholesterol, RMSEPs were calculated as 9.96mg/dl, 17.41mg/dl, 14.05mg/dl, 8.22mg/dl, 8.3mg/dl, 7.49mg/dl, 10.85mg/dl, 11.27mg/dl and 8.19mg/dl by using PLS-SPXY, PLS-0thD-SPXY, PLS-1stD-SPXY, PLS-2ndD-SPXY, PLS-C-SPXY, DSFPLS-C-SPXY, PLS-0thD-C-SPXY, PLS-1stD-C-SPXY and PLS-2ndD-C-SPXY model respectively.

On the other hand, there are studies indirectly determination of the concentration of glucose, urea, cholesterol, triglycerides, albumin and total protein. In these studies, drying process are applied to blood, plasma and serum samples. In the study of Budinova, Salva et al.[51], whole blood and serum samples were dried on polyethylene carrier. Transmission spectra were recorded in wavenumber range between 450-4000cm^{-1} by using Nicolet 210 FTIR spectrometer equipped with DTGS detector. An empty cell was background. RMSEPs were calculated as 23.6mg/dl for glucose and 32.4mg/dl for cholesterol in whole blood and 16.9mg/dl for glucose and 24.8mg/dl for cholesterol in serum by using entire spectral region. Also RMSEPs were calculated by using selected spectral region for glucose as 28.7mg/dl in whole blood and 32.5mg/dl in serum. Werner, Boecker et al.[52] studied to prediction of the concentration of the glucose, total protein, cholesterol, triglycerides, hemoglobin and urea in whole blood and serum samples. The samples were dried on a disposable carrier and analyzed in wavenumber range between 500-5000cm^{-1} by using Bruker IFS66FT spectrometer eqiupped with MCT detector. Diffuse reflectance and transmission techniques were applied. PLS algorithm was used in matlab as multivariate method to determine glucose, total protein, cholesterol, triglycerides, hemoglobin and urea. RMSEPs were evaluated as 18mg/dl for glucose, 17.5mg/dl for cholesterol and 23.5mg/dl for triglycerides in the dried blood samples and 8.7mg/dl for glucose, 0.0023g/l for total protein, 14.9mg/dl for cholesterol, 8mg/dl for triglycerides and 0.23mg/dl for urea. Study of Shaw, Kotowich et al.[53] was about determining of concentrations of glucose, total protein, cholesterol, triglycerides, uric acid, urea, albumin and creatinine in dried films of serum samples by using Digilab FTS40 spectrometer equipped with MTC detector and PLS algorithm for multivariate analysis.

RMSEP results were given as 7.39mg/dl, 2.8g/l, 10.81mg/dl, 0.20mg/dl, 6.61mg/dl and 2.2g/l for glucose, total protein, cholesterol, triglycerides, urea and albumin. Low-Ying, Shaw et al.[54] studied dried films of whole blood samples and determined the concentration of glucose and urea in the films by using Bio-Rad FTS-40A spectrometer equipped with MCT detector and multivariate calibration method which was PLS. RMSEP values were 12.61mg/dl for glucose and 7.21mg/dl for urea. In the study of Kocherscheidt et al.[55], serum samples were dried on a carrier and analyzed with a spectrometer which was Bruker Matrix HTS-XT equipped with DLaTGS detector, to determine the concentrations of the glucose, total protein, cholesterol, triglycerides, uric acid and urea in the dried serum samples. PLS was employed as multivariate analysis method. RMSEPs were evaluated as 14.7mg/dl, 3.28g/l, 16.1mg/dl, 18.1mg/dl and 3.3mg/dl for glucose, total protein, cholesterol, triglycerides and urea. In the study of Perez-Guaita, Sanchez-Illana et al.[56], they determined lipidic parameters in dried serum samples. Bruker IFS66V ATR spectrometer eqipped with MCT detector and ZnSe ATR crystal, was used to analyse dried films of serum samples. PLS was applied as a multivariate method. RMSEP results were found 32.65mg/dl for cholesterol and 31.36mg/dl for triglycerides. Figure 3.1. shows the summary of the information of the literature reviews.

Table 3.1. Summary of the literature studies for instrumentation, analysis technique and sample type and size.

	Year	Instruments	Speciments	Multivariate Methods	Wavenumber-Resolution-Scan	Samples	Sample size	Analyzes type
1	1989	PE 1800, Bruker IFS113V (ATR)	DTGS*, $ZnSe^{+}$,	PLS	750-1750cm^{-1}, 8cm^{-1}, 20scans	Plasma	x	Direct
2	1992	PE 1710 (ATR)	DTGS*, $ZnSe^{+}$,	PLS, PCR, UPA, UPH	450-4000cm^{-1}	PBS	31 PBS solution	Direct
3	1993	PE 1750 (ATR)	DTGS*, $ZnSe^{+}$	PLS, PCR, ANN	750-1500cm^{-1}, 8cm^{-1}, 20scans	Whole Blood	96 Undiluted blood	Direct
4	1994	PE 1710 (ATR)	DTGS*, $ZnSe^{+}$,	PLS, PCR, ANN	450-4000cm^{-1}, 8cm^{-1}, 100scans	PBS	x	Direct
5	1994	Bruker IFS66FT (ATR)	KBr^{-}, MCT*, $ZnSe^{+}$	PLS	950-3100cm^{-1}, 4cm^{-1}, 500 scans	Plasma	126 Plasma	Direct
6	1997	Nicolet 210 (Transmission)	KBr^{-} , DTGS*	PLS	450-4000cm^{-1}, 8cm^{-1}, 64scans	Whole blood, serum	131 Whole blood, 136 serum	Dried on polyethylene carrier

(Cont. on next page)

Table 3.1.(Cont.)

7	1998	Bruker IFS66FT (Transmission, Diffuse Reflectance)	KBr^{-} , MCT*	PLS	500-5000cm^{-1}, 4cm^{-1}, 16scans	Blood, Serum	300 Serum, 90 blood	Dried on a disposable carrier
8	1998	Digilab FTS40 (Transmission)	MCT*	PLS	800-4000cm^{-1}, 4cm^{-1}, 256scans	Serum	300 Serum	Dried films
9	1998	Bruker IFS66FT (Transmission)	CaF_2^{-}, InSb*	PLS-RVC	420-6800cm^{-1}, 32cm^{-1}, 1500 scans	Plasma	126 Plasma	Direct
10	2002	Bio-Rad FTS-40A (Transmission)	MCT*	PLS	4cm^{-1}, 256scans	Whole blood	200 Whole blood	Dried film
11	2003	Bruker IFS113V (Transmission)	KBr^{-}, MCT316*	4V-PLS	500-7000cm^{-1}, 4cm^{-1}, 32scans	Whole Blood	28 Whole blood	Direct
12	2005	Bruker Matrix HTS-XT (Transmission)	DLaTGS*	PLS	500-4000cm^{-1}, 4cm^{-1} ,32scans	Serum	247 Serum	Dried on the carrier for IR
13	2012	Bruker Tenson27 (ATR)	DLaTGS*, $ZnSe^{+}$	PLS	600-4000cm^{-1}, 4cm^{-1}, 100 scans	Serum	1500 Serum	Direct
14	2012	1)Bruker Tenson27 (ATR), 2)Bruker IFS66V(ATR)	1)DLaTGS*, 2)MCT*	PLS-AS,KP,SPA	600-4000cm^{-1}, 4cm^{-1}, 100 scans	Whole Blood, Serum	x	Direct
15	2013	Bruker Tenson27 (ATR)	DTGS*, $ZnSe^{+}$	PLSR, MLW-PLSR	600-4000cm^{-1}, 4cm^{-1}, 100 scans	Serum	1400 Serum	Direct
16	2013	Bruker IFS66V (ATR)	MCT*, $ZnSe^{+}$	PLS	600-4000cm^{-1}, 4cm^{-1}, 300 scans	Serum	x	Dry film
17	2014	Bruker Tenson27 (Transmission)	MCT*	PLS	950-3100cm^{-1}, 4cm^{-1}, 128 scans	Plasma	144-170 Plasma	Direct
18	2017	Bruker Alpha (ATR)	DTGS*,$ZnSe^{+}$	iPLS, HSE	850-4000cm^{-1}, 6cm^{-1}, 64 scans	Whole blood	50-58 Whole blood	Direct
19	2017	Bruker Alpha (ATR)	DTGS*,$ZnSe^{+}$	FD-PLS	850-4000cm^{-1}, 6cm^{-1}, 64 scans	Whole Blood	60 Whole blood	Direct

(*: Detector, +: ATR crystal, -: beamsplitter, PLS: Partial least square, PCR: Principal component analysis, UPA: Univariate peak area analysis, UPH: Univariate peak height analysis, ANN: Artificial neural network, PBS: Phosphate buffered saline, RCV: Regression vector choices, iPLS: Interval PLS, FD-PLS: Fusing different PLS, MLW-PLS: Modified locally weighted-PLS Regression, AS: Aleatory selection, KS: Kennard–Stone, 4V-PLS: 4 vector-PLS, HSE: Hybrid spectra space. Articles: 1[38], 2[39], 3[40], 4[41], 5[42], 6[51], 7[52], 8[53], 9[43], 10[54], 11[44], 12[55], 13[45], 14[46], 15[47], 16[56], 17[48], 18[49], 19[50])

3.2. Introduction

Today, advances in the fields of computer, software, statistics and applied mathematics have led to the birth of a new discipline called chemometrics, especially in the analytical chemistry for the solution of complex systems. These developments have led to new areas of study in analytical chemistry and researchers in neighboring fields, using chemometric methods that use multidimensional and multivariable parameters that provide new possibilities for solving analytical problems. Chemometrics is a discipline of chemistry that involves the processing of chemical data using computers with statistics and mathematics. It is a powerful tool in chemical analyzes, allowing the extraction of actual information from chemical data or the disclosure of hidden information. One of the basic applications of chemometrics is analytical chemistry.[57-58]

As a word, chemometrics began to be promulgated in 1970s for statistics and mathematical methods, as well as for chemistry applications where computers and software are used. The concept of chemometrics was first put forward by the Swedish Svante Wold and the American Bruce R. Kowalski in 1972 and the first official statement of this discipline was made by the international chemometrics association in 1974. In the following years, it is observed that national and international chemometrics conferences have been organized in the world as well.[59-73]

The desirability of these chemometrics methods can be attributed to providing flexible and versatile solutions for rapid, accurate, precise and reliable results in the analysis of complex samples in chemistry and analytical chemistry. The results of published scientific work have shown that analytical chemists are the greatest users of chemometric methods for processing multivariate and multidimensional measurement data obtained from advanced analytical devices for analyzing analytical problems over the past 25 years.[57-74]

The largest users of the chemometrics methods are being observed from published educational notes and published scientific articles that are used in neighboring branches performing laboratory and analysis work, as well as analytical chemists. The relation of chemometrics with different disciplines is presented in figure 1.

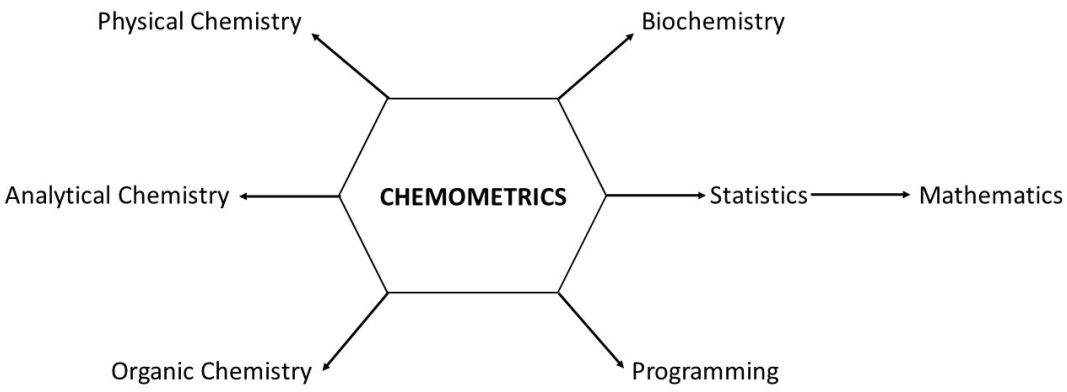

Figure 3.1. Disciplines related to Chemometrics.

From the above schematic (Figure 1) it is clear that in chemometrics studies, analytical chemists and other related disciplines need to have applied mathematics and statistics knowledge to the extent of their needs. Programming is very important here. Most of the chemometrics applications involve complex calculations. Computer programs are needed because these calculations cannot be performed manually or by simple calculators. Chemometrics calculations usually use EXCEL, MATLAB, and other packaged programs.

3.2.1. Univariate Calibration

Univariate calibration is defined as a zero-point calibration and includes measurements of a given wavelength from a device to determine the concentration of a single analyte. This calibration method is based on the principle that the device signal is connected to the relevant component without any interference. In practice, however, this is not possible. In addition to having multiple components, actual samples may also contain other components that may interfere or have a detrimental effect.

Univariate calibration consists of two steps, calibrating and estimating. A calibration model is established that gives the relationship between instrument signals and concentrations of standard samples, whose contents are known in advance at the calibration step. In the estimation step, the device signal is taken for the unknown analyte and the concentration of this analyte is calculated by using the calibration model generated at the calibration step. Univariate calibration models are considered linear in

accordance with Beer's law and the relationship between the analyte concentration (c) and the signal at a frequency (r):

$$r = f(c) + e_r \quad (3.1)$$

is defined as the calibration function.

3.2.2. Multivariate Calibration

3.2.2.1. Classical Least Squares Method

The classical smallest squares calibration method is applied to the systems of linear equations consisting of measurement data obtained from spectrophotometric or other analytical devices, to the Beer's law. The explanations here are made for spectrophotometric studies. A = K x C (according to the Beer law).

Advantages of the method:

i. Calculations are quick

ii. Do not require wavelength selection in calibrations

iii. Even if the number of wavelengths is greater than the number of components, it can be used.

iv. A large spectral range can be used to calibrate the absorbance measurements of multiple wavelengths.

v. It has a simple mathematics according to PCR and PLS.

Disadvantages of the method:

i. At this calibration, the exact composition of the calibration mixtures must be known for each component.

ii. Spectrophotometry is not suitable for the analysis of mixtures with interacting components for CLS calibration as well as for the application of graphical methods.

3.2.2.2. Inverse Least Squares Method

The ILS method involves the application of the system of linear equations to the system of linear equations of the inverse representation of the Beer's law in spectroscopy:

$$C = P \times A \tag{3.4}$$

In the above equations system, A=measured absorbance value, P=calibration factor, C=concentration of the component.

Advantages of the method:

i. It is possible to calculate the direct concentration when the measured absorbance values for the sample are substituted in the formula. Which removes time lost in calculations.

Ii. Provided that the analytical compounds are known, this calibration model allows for the analysis of very complex mixtures.

Disadvantages of the method:

i. The choice of wavelength used for calibration can be difficult and time consuming.

ii. Models are used that their wavelength are limited with size of their calibration samples.

iii. It is usually necessary to use a large number of samples for accurate calibration, because the matrix determinant value of "0" in the calculation of the coefficient matrix is problematic because it requires an infinite solution. it is necessary to increase the serial number in the calibration set to overcome this.

iv. The preparation of the calibration samples and the measurement by means of a pre-calibration is extremely difficult and troublesome.

3.2.2.3. Principal Component Regression (PCR) Method

The principal component regression method, which is one of the methods of chemometrics calibration, is based on the principle that the decomposition of the measured absorbance data for the concentration set is made perpendicular to each other. The obtained lines are the coordinate system of the calibration to be established.

The PCR algorithm described here is explained by the scheme given by Martens and Naes (1984).[75] The steps for setting up the PCR calibration are as follows.

The concentration of the substance to be analyzed and the variance-covariance of the absorbance data are found. The eigenvectors and eigenvalues of the variance-covariance scattering matrix are calculated. The selected eigenvalue is the linear component of the corresponding eigenvector calibration.

Advantages of the method:

i. Does not require wavelength selection. Generally the whole spectral range or a wide region of this spectral range can be used.
ii. It can be used for multiple component analysis
iii. Allows the use of ILS regression processing for PCR data processing and calculation of calibration coefficients.
iv. Can be used for very complex mixtures provided that the components to be analyzed are known.
v. It can sometimes be used to quantify component samples in the original calibration mix but not in the sample.
vi. Allows for the elimination of noise from the experimental environment and measuring instruments of selected eigenvalues versus appropriate eigenvectors after deconvolution of the measured absorbances for calibration.

Disadvantages of the method:

i. Calculations are slower than classical methods.
ii. The optimization of the method requires some of the basic calibration components to be known (for very complex models to be understood and interpreted).

iii. The vectors based on the calibration may not correspond to the components to be analyzed.

iv. The use of a large number of calibration samples is usually necessary for an accurate calibration.

v. The preparation of the calibration samples is difficult due to the fact that they are out of linearity with the concentrations of the components.

3.2.2.4. Partial Least Squares Regression Method

One of the most common and popular methods for chemometric calibrations is the PLS method. In the PLS method, there are orthogonalized PLS algorithm and nonorthogonal PLS algorithm according to the PLS algorithms used to establish the calibration. The main difference between orthogonal PLS and non-orthogonal PLS is that factors subtract from X. There are two types of PLS calibration, PLS1 and PLS2. PLS1 is also in a compound model; All compounds in PLS2 are included in the model.[61]

The PLS algorithm given by Wold and Martens is the most common. The PLS calibration is based on the relationship between the X- and Y-blocks through the number vectors. According to the PLS algorithm, the matrix of the X-variable centered around zero and the division of the Y-variable centered around zero are given as follows.[61, 75]

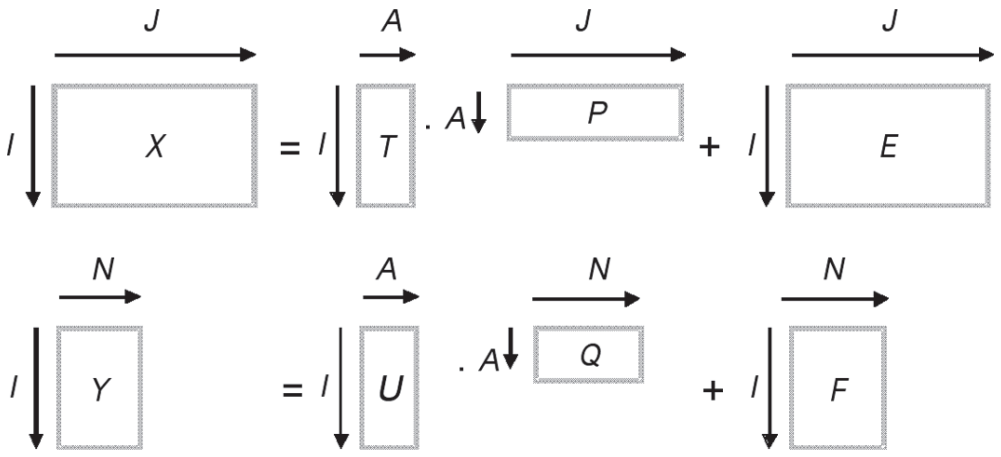

Figure 3.2. PLS2 calibration.[57]

$$X = T P^T + E$$
$$Y = U Q^T + F \qquad (3.12)$$
$$Y = X B + F$$
$$B = W (P^T W)^{-1} Q^T$$

where X = the dependent variable (e.g. absorbance data), Y = the independent variable (e.g. concentration), the number matrix for T = X, the numerator matrix for U = Y, the load matrix for P = X, the load matrix for Q = -reduction matrix, F = Y-residue matrix, W = max (covariance (E, F))

As in the PCR algorithm, these coefficients are calculated by replacing the absorbance values of the sample to be analyzed with (B) in the linear regression equation.

Advantages of the method:

i. PLS calibration process includes CLS and ILS calculation techniques.
ii. Requires a single-stage decomposition and regression process. The eigenvectors used in the calibration are directly related to the components that are analyzed and the region with the largest common spectral change.
iii. Calibrations will usually provide more confidence that the calibration set reflects the different concentrations expected from unknown samples.
iv. It can only be used for complex mixtures provided that the components to be analyzed are known.
v. In some cases it may be used to quantify samples of components in the original calibration mix but not in the sample.
vi. While all of these techniques are applied for spectral quantitative analysis, the reasons in the literature often indicate that the estimated power of PLS is high. In many cases, PLS methods give better results than PCR.

Disadvantages of the method:

i. PLS calculations are slower than classical methods.
ii. PLS model is highly abstract and is difficult to understand and interpret.
iii. An accurate calibration is usually required for a large number of samples.
iv. The preparation of the calibration samples is difficult since they are out of linearity with the concentrations of the components.

3.3. Experimental

Fourier Transform Infrared spectroscopic analyses were performed with Perkin Elmer Spectrum II FTIR spectrometer which equipped with diode laser as a light source, a DTGS (Deuterated Triglycine Sulphate) as a detector, and KBr as a beam splitter. FTIR spectra of artificial samples were collected using 1 reflection Diamond ATR (Attenuated Total Reflectance) accessory, between 4000 – 650 cm^{-1} with the spectral resolution of 4 cm^{-1}. Each spectrum was recorded as transmission against to air background and saved in order to generate multivariate calibration models. We should have done the measurements with water background because artificial serum is high amount of water in average that with the background of air the required data may be hidden in the peak of water instead of water background. However, we didn't want extra steps for the measurement of the quick analysis of blood sample in the future, so we used air as a background. Calibration and independent validation sets were prepared as text files with the aid of Microsoft Excel (MS Office 2016, Microsoft Corporation) program using the artificial serum samples given in the Table 3.2. The Partial Least Squares (PLS) multivariate calibration methods was applied in Minitab statistical software (2012 Minitab Inc.).

Table 3.2. Concentration range of components in artificial serum samples.

Components	Min(mg/dl)	Max(mg/dl)
Glucose	67	454
Total Protein	4150	10080
Albumin	2520	5000
Cholesterol	103	437
Triglyceride	35	1344

Table 3.3. Concentration of Components in artificial serum samples determined by biological methods.

Sample No.	Glucose	Total Protein	Albumin	Cholestrol	Triglyceride	Sample No.	Glucose	Total Protein	Albumin	Cholestrol	Triglyceride
1	132	6.82	4.73	114	117	**60**	91	NAN	4.24	180	199
2	86	6.36	4.07	178	154	**61**	96	NAN	4.28	256	206
3	226	7.83	4.06	NAN	NAN	**62**	110	6.46	4.18	NAN	NAN
4	112	NAN	3.4	174	148	**63**	132	5.82	3.13	142	162
5	114	NAN	4.2	189	56	**64**	112	6.97	4.45	295	244
6	79	5.74	3.58	NAN	NAN	**65**	103	6.26	3.72	158	69
7	86	7.3	4.53	240	98	**66**	90	10.08	3.44	NAN	NAN
8	67	6.8	4.01	NAN	NAN	**67**	96	NAN	NAN	189	60
9	91	7.85	4.59	NAN	NAN	**68**	102	7.03	4.1	NAN	NAN
10	NAN	NAN	NAN	437	1344	**69**	95	NAN	NAN	151	112
11	159	NAN	4.87	NAN	NAN	**70**	268	NAN	3.86	NAN	NAN
12	94	5.67	3.52	226	156	**71**	122	NAN	4.19	207	214
13	98	NAN	NAN	232	160	**72**	NAN	8.31	5	NAN	NAN
14	NAN	NAN	NAN	NAN	NAN	**73**	93	6.84	4.09	267	133
15	107	6.7	4.2	NAN	NAN	**74**	121	NAN	NAN	239	136
16	90	NAN	NAN	165	181	**75**	94	7.17	4.53	154	408
17	95	NAN	4.77	226	258	**76**	97	5.45	3.02	NAN	NAN
18	164	7.36	4	NAN	NAN	**77**	141	6.92	4.28	191	62
19	97	NAN	4.09	182	71	**78**	92	NAN	NAN	158	157
20	92	NAN	NAN	193	349	**79**	74	7.22	4.05	290	272
21	94	6.24	3.65	NAN	NAN	**80**	78	4.15	3.32	NAN	NAN
22	129	NAN	NAN	256	144	**81**	98	NAN	4.36	172	83
23	355	NAN	NAN	NAN	NAN	**82**	238	NAN	NAN	NAN	NAN
24	106	NAN	4.62	284	141	**83**	92	7.4	4.2	NAN	NAN
25	196	7.19	3.39	NAN	NAN	**84**	98	NAN	NAN	235	68
26	103	NAN	4.36	106	152	**85**	454	7.07	4.27	233	110
27	83	NAN	NAN	130	117	**86**	284	NAN	4.87	235	249
28	87	7.48	3.87	NAN	NAN	**87**	216	NAN	3.9	NAN	NAN
29	108	7.01	4.06	192	181	**88**	101	7.68	4.19	247	833
30	NAN	5.85	3.48	NAN	NAN	**89**	87	5.83	3.82	120	87
31	100	NAN	NAN	144	81	**90**	223	0	4.3	286	354
32	NAN	6.21	4.18	NAN	NAN	**91**	97	NAN	NAN	142	54
33	121	7.42	4.76	NAN	NAN	**92**	104	0	3.65	156	112
34	NAN	7.09	3.92	266	151	**93**	116	6.78	4.33	164	78
35	96	NAN	4.22	241	201	**94**	91	0	4.74	134	98
36	112	6.89	4.28	196	189	**95**	94	6.91	3.9	233	161
37	86	6.92	4.1	245	56	**96**	125	7.11	4.4	198	355
38	90	NAN	NAN	293	210	**97**	112	7.08	4.44	223	98
39	101	7.01	3.89	168	107	**98**	69	6.25	3.57	NAN	NAN
40	158	NAN	4.01	239	226	**99**	102	7.83	4.86	NAN	NAN
41	84	6.39	4.24	249	108	**100**	116	5.34	2.52	103	119
42	108	NAN	NAN	132	133	**101**	282	NAN	NAN	163	124
43	88	7.03	4.17	NAN	NAN	**102**	88	6.52	3.82	209	179
44	128	NAN	NAN	168	165	**103**	82	7.31	4.72	232	59
45	229	NAN	NAN	227	237	**104**	107	7.09	4.31	231	157
46	132	NAN	NAN	231	249	**105**	120	6.62	4.24	189	147
47	107	7.27	4.44	NAN	NAN	**106**	142	6.42	3.81	NAN	NAN
48	78	NAN	2.97	NAN	NAN	**107**	89	NAN	4.49	191	117
49	94	NAN	NAN	144	81	**108**	103	7.89	4.68	172	141
50	85	7.34	4.26	199	115	**109**	85	7.62	4.21	246	86
51	281	NAN	NAN	151	35	**110**	NAN	6,98	4,44	168	749
52	96	NAN	NAN	202	59	**111**	106	7,19	4,58	236	152
53	93	NAN	3.98	235	148	**112**	99	7,12	4,02	261	425
54	130	7.47	402	NAN	NAN	**113**	195	7,27	4,37	NAN	NAN
55	133	NAN	NAN	189	48	**114**	66	7,46	4,21	NAN	NAN
56	80	6.81	4.08	181	107	**115**	94	NAN	4,15	225	155
57	96	NAN	4.02	224	82	**116**	90	7,5	4,16	146	97
58	126	7.47	3.75	NAN	NAN	**117**	233	7,01	4,06	NAN	NAN
59	97	6.47	3.77	149	129	**118**	90	6,75	4,22	210	141

118 artificial serum samples were prepared by as shown in Table 3.2. We used 37 of them. For each measurement, 10µl serum sample was put onto PE spectrum II ATR-IR spectrometer and its spectrum was recorded.

3.4. Discussion

In the study, a FTIR spectroscopic method based on multivariate calibration data analysis for the determination of glucose, cholesterol, triglycerides, albumin and total protein components in artificial serum samples was performed. 37 artificial serum samples were prepared in our laboratory. Artificial serum samples were analyzed with FTIR and were saved. Multivariate calibration technique (PLS) was performed on data of the spectra. After analyzing data with chemometric methods, the results were evaluated and compared.

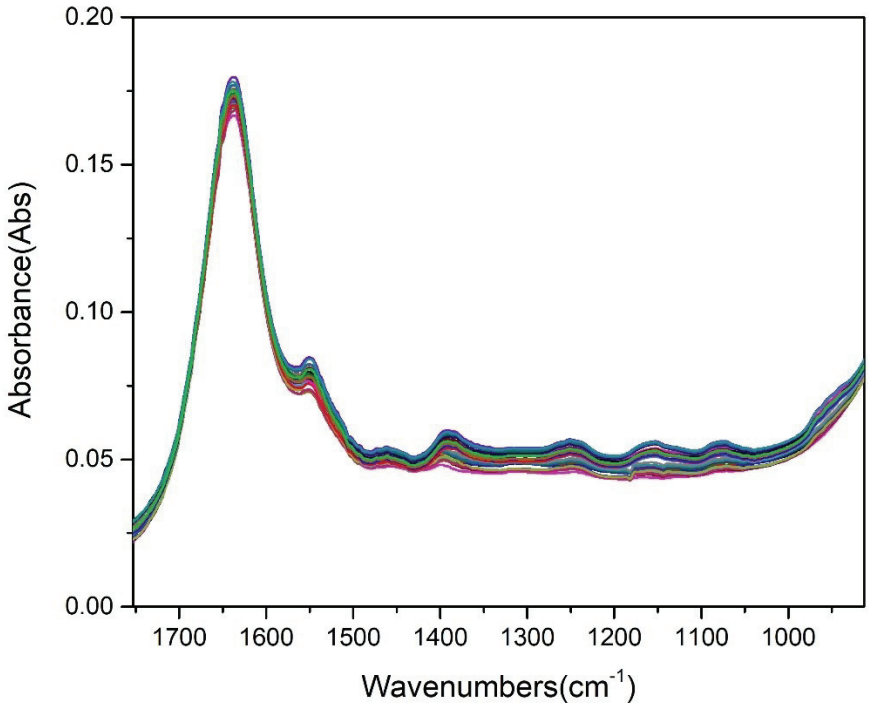

Figure 3.3. IR Spectrums of artificial serum samples

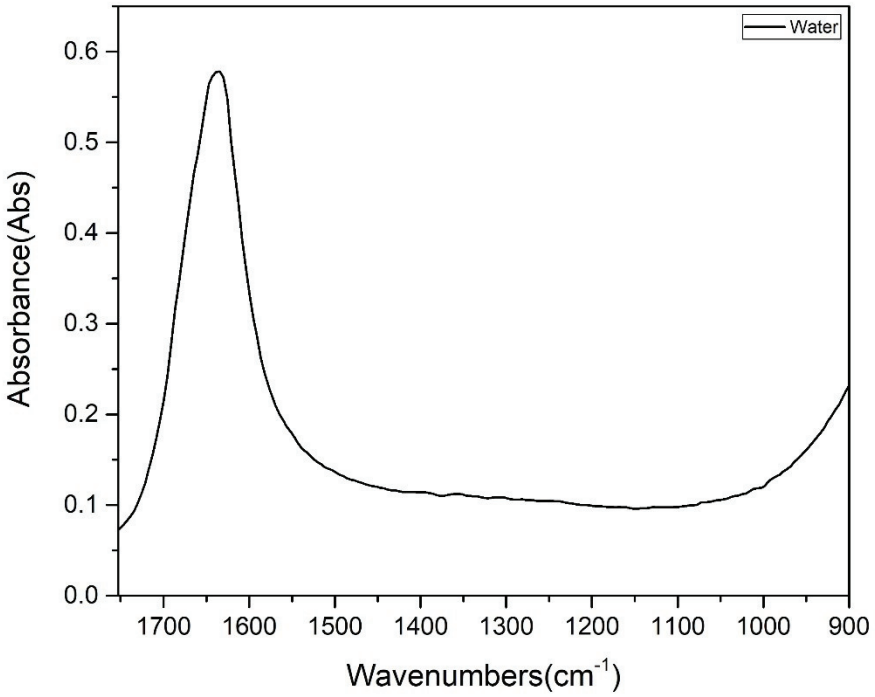

Figure 3.4. Reference IR Spectrums of Water

After our all measurements, we plotted IR spectrum as seen figure 3.3. When we analyzed the graph, there were similarities with reference IR water absorption spectra as shown figure 4.4. and we could say that there was certainly water absorption. We expected as we mentioned before. However, there were differences too from the reference IR water absorption spectra at around 1551, 1462, 1391, 1251, 1153, 1073, and 955cm^{-1}. These peaks might be related to our components that we tried to determine their concentration in artificial serum.

Multivariate calibration models (given in Table 3.3) were generated with synthetically prepared samples by using PLS1 and PLS2 models and artificial serum samples were predicted with these models. Firstly, we generated a PLS2 calibration model for whole and selected wavenumber regions. Selected wavenumber regions were between 920-1730cm^{-1}, 1960-2616cm^{-1} and 2840-3670cm^{-1}. In the PLS2 model, a calibration model can be created using more than one concentration. By this way, multiple concentration values can be predicted.

We had 3351 rows for one vector in the spectrum data. Minitab can analyze maximum 1000 variables at a time, so we used MATLAB to decrease number of data at a vector. We used a code in MATLAB that it chose each 4th in the vector. By this way, we decreased the number of wavenumbers to 838. After that, we split the spectrum data as 24 calibration samples and 11 validation samples for whole spectrum data and 23 calibration samples and 12 validation for selected wavenumber regions. We did not use sample 12 and sample 13. Since concentration of 12. glucose sample was 454mg/dl and concentration of 13. triglycerides sample was 833mg/dl, we assumed they were outliers.

Firstly, we applied PLS2 analysis in Minitab. Because more than one component can be predicted by using PLS2. For whole spectrum, maximum number of components was chosen as 5. However, the PLS2 chose the maximum number of components as 2.

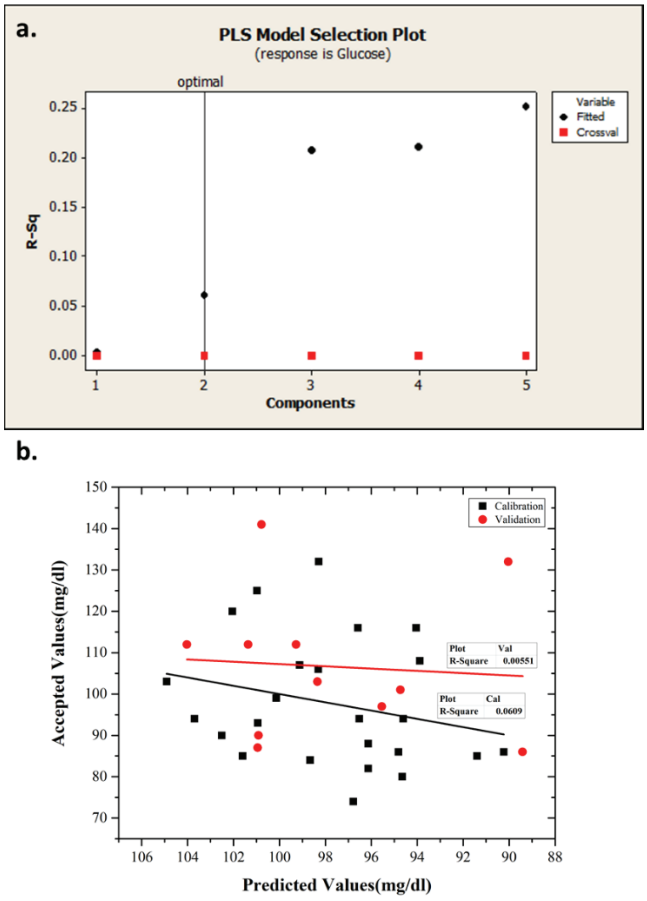

Figure 3.5. a) Glucose PLS2 model selection plot (whole spectrum) b) Accepted glucose values vs Predicted glucose values from PLS2 model with 2 factors. (whole spectrum)

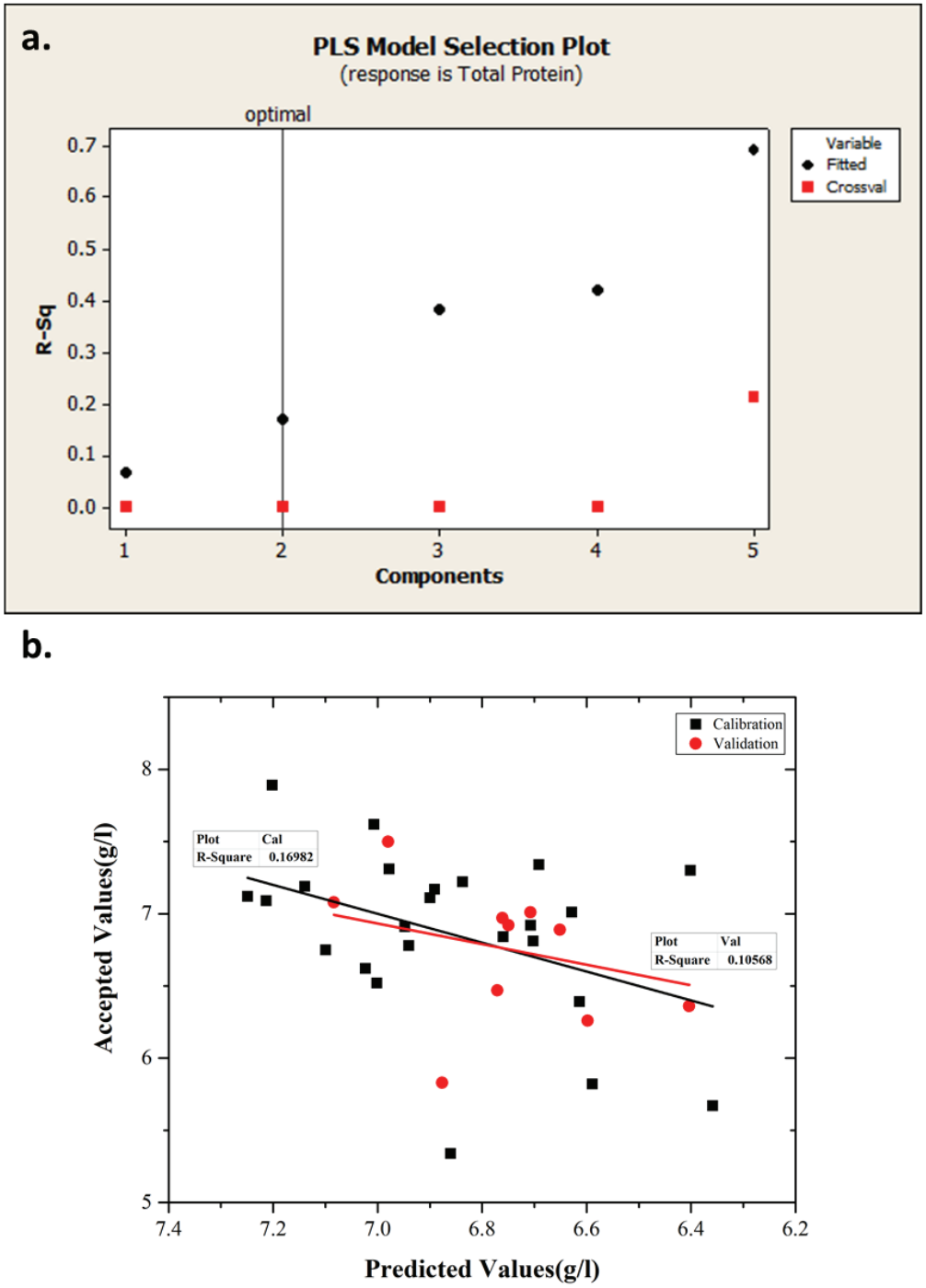

Figure 3.6. a) Total protein PLS2 model selection plot (whole spectrum) b) Accepted total protein values vs Predicted total protein values from PLS2 model with 2 factors. (whole spectrum)

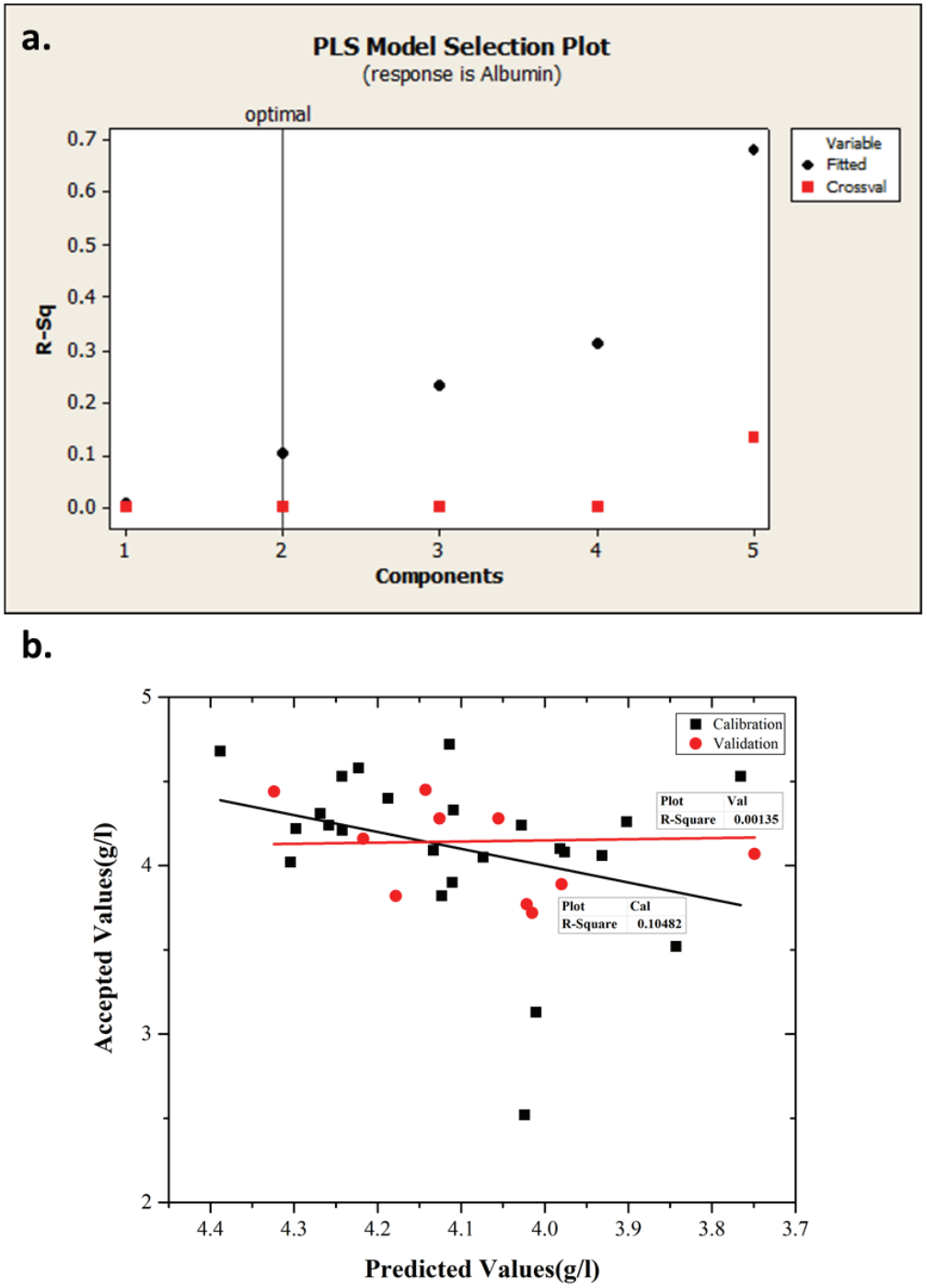

Figure 3.7. a) Albumin PLS2 model selection plot (whole spectrum) b) Accepted albumin values vs Predicted albumin values from PLS2 model with 2 factors. (whole spectrum)

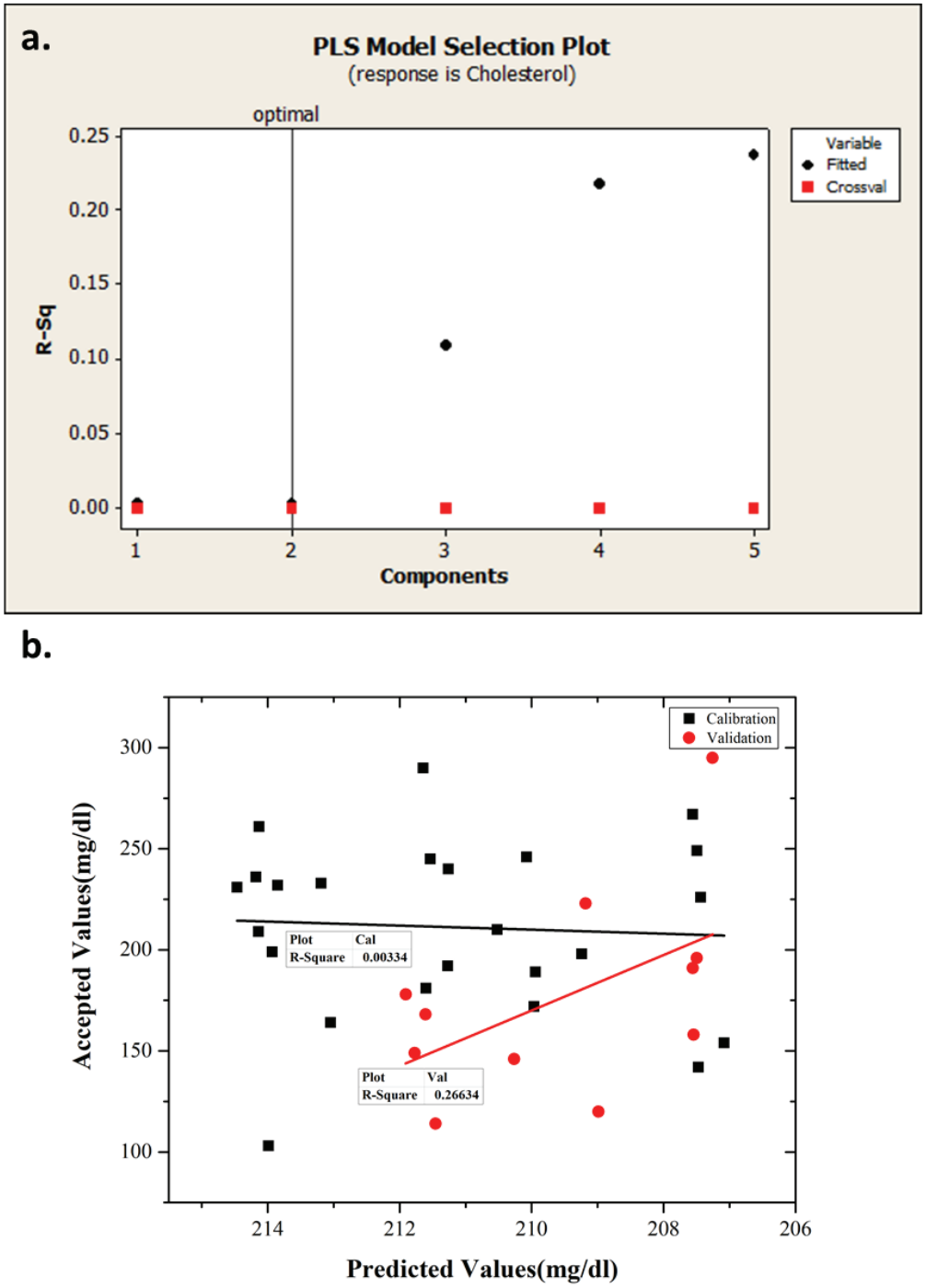

Figure 3.8. a) Cholesterol PLS2 model selection plot (whole spectrum) b) Accepted cholesterol values vs Predicted cholesterol values from PLS2 model with 2 factors. (whole spectrum)

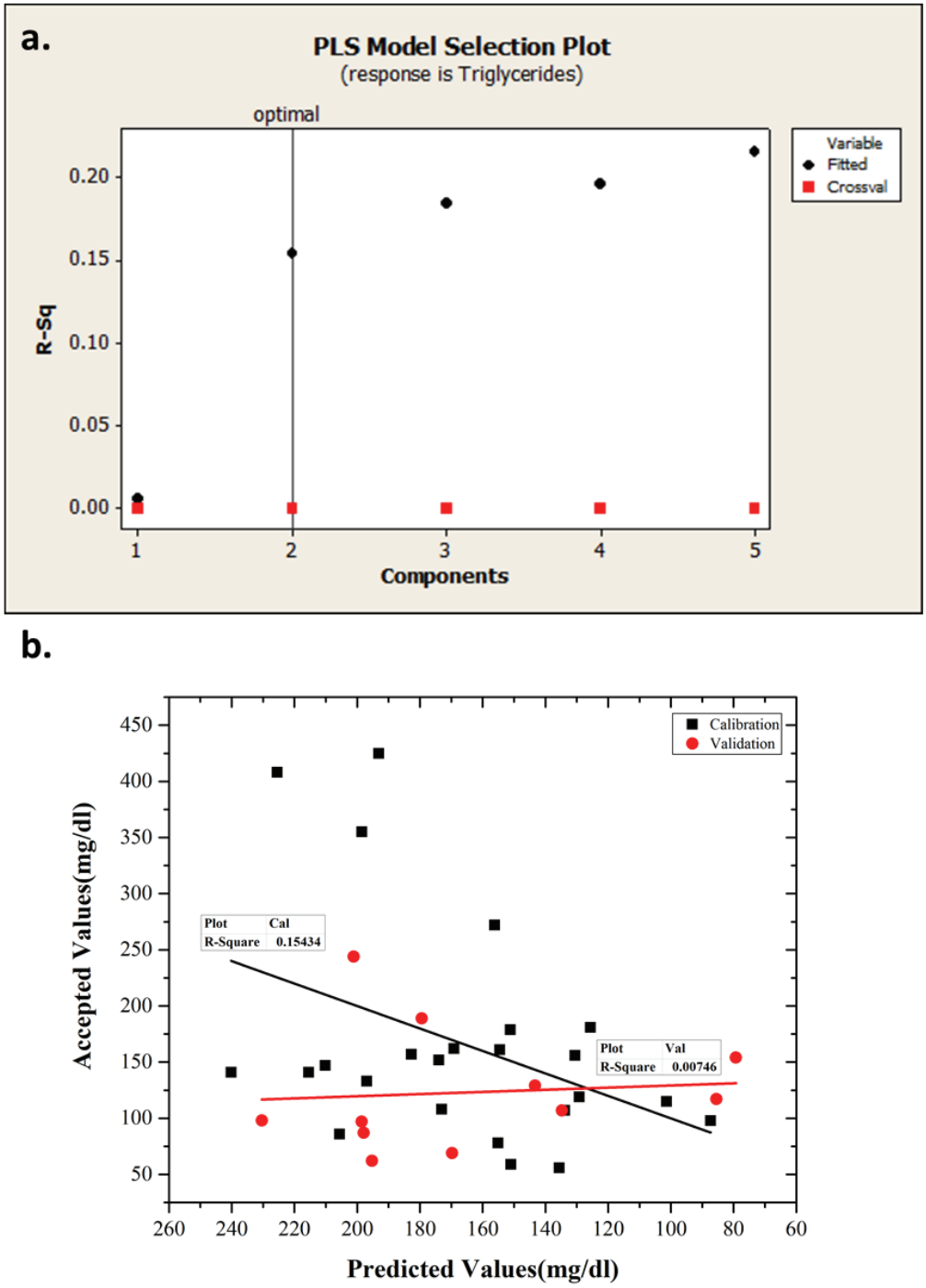

Figure 3.9. a) Triglycerides PLS2 model selection plot(whole spectrum) b) Accepted triglycerides values vs Predicted triglycerides values from PLS2 model with 2 factors. (whole spectrum)

Figure 3.5, 3.6, 3.7, 3.8 and 3.9 show PLS2 model selection plot of whole spectrum and accepted values vs. predicted values plots for glucose, total protein, albumin, cholesterol and triglycerides. From the quintet whole spectrum PLS2 model graphs of artificial blood samples, the correlation coefficients for glucose, total protein, albumin, cholesterol and triglycerides were found as 0.0609, 0.1698, 0.1048, 0.0033 and 0.1543 for calibration and 0.0055, 0.1057, 0.0014, 0.2663 and 0.0075 for validation respectively. In addition, RMSEC values of the model were 14.4487mg/dl, 0.5223g/l, 0.4527g/l, 42.8350mg/dl and 88.7472mg/dl for glucose, total protein, albumin, cholesterol and triglycerides respectively and RMSEP values of the model were 19.3190mg/dl, 0.4228g/l, 0.3706g/l, 59.7631mg/dl and 83.9608mg/dl for glucose, total protein, albumin, cholesterol and triglycerides respectively.

Table 3.4. R-squares and % errors for calibration and validation sets for PLS2 whole spectrum model

		Glucose	Total Protein	Albumin	Cholesterol	Triglycerides
PLS2 Whole Spectrum	R-Squares of Calibration	0.0609	0.1698	0.1048	0.0033	0.1543
	R-Squares of Validation	0.0055	0.1057	0.0014	0.2663	0.0075
	% Error of Calibration	12.3920	6.2093	8.5437	19.1378	48.1010
	% Error of Validation	12.0591	5.0002	6.7613	33.8746	78.4885

Table 3.4 shows r-square values and % errors of calibration and validation sets. Because the total number of components selected was not sufficient to explain the system and the total number of samples was low, they caused the high % errors.

After that, PLS2 analysis was applied for selected wavenumber regions. Maximum number of components was chosen as 5. However, the PLS2 chose the maximum number of components as 2, again.

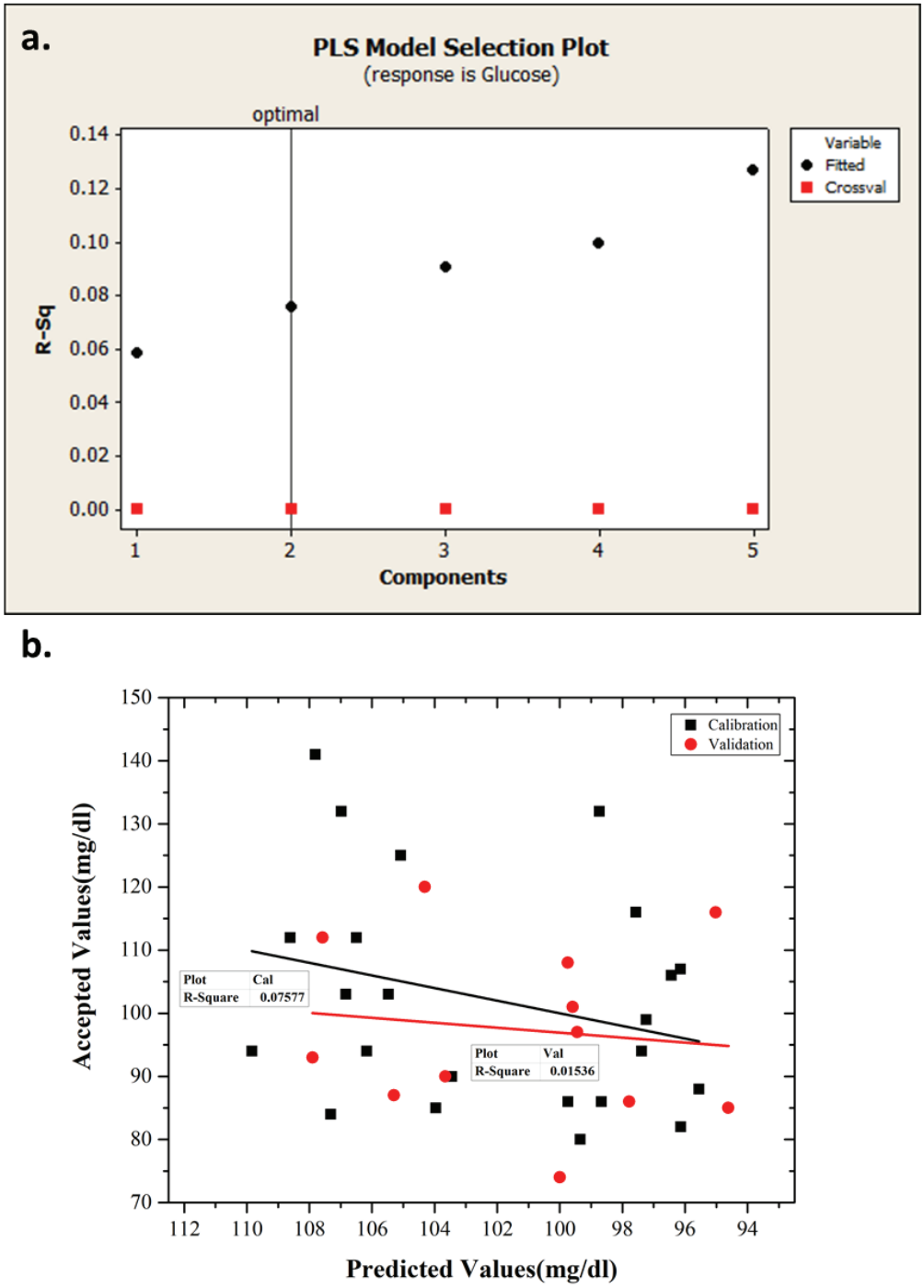

Figure 3.10. a) Glucose PLS2 model selection plot (selected wavenumber regions) b) Accepted glucose values vs Predicted glucose values from PLS2 model with 2 factors. (selected wavenumber regions)

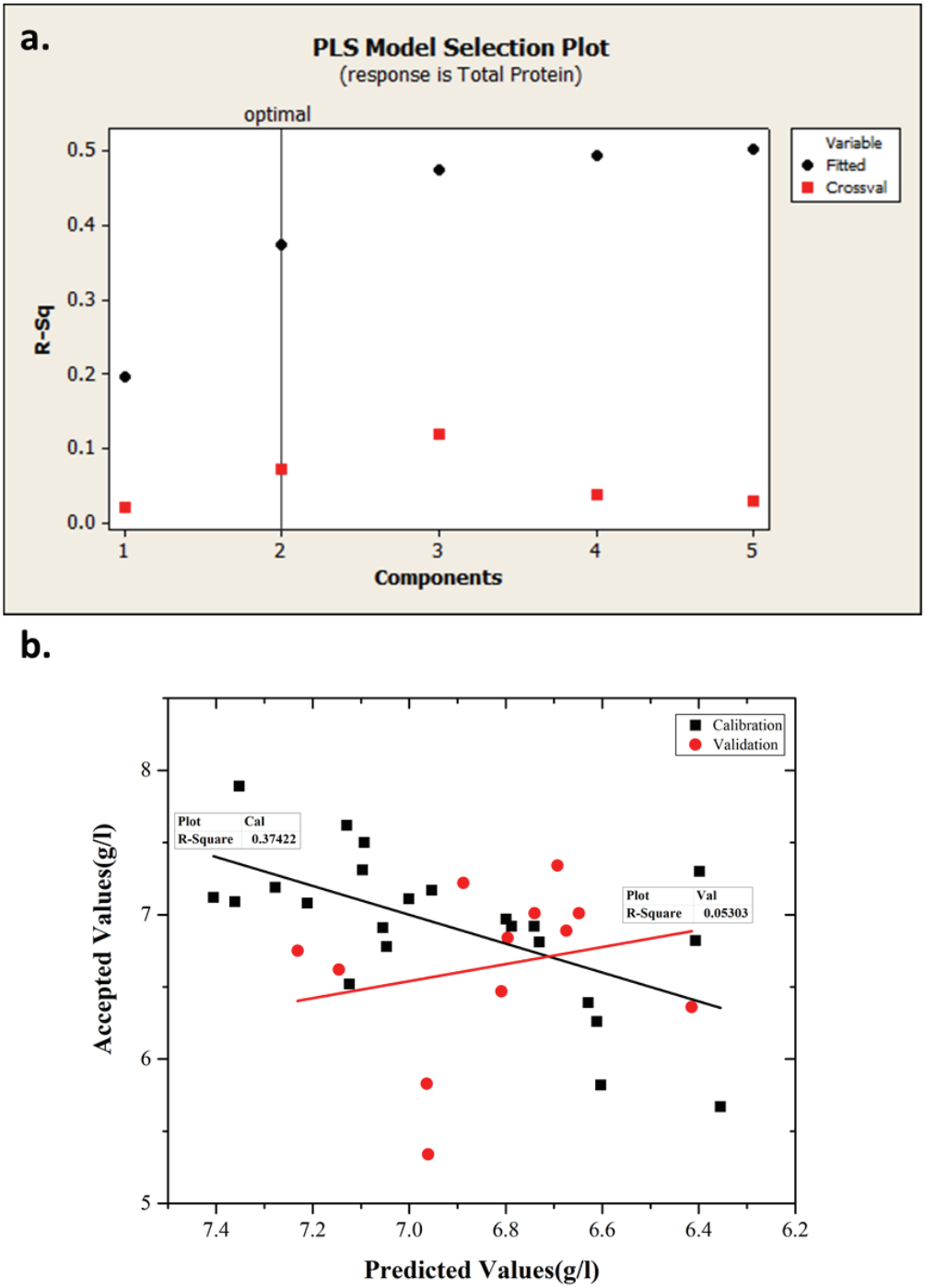

Figure 3.11. Total protein PLS model2 selection plot(selected wavenumber regions) b) Accepted total protein values vs Predicted total protein values from PLS2 model with 2 factors. (selected wavenumber regions)

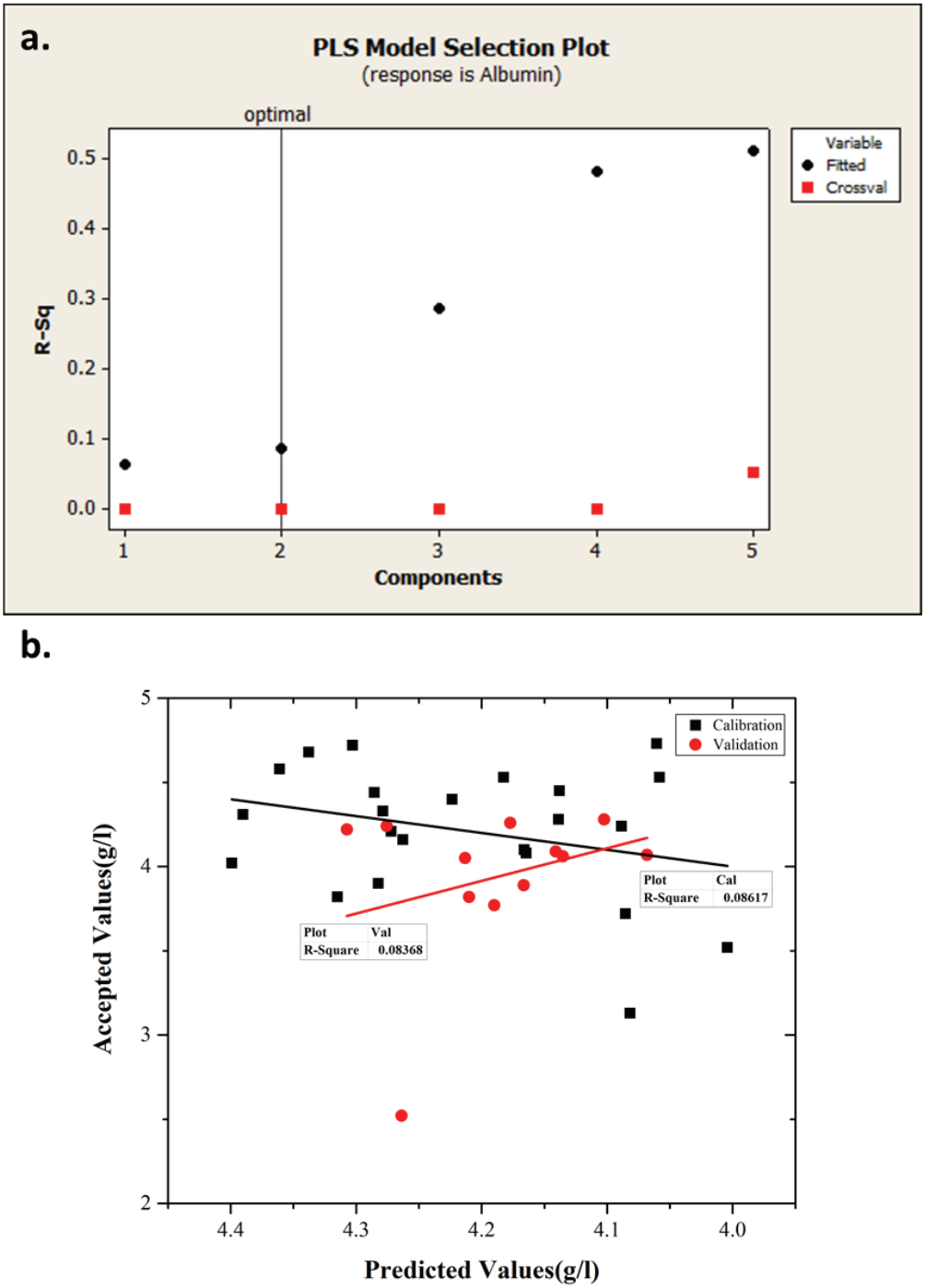

Figure 3.12. Albumin PLS2 model selection plot (selected wavenumber regions) b) Accepted albumin values vs Predicted albumin values from PLS2 model with 2 factors. (selected wavenumber regions)

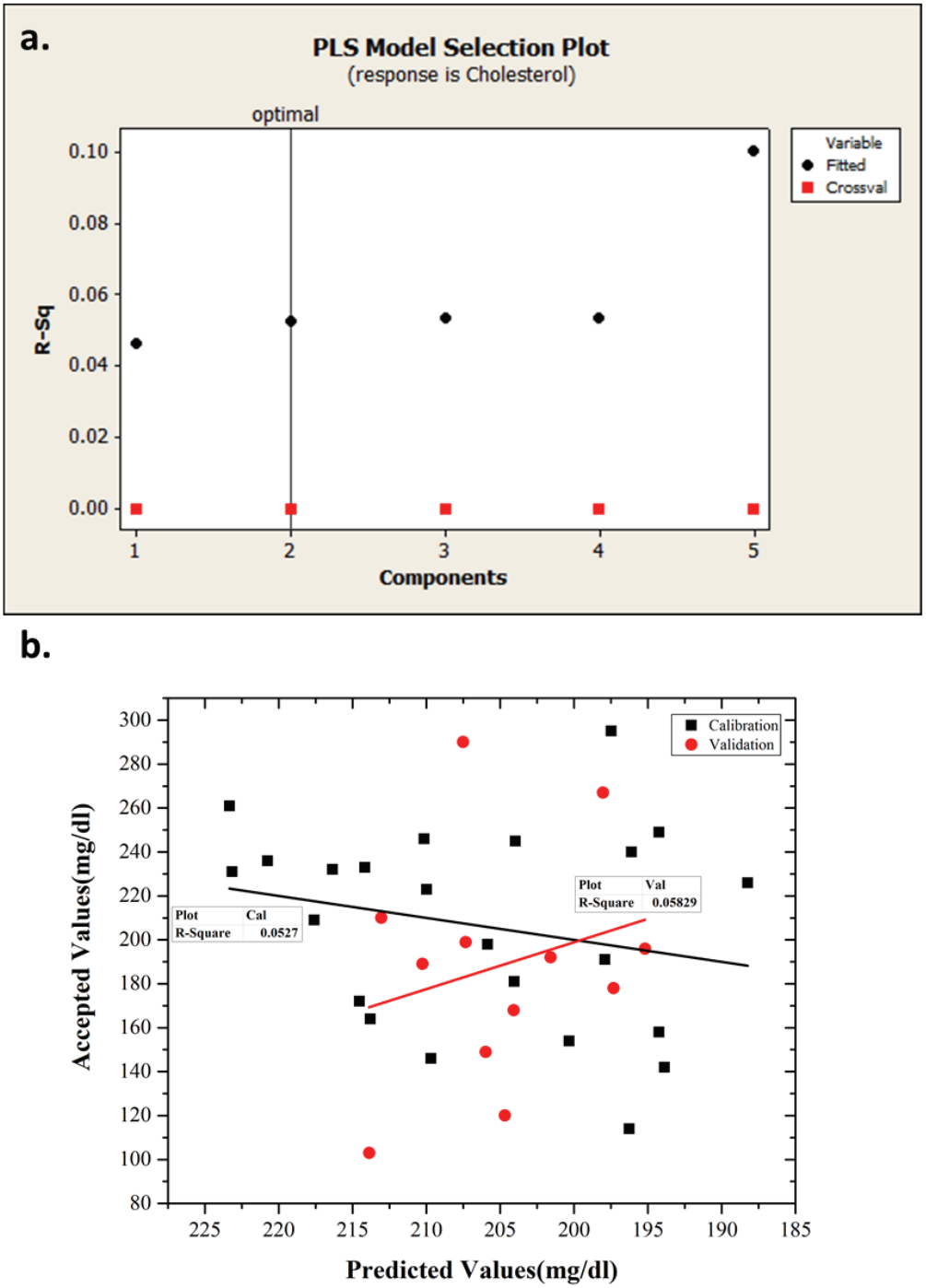

Figure 3.13. Cholesterol PLS2 model selection plot(selected wavenumber regions) b) Accepted cholesterol values vs Predicted cholesterol values from PLS2 model with 2 factors. (selected wavenumber regions)

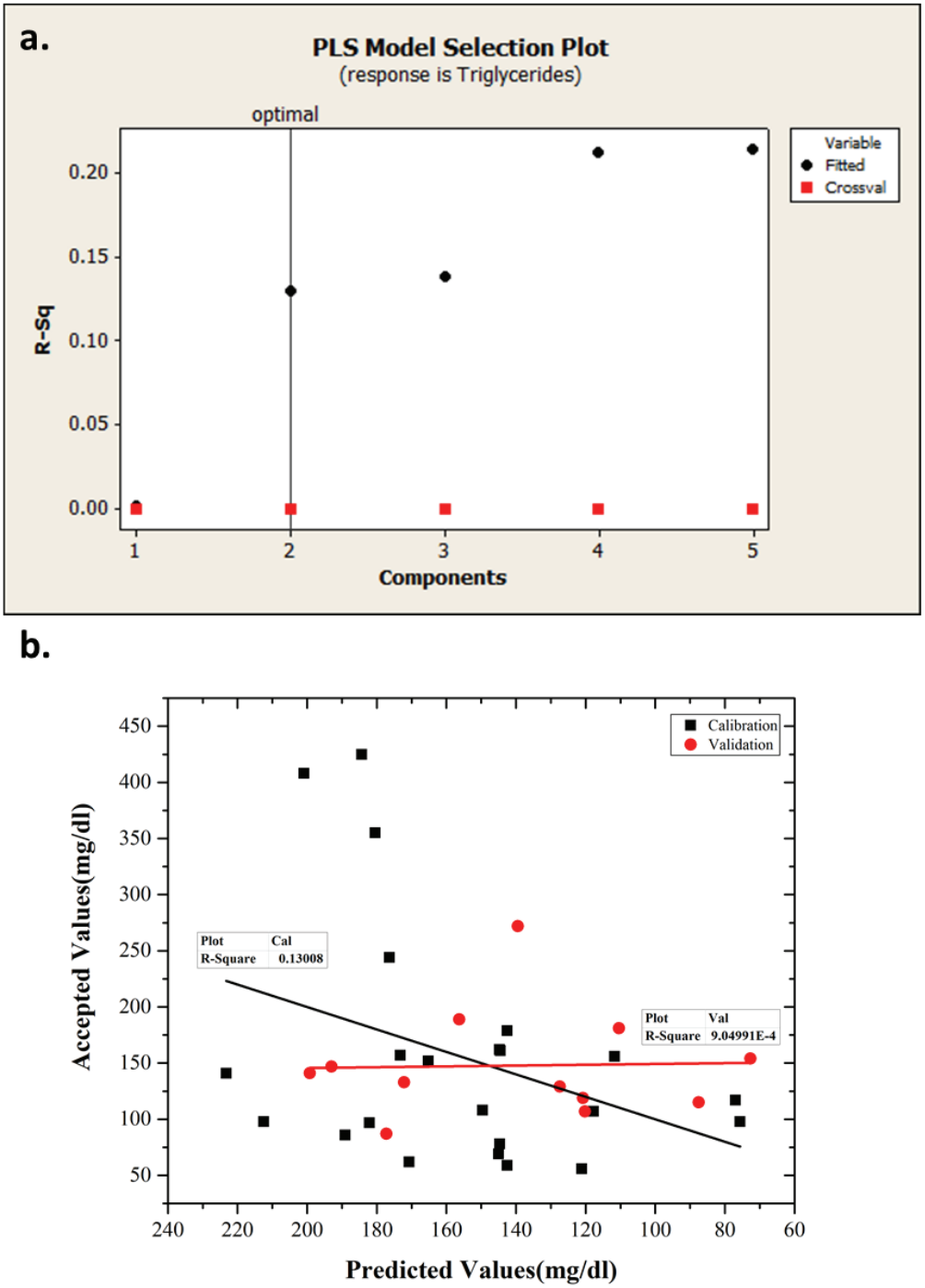

Figure 3.14. Triglycerides PLS2 model selection plot(selected wavenumber regions) b) Accepted triglycerides values vs Predicted triglycerides values from PLS2 model with 2 factors. (selected wavenumber regions)

Figure 3.10, 3.11, 3.12, 3.13 and 3.14 show PLS2 model selection plots and accepted values vs. predicted values plots for glucose, total protein, albumin, cholesterol and triglycerides. From the quintet PLS2 model graphs of artificial blood samples, the correlation coefficients for glucose, total protein, albumin, cholesterol and triglycerides were found as 0.0758, 0.3742, 0.0862, 0.0527 and 0.1301 for calibration and 0.0154, 0.0530, 0.0837, 0.0583 and 0.0009 for validation respectively. In addition, RMSEC values of the model were 16.5763mg/dl, 0.4048g/l, 0.3712g/l, 43.3844mg/dl and 96.7074mg/dl for glucose, total protein, albumin, cholesterol and triglycerides respectively and RMSEP values of the model were 14.2369mg/dl, 0.6658g/l, 0.5422g/l, 55.2026mg/dl and 62.1349mg/dl for glucose, total protein, albumin, cholesterol and triglycerides respectively.

Table 3.5. R-squares and % errors for calibration and validation sets for PLS2 selected wavenumber regions model

		Glucose	Total Protein	Albumin	Cholesterol	Triglycerides
PLS2 Selected Wavenumber Regions	R-Squares of Calibration	0.0758	0.3742	0.0862	0.0527	0.1301
	R-Squares of Validation	0.0154	0.0530	0.0837	0.0583	0.0009
	% Error of Calibration	13.6354	4.9470	7.4514	19.6162	60.4431
	% Error of Validation	13.2536	8.0965	9.4856	27.1108	33.5408

Table 3.5 shows r-square values and % errors of calibration and validation sets. Because the total number of components selected was not sufficient to explain the system and the total number of samples was low, they caused the high % errors. According to these models, while glucose, total protein and albumin had lower % errors at PLS2 whole spectrum model, cholesterol and triglycerides had lower % errors at PLS2 selected wavenumber regions.

Next step, PLS1 models were generated for whole spectrum and selected wavelengths. Firstly, PLS1 model was created for whole spectrum. Because concentration of 12. glucose sample was 454mg/dl and concentration of 13. triglycerides sample was 833mg/dl, we did not put them into model. We assumed they were outliers.

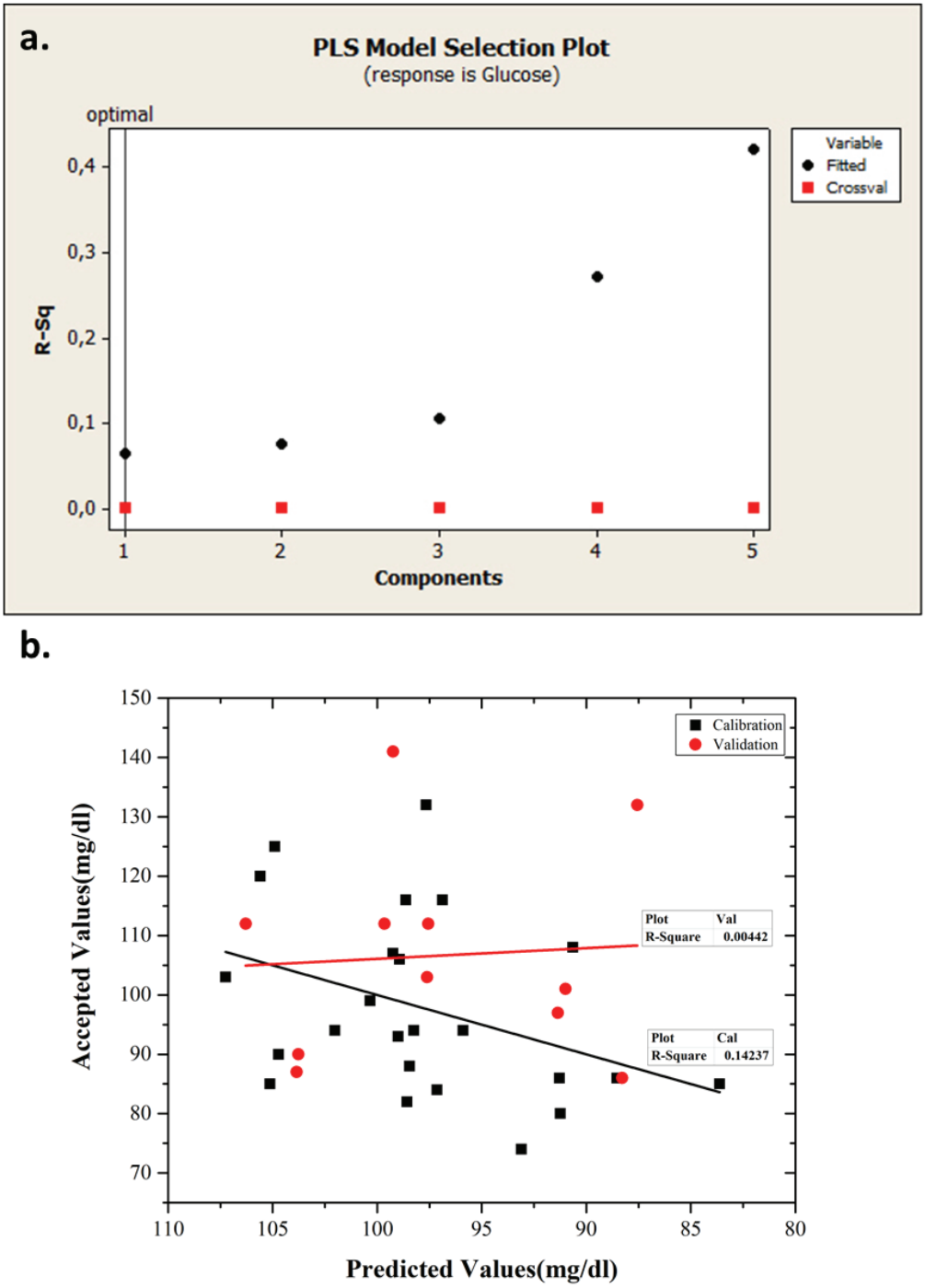

Figure 3.15. a) Glucose PLS1 model selection plot (whole spectrum) b) Accepted glucose values vs Predicted glucose values from PLS1 model with 1 factors. (whole spectrum)

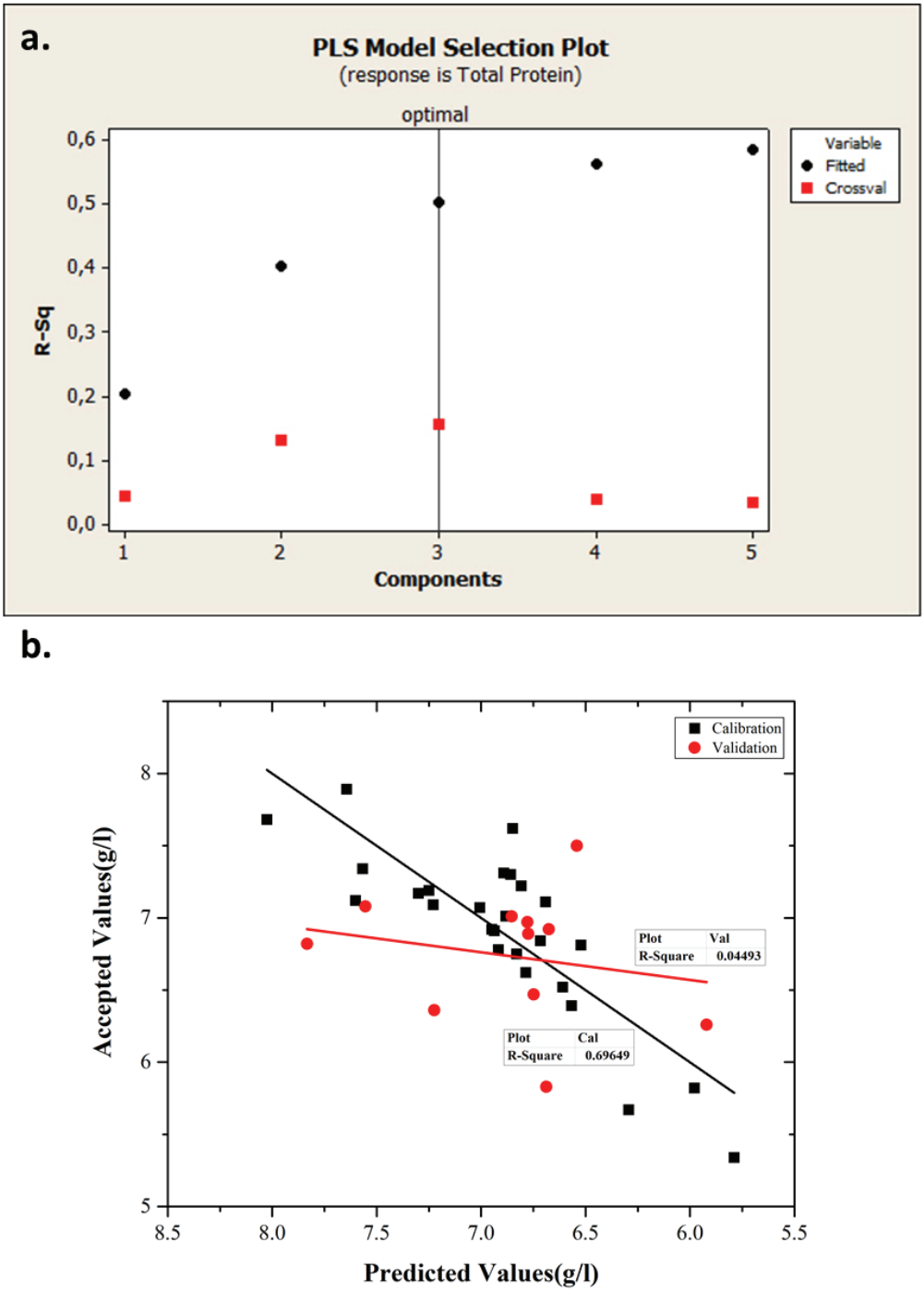

Figure 3.16. a) Total protein PLS1 model selection plot (whole spectrum) b) Accepted total protein values vs Predicted total protein values from PLS1 model with 3 factors. (whole spectrum)

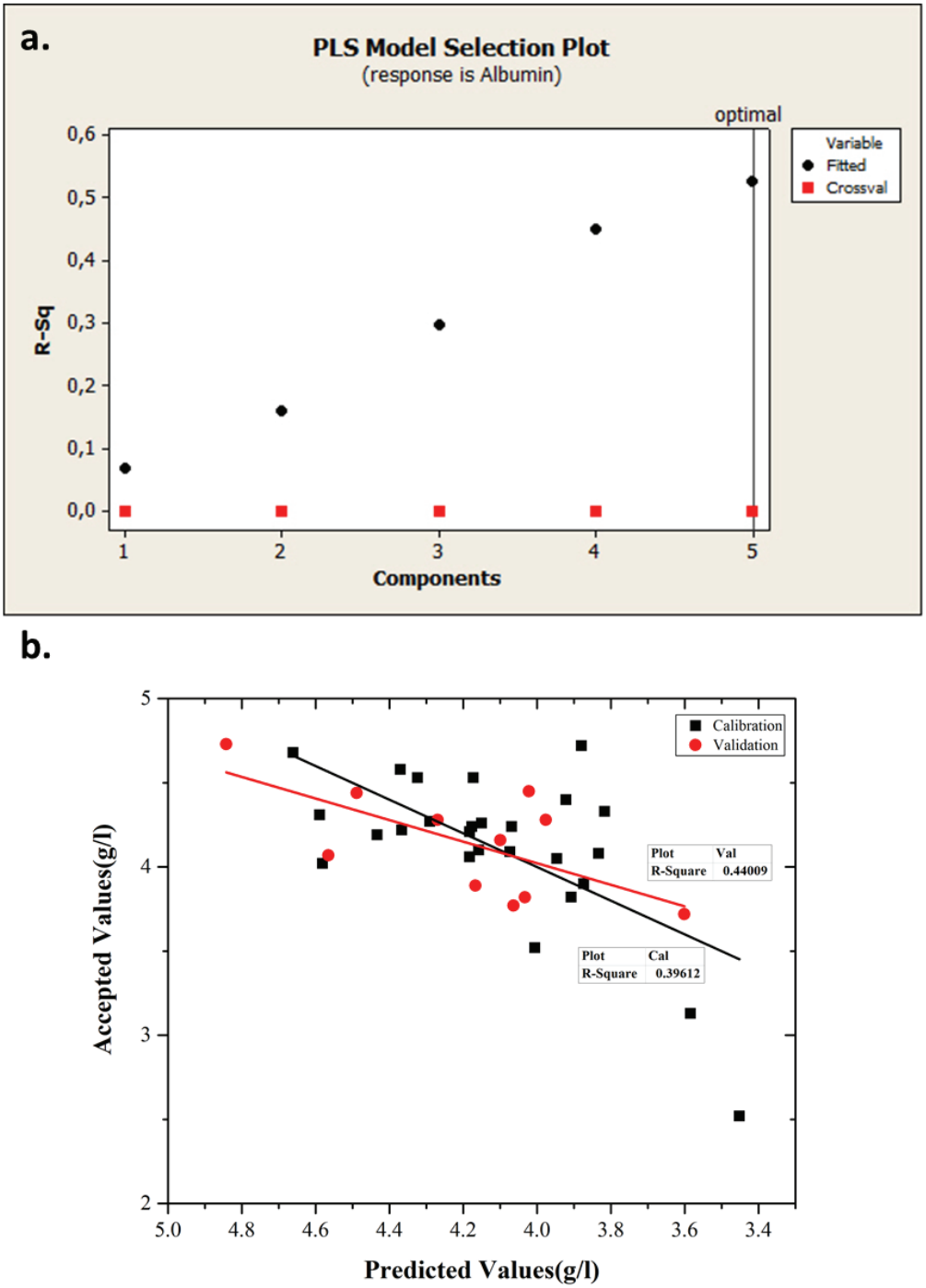

Figure 3.17. Albumin PLS1 model selection plot (whole spectrum) b) Accepted albumin values vs Predicted albumin values from PLS1 model with 5 factors. (whole spectrum)

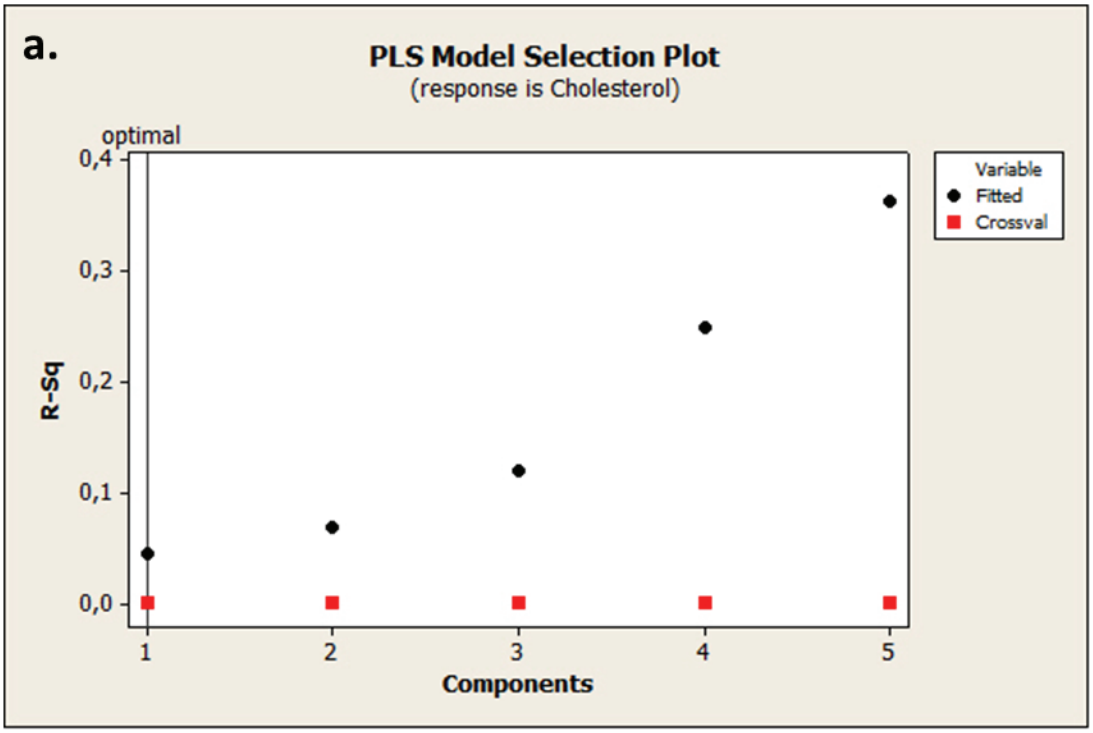

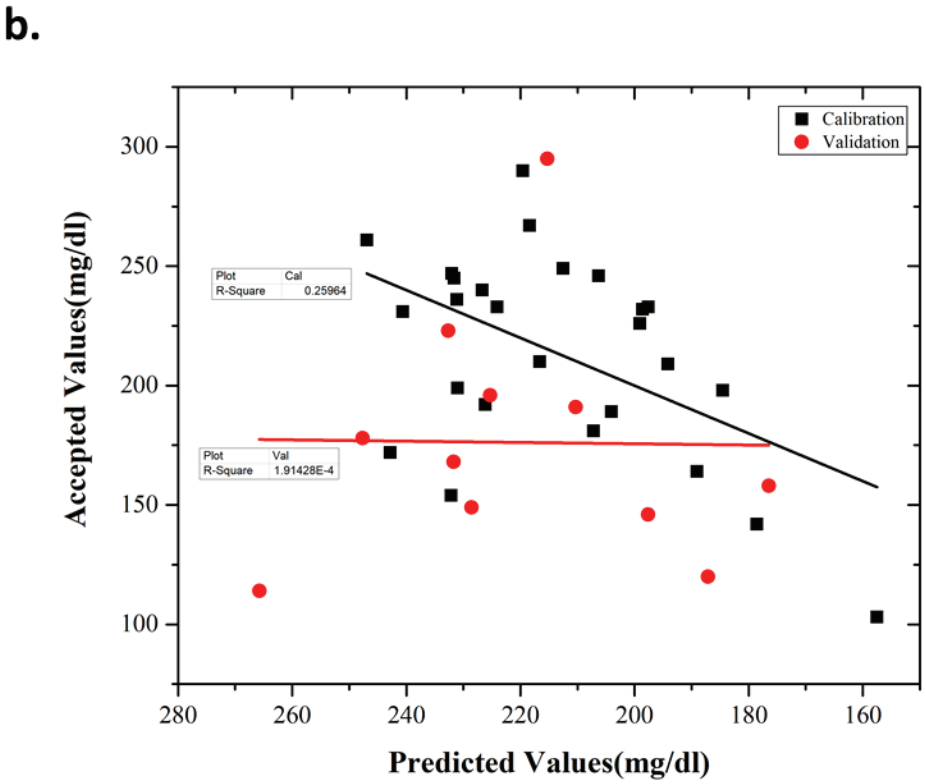

Figure 3.18. Cholesterol PLS1 model selection plot (whole spectrum) b) Accepted cholesterol values vs Predicted cholesterol values from PLS1 model with 1 factors. (whole spectrum)

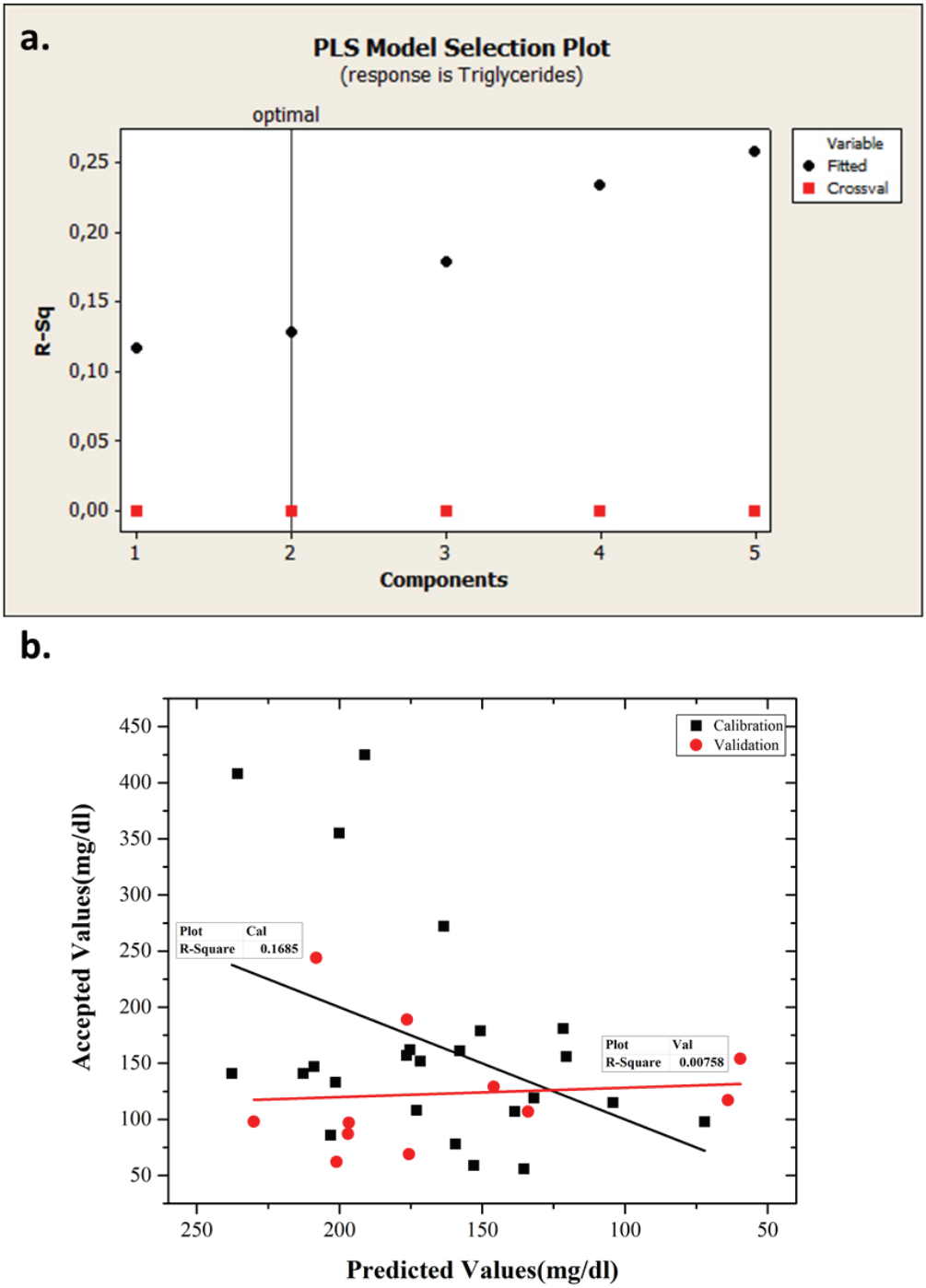

Figure 3.19. Triglycerides PLS1 model selection plot (whole spectrum) b) Accepted triglycerides values vs Predicted triglycerides values from PLS1 model with 2 factors. (whole spectrum)

Figure 3.15, 3.16, 3.17, 3.18 and 3.19 show PLS1 model selection plot of whole spectrum for glucose, total protein, albumin, cholesterol and triglycerides. From the PLS1 model graphs of artificial blood samples it was apparent that the correlation coefficients for glucose, total protein, albumin, cholesterol and triglycerides were found as 0.1424, 0.6965, 0.3961, 0.2596 and 0.1685 for calibration and 0.0044, 0.0449, 0.4401, 0.0002 and 0.0076 for validation respectively. In addition, RMSEC values of the model were 14.0218mg/dl, 0.3247g/l, 0.3644g/l, 36.8096mg/dl and 89.2821mg/dl for glucose, total protein, albumin, cholesterol and triglycerides respectively and RMSEP values of the model were 19.9008mg/dl, 0.5757g/l, 0.2519g/l, 66.7469mg/dl and 83.8547mg/dl for glucose, total protein, albumin, cholesterol and triglycerides respectively.

Table 3.6. R-squares and % errors for calibration and validation sets for PLS1 whole spectrum model

		Glucose	**Total Protein**	**Albumin**	**Cholesterol**	**Triglycerides**
PLS1 Whole Spectrum	**R-Squares of Calibration**	0.1424	0.6965	0.3961	0.2596	0.1685
	R-Squares of Validation	0.0044	0.0449	0.4401	0.0002	0.0076
	% Error of Calibration	11.7048	3.7351	6.8677	15.6382	49.1056
	% Error of Validation	13.6898	7.5049	5.2476	38.4516	82.6550

The total number of components did not represent the whole sample correlation, so errors were so high and also the total number of samples were low.

Secondly, PLS1 model was created for selected wavenumber regions. Because concentration of 12. glucose sample was 454mg/dl and concentration of 13. triglycerides sample was 833mg/dl, we did not put them into model. We assumed they were outliers.

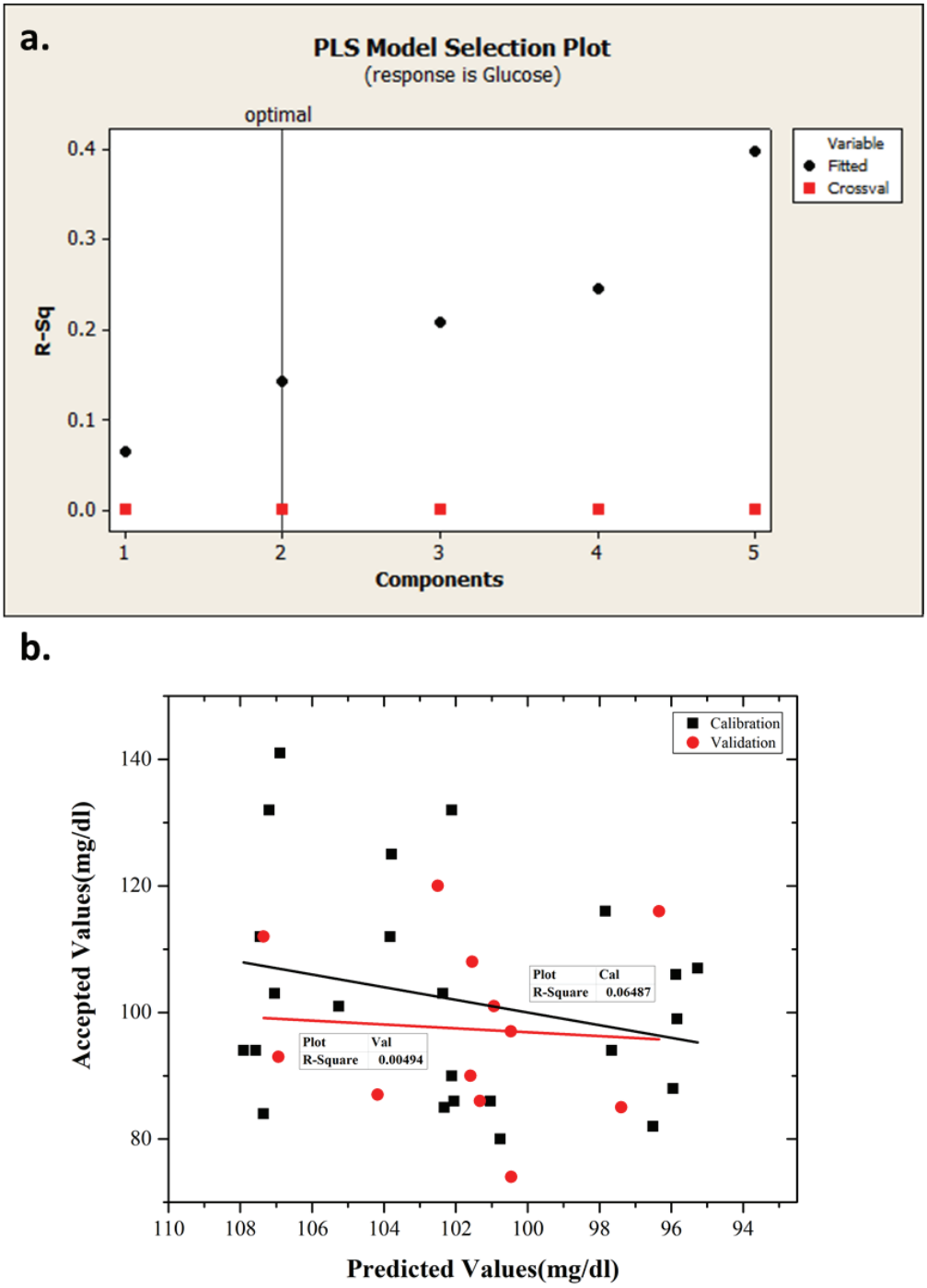

Figure 3.20. a) Glucose PLS1 model selection plot (selected wavenumber regions) b) Accepted glucose values vs Predicted glucose values from PLS1 model with 2 factors. (selected wavenumber regions)

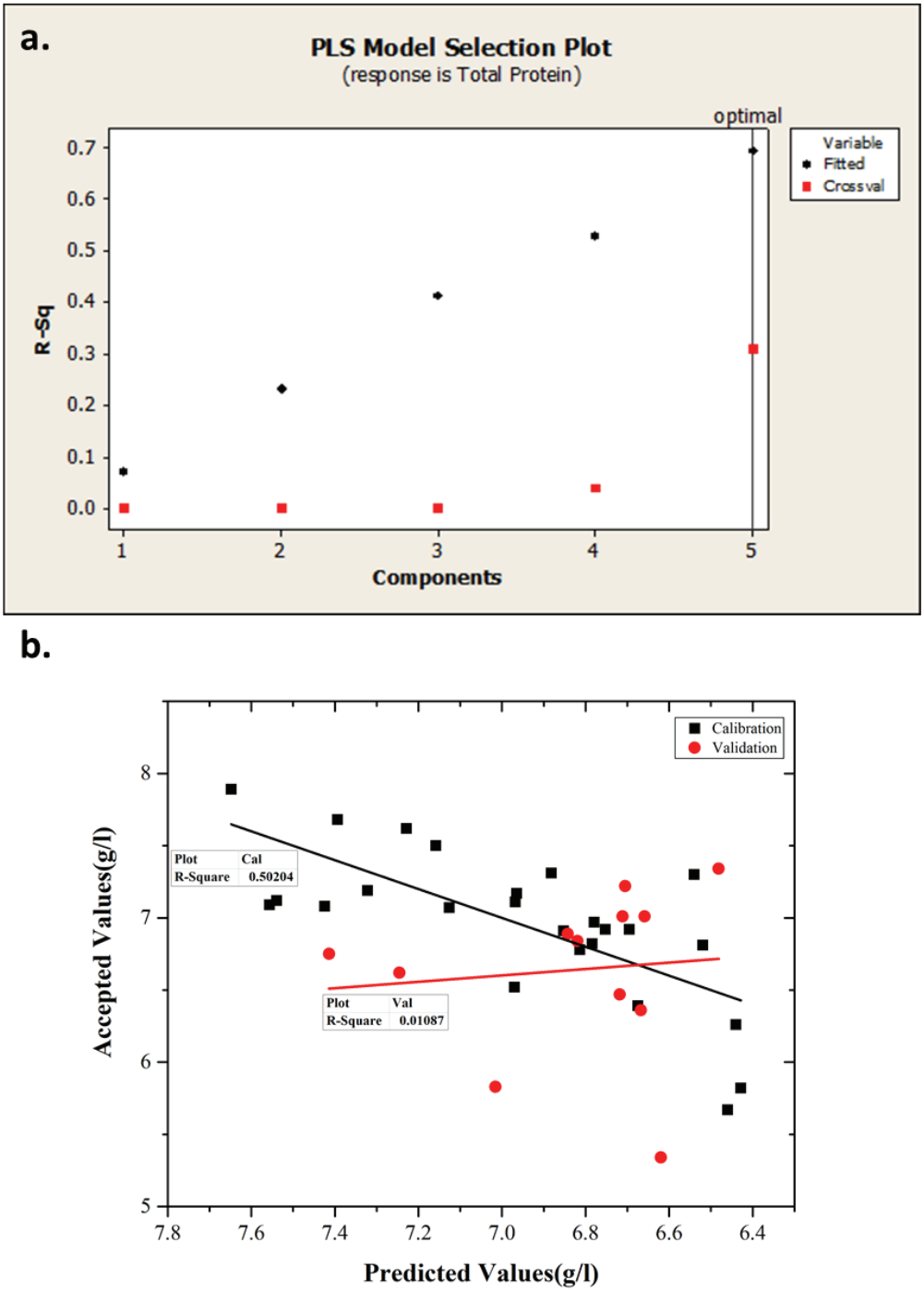

Figure 3.21. a) Total protein PLS1 model selection plot (selected wavenumber regions) b) Accepted total protein values vs Predicted total protein values from PLS1 model with 5 factors. (selected wavenumber regions)

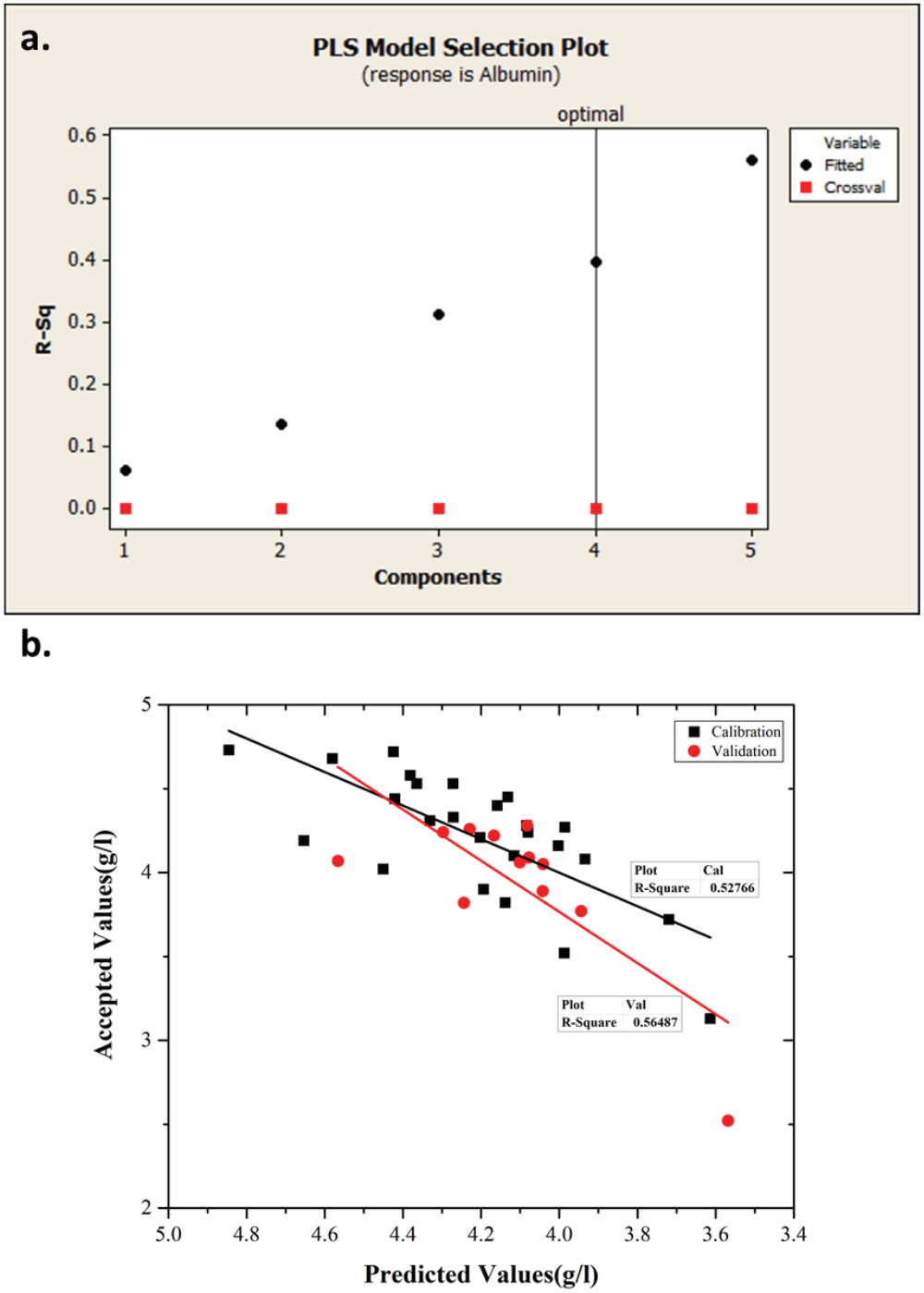

Figure 3.22. a) Albumin PLS1 model selection plot (selected wavenumber regions) b) Accepted albumin values vs Predicted albumin values from PLS1 model with 4 factors. (selected wavenumber regions)

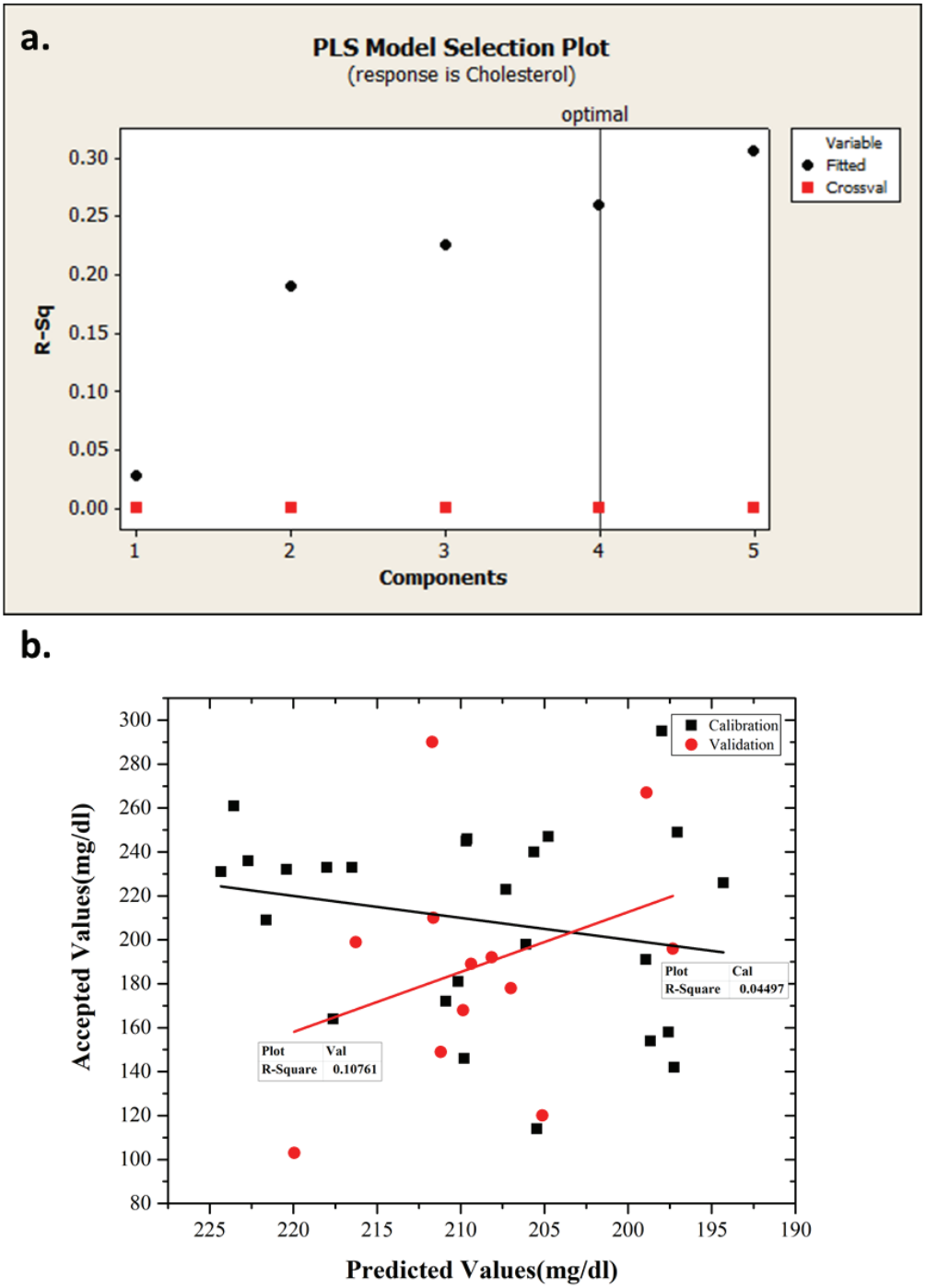

Figure 3.23. a) Cholesterol PLS1 model selection plot (selected wavenumber regions) b) Accepted glucose values vs Predicted glucose values from PLS1 model with 4 factors. (selected wavenumber regions)

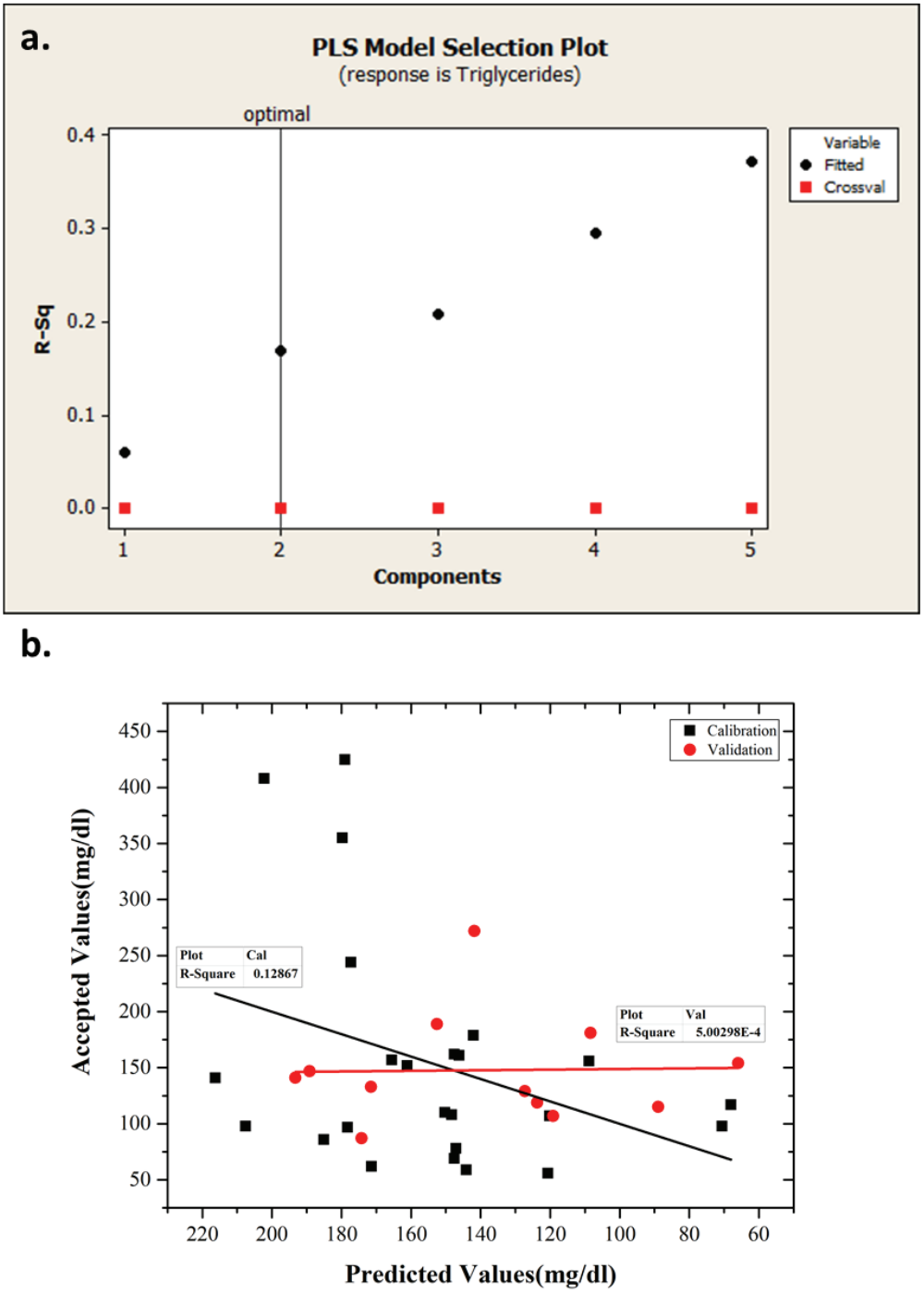

Figure 3.24. Triglycerides PLS1 model selection plot (selected wavenumber regions) b) Accepted glucose values vs Predicted glucose values from PLS1 model with 2 factors. (selected wavenumber regions)

Figure 3.20, 3.21, 3.22, 3.23 and 3.24 show PLS1 model selection plot of selected wavenumber regions for glucose, total protein, albumin, cholesterol and triglycerides. From the PLS1 model graphs of artificial blood samples it was apparent that the correlation coefficients for glucose, total protein, albumin, cholesterol and triglycerides were found as 0.0649, 0.5020, 0.5277, 0.04497 and 0.1287 for calibration and 0.0049, 0.0109, 0.5649, 0.1076 and 0.0005 for validation respectively. In addition, RMSEC values of the model were 16.3244mg/dl, 0.3623g/l, 0.2561g/l, 42.7682mg/dl and 95.1264mg/dl for glucose, total protein, albumin, cholesterol and triglycerides respectively and RMSEP values of the model were 14.3760mg/dl, 0.6615g/l, 0.3681g/l, 57.1047mg/dl and 61.7378mg/dl for glucose, total protein, albumin, cholesterol and triglycerides respectively.

Table 3.7. R-squares and % errors for calibration and validation sets for PLS1 selected wavenumber regions model

		Glucose	**Total Protein**	**Albumin**	**Cholesterol**	**Triglycerides**
PLS1 Selected Wavenumber Regions	**R-Squares of Calibration**	0.0649	0.5020	0.5277	0.0449	0.1287
	R-Squares of Validation	0.0049	0.0109	0.5649	0.1076	0.0005
	% Error of Calibration	13.5703	4.4287	5.1508	19.1763	59.3433
	% Error of Validation	13.4215	8.4466	6.9070	29.1049	33.2153

The total number of components did not represent the whole sample correlation, so errors were so high and also the total number of samples were low. While PLS1 whole spectrum model had lower % error rate for total protein and albumin, PLS1 selected wavenumber regions model had lower % error rate for the others.

3.5. Conclusion

As a result, we measured 118 artificial serum samples that were prepared in our laboratory. We used PE spectrum II UATR-IR. It set 4 cm^{-1} resolution, 20 scans and for between 650-4000cm^{-1} wavenumbers to get spectra. After these measurements we obtained 118 separate spectra data. We used the multivariate calibration method to distinguish 118 artificial serum spectra that seemingly identical. We knew that they contained the components at different concentrations. We used multivariate calibration method instead of univariate calibration method, because univariate calibration method is based on a single peak point. The spectra may contain more than one significant peak and complementary points, or the peak points of the molecules may be superimposed on each other. However, univariate calibration method ignores these points. Multivariate calibration method scans the entire spectral data and creates a calibration model by selecting points that may be significant. Then, it uses the calibration model to predict concentrations of components in unknown samples. So, the partial least squares (PLS) calibration method was chosen as the multivariate calibration method. Advantages and disadvantages of PLS was discussed in the previous sections.

The aim of this study was a preliminary study to determine concentrations of glucose, cholesterol, triglycerides, albumin and total proteins in artificial serum samples from the mid infrared region spectrum. We have obtained IR spectra of 37 artificial serum samples that were prepared in our laboratory. We used PE spectrum II UATR-IR which was set to 4 cm^{-1} resolution, 20 scans and 650-4000cm^{-1} wavenumber range was used.

The mean squares of prediction errors (RMSEP) obtained from PLS results was shown in table 3.5. The results we had come up above acceptable error limits as expected due to this study being preliminary. We expressed our ideas on what we should do to improve it in the following. PLS2 and PLS1 models were performed to the data by using Minitab PLS algorithm. The difference between PLS2 and PLS1 were observed and compared the literature RMSEPs.

Table 3.8. Root mean square error of calibration prediction (RMSEC) and root mean square error of validation prediction (RMSEP)

		Glucose	Total Protein	Albumin	Cholesterol	Triglycerides
PLS2 Whole Spectrum	**RMSEC**	14.4487	0.5223	0.4527	42.8350	88.7472
	RMSEP	19.3191	0.4228	0.3706	59.7631	83.9608
PLS1 Whole Spectrum	**RMSEC**	14.0218	0.3246	0.3644	36.8096	89.2821
	RMSEP	19.9008	0.5757	0.2520	66.7469	83.8547
PLS2 Selected Wavelengths	**RMSEC**	16.5763	0.4048	0.3712	43.3844	96.7074
	RMSEP	14.2370	0.6658	0.5422	55.2026	62.1349
PLS1 Selected Wavelengths	**RMSEC**	16.3244	0.3623	0.2561	42.7682	95.1264
	RMSEP	14.3760	0.6615	0.3681	57.1047	61.7378

When we examined based on the RMSEP of the validation set, it was observed that for the prediction of glucose, PLS2 selected wavenumber model gave the lowest RMSEP in our study so this model was better than the other models for glucose prediction. For the prediction of total protein, PLS2 whole spectrum model gave the lowest RMSEP in our study so PLS2 whole spectrum model was better than the other models. For the prediction of albumin, PLS1 whole spectrum model gave the lowest RMSEP in our study so PLS1 whole spectrum model was better than the other models. For the prediction of cholesterol, PLS2 selected wavenumber regions model gave the lowest RMSEP in our study so PLS2 selected wavenumber regions model was better than the other models. For the prediction of triglycerides, PLS1 selected wavenumber regions model gave the lowest RMSEP in our study so PLS1 selected wavenumber regions model was better than the other models. When we compared PLS2 whole spectrum model and PLS2 selected wavenumber model, PLS2 whole spectrum model was better for total protein and albumin while PLS2 selected wavenumber model was better for the other. When we compared PLS1 whole spectrum model and PLS1 selected wavenumber model, PLS1 whole spectrum model was better for total protein and albumin while PLS1 selected wavenumber model was better for the other. In order to allow easier comparison, table 3.6. is formed that shows RMSEPs of the studies previously done in the literature.

Table 3.9. RMSEP values in the previous studies.

1	**1989**	**RMSEP**	**Glucose**	**TP**	**Cholesterol**	**TG**	**Uric acid**	**Urea**
			22mg/dl	2.1g/l	31mg/dl	33mg/dl	1.6mg/dl	4.4mg/dl
2	**1992**	**RMSEP**	**Albumin**	**Ethanol**	**Cholesterol**	**Lactic acid**	**Urea**	
		PCR	49.1mg/dl	15.7mg/dl	8.0mg/dl	3.8mg/dl	8.5mg/dl	
		PLS	51.5mg/dl	7.8mg/dl	7.9mg/dl	3.4mg/dl	8.4mg/dl	
		Peak area	60.5mg/dl	25.2mg/dl	19.4mg/dl	21.8mg/dl	37.6mg/dl	
		Peak height	59.1mg/dl	22.4mg/dl	11.8mg/dl	11.4mg/dl	17.7mg/dl	
3	**1993**	**RMSEP**	**Glucose PCR**	**Glucose PLS**	**Glucose PLS-ANN**			
			24.0mg/dl	21.5mg/dl	15.6mg/dl			
4	**1994**	**RMSEP**	**Total area 1180-950cm-1**	**Peak height 1035cm^{-1}**	**Peak height 1079cm^{-1}**	**PLS 1425-930cm^{-1}**	**PCR 1425-930cm-1**	**PC-ANN 1425-930cm-1**
		Glucose	47.3mg/dl	40.1mg/dl	42.0mg/dl	16.5mg/dl	18.3mg/dl	18.3mg/dl
5	**1994**	**RMSEP**	**Glucose**	**TP**	**Cholesterol**	**TG**	**Uric acid**	**Urea**
			10.4mg/dl	1.21g/L	1.42mg/dl	10.3mg/dl	0.99mg/dl	2.9mg/dl
6	**1997**	**RMSEP**	**Glucose^{W}**	**Glucose^{R}**	**Cholesterol^{R}**	**R= Entire spectral region**		
		Whole blood	28.7mg/dl	23.6mg/dl	32.4mg/dl	**W= Selected peak wavenumber**		
		Serum	32.5mg/dl	16.9mg/dl	24.8mg/dl			
7	**1998**	**RMSECV**	**Glucose**	**TP**	**Cholesterol**	**TG**	**Hemoglobin**	**Urea**
		Blood	18mg/dl	x	17.5mg/dl	23.5mg/dl	0.77g/dl	x
		Serum	8.7mg/dl	0.0023g/l	14.9mg/dl	8mg/dl	x	0.23mg/dl
8	**1998**	**RMSEP**	**Glucose**	**TP**	**Cholesterol**	**TG**	**Uric acid**	**Urea**
			7.39mg/dl	2.8g/l	10.81mg/dl	0.20mg/dl	2.19mg/dl	6.61mg/dl
			Albumin	**Creatinine**				
			2.2g/l	0.79mg/dl				
9	**1998**	**RMSEP**	**Glucose**	**TP**	**Cholesterol**	**TG**	**Urea**	
		1. chosen range	18.0mg/dl	0.98g/L	8.3mg/dl	13.7mg/dl	5.6mg/dl	
		2. chosen range	16.3mg/dl	0.98g/L	7.8mg/dl	12.8mg/dl	5.3mg/dl	
10	**2002**	**RMSEP**	**Glucose**	**Urea**				
			12.61mg/dl	7.21mg/dl				
11	**2003**	**RMSEP**	Glucose	10.63mg/dl				
12	**2005**	**RMSEP**	**Glucose**	**TP**	**Cholesterol**	**TG**	**Uric acid**	**Urea**
		For Mid-IR	14.7mg/dl	3.28g/l	16.1mg/dl	18.1mg/dl	1.4mg/dl	3.3mg/dl
		For Raman	17.1mg/dl	1.76g/	11.5mg/dl	20.7mg/dl	1.1mg/dl	4.4mg/dl
			LDL	**HDL**				
		For Mid-IR	19.4mg/dl	11.9mg/dl				
		For Raman	15.7mg/dl	11.0mg/dl				
13	**2012**	**RMSEP**	**Glucose**	**Creatinine**	**Cholesterol**	**TG**	**LDL**	**HDL**
			17.8mg/dl	1.78mg/dl	26.3mg/dl	43.9mg/dl	27.5mg/dl	11.9mg/dl
			Urea	**Uric acid**				
			10.6mg/dl	1.3mg/dl				
14	**2012**	**RMSEP**	**Albumin**	**Total globulin**	**γ-globulin**	**Hemoglobin**	**TOH in blood**	
			0.191g/dl	0.093g/dl	0.160g/dl	1.08g/dl	**Untreated**	
						0.71g/dl	**SDS**	
						0.63g/dl	**F/UF**	
15	**2013**	**RMSEP**	**Glucose**	**TP**	**Urea**	**TG**		
		PLS$_a$	24.7mg/dl	0.253g/dl	13.4mg/dl	45.0mg/dl		
		LW-PLSR$_a^*$	22.2mg/dl	0.243g/dl	11.6mg/dl	43.2mg/dl		
		LW-PLSR$_w^{**}$	19.7mg/dl	0.240g/dl	11.3mg/dl	50.6mg/dl		
		LW-PLSR$_m^{***}$	17.1mg/dl	0.240g/dl	9.5mg/dl	40.1mg/dl		
16	**2013**	**RMSEP**	**LDL**	**HDL**	**Cholesterol**	**TG**		
			24.64mg/dl	10.25mg/dl	32.65mg/dl	31.36mg/dl		
17	**2014**	**RMSEP**	**Glucose**	**TP**	**Cholesterol**	**TG**	**Albumin**	**Urea**
			4.14mg/dl	0.88g/L	4.25mg/dl	5.31mg/dl	0.49g/L	25mg/dl
18	**2017**	**RMSEP**	**Glucose**	**Cholesterol**				
			6.34mg/dl	7.92mg/dl				
19	**2017**	**RMSEP**	**PLS-SPXY**	**PLS-0thD-SPXY**	**PLS-1stD-SPXY**	**PLS-2ndD-SPXY**	**PLS-C-SPXY**	**DSFPLS-C-SPXY**
		Glucose(mg/dl)	13.62	22.68	11.23	29.78	9.59	6.58
		Cholesterol(mg/dl)	9.96	17.41	14.05	8.22	8.3	7.49
			PLS-0thD-C-SPXY	**PLS-1stD-C-SPXY**	**PLS-2ndD-C-SPXY**			
		Glucose(mg/dl)	14.18	10.25	8.02			
		Cholesterol(mg/dl)	10.85	11.27	8.19			

(Articles: 1[38], 2[39], 3[40], 4[41], 5[42], 6[51], 7[52], 8[53], 9[43], 10[54], 11[44], 12[55], 13[45], 14[46], 15[47], 16[56], 17[48],18[49],19[50])

Some studies were including different error definitions like SEP and PRESS$^{1/2}$. When we checked their calculations, they performed RMSEP calculations however defined as SEP. In Richard Kramer's book[76], he says "RMSEP is wrongly called the SEP. Fortunately, the difference between the two is usually negligible." In this direction, we rearranged error definitions and created the table. Table 3.6 contains the RMSEP values of all the components predicted in the studies. However, we only studied for glucose, cholesterol, triglyceride, albumin and total protein predictions. That's why we had created column charts based on the RMSEP of the components with the RMSEP of our work. We could see how good we were in this respect compared to the studies in the literature.

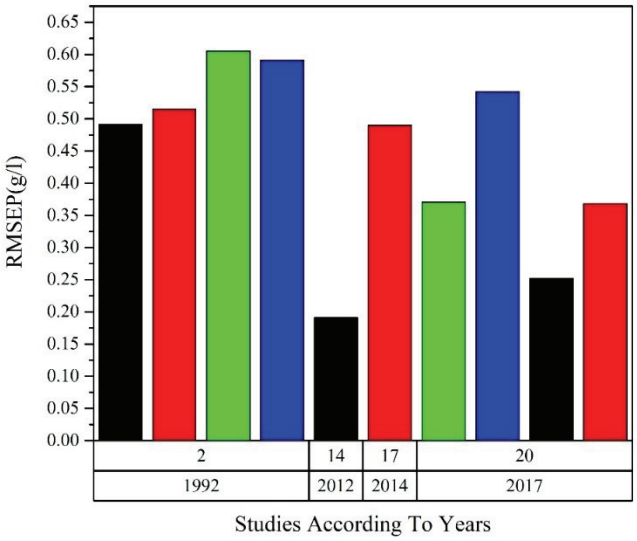

Figure 3.25. RMSEP of Albumin in literature and RMSEP of our study (at 20/2017, green bar is PLS2 model RMSEP for whole spectrum, blue bar is PLS2 model RMSEP for selected wavenumber regions, black bar is PLS1 model RMSEP for whole spectrum and red bar is PLS1 model RMSEP for selected wavenumber regions)

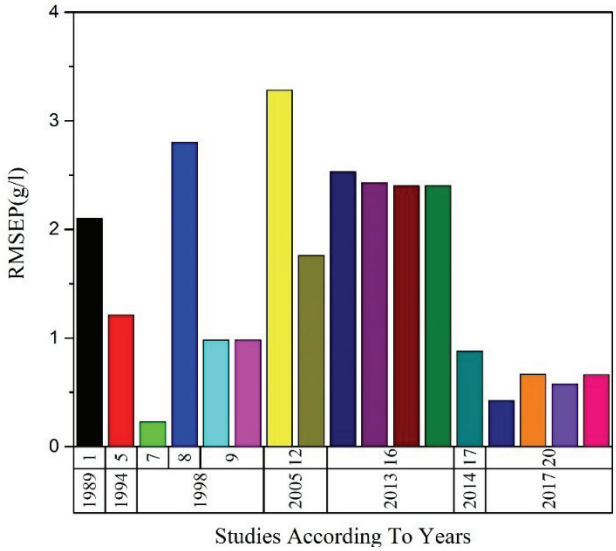

Figure 3.26. RMSEP of Total protein in literature and RMSEP of our study (at 20/2017, blue bar is PLS2 model RMSEP for whole spectrum, orange bar is PLS2 model RMSEP for selected wavenumber regions, purple bar is PLS1 model RMSEP for whole spectrum and pink bar is PLS1 model RMSEP for selected wavenumber regions)

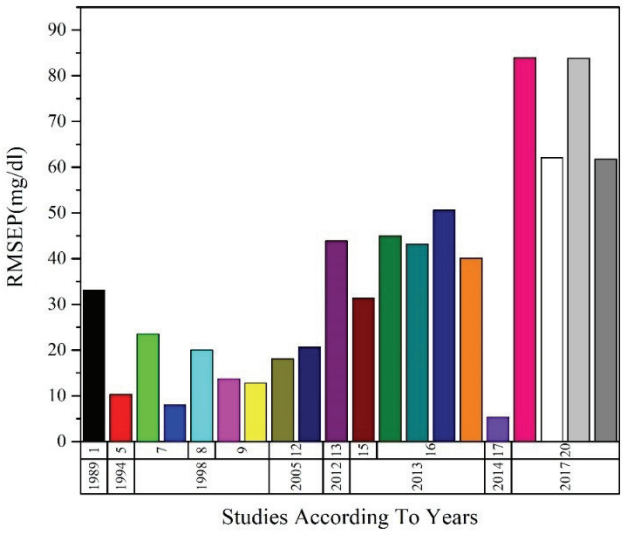

Figure 3.27. RMSEP of triglycerides in literature and RMSEP of our study (at 20/2017, pink bar is PLS2 model RMSEP for whole spectrum, white bar is PLS2 model RMSEP for selected wavenumber regions, grey bar is PLS1 model RMSEP for whole spectrum and darker grey bar is PLS1 model RMSEP for selected wavenumber regions)

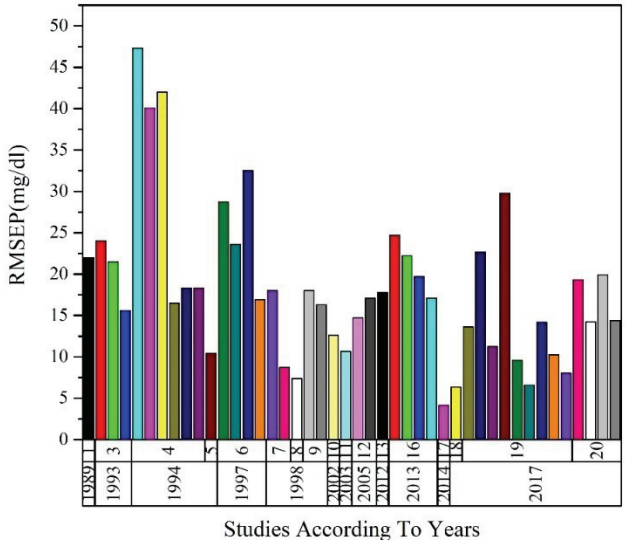

Figure 3.28. RMSEP of glucose in literature and RMSEP of our study (at 20/2017, pink bar is PLS2 model RMSEP for whole spectrum, white bar is PLS2 model RMSEP for selected wavenumber regions, grey bar is PLS1 model RMSEP for whole spectrum and darker grey bar is PLS1 model RMSEP for selected wavenumber regions)

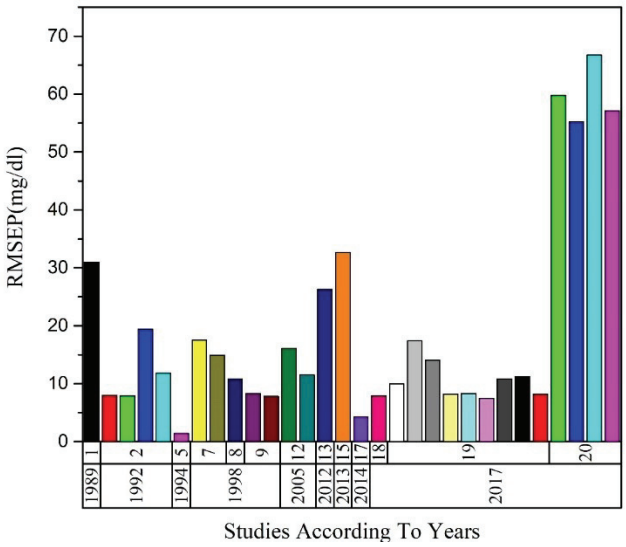

Figure 3.29. RMSEP of cholesterol in literature and RMSEP of our study (at 20/2017, green bar is PLS2 model RMSEP for whole spectrum, blue bar is PLS2 model RMSEP for selected wavenumber regions, light blue bar is PLS1 model RMSEP for whole spectrum and magenta bar is PLS1 model RMSEP for selected wavenumber regions)

According these comparison between RMSEP values show where we stood in these studies with our work. For albumin, RMSEP of PLS1 model of whole spectrum gave the second-best results. For total protein, PLS2 model of whole spectrum was the second-best result and the other models were the third-best, the forth best and the fifth best results in the literature. For triglycerides, our results were the worst when we compared with the literature RMSEPs. While our best result was 61.7378mg/dl, the worst result in the literature was 50.6mg/dl. That meant the worst model for triglycerides. For glucose, our results were average that compared the literature results. For cholesterol, again our results were the worst. While our best result were 55.2027mg/dl, the worst result in the literature was 32.65mg/dl. The differences were nearly twice. The results obtained with these models were found nearly doubled form when we compared other PLS and its combinations results according to RMSEP values in the literature studies for cholesterol and triglycerides. This can be explained by the algorithm of other methods chooses the data in the best compatible wavenumber while modeling from the parameters of spectral data, unlike PLS of Minitab.

When we investigated the reasons for this, we could summarize the reasons for the differences as follows:

1. Due to differences in the instruments used during the measurement.
2. Some studies were using dried samples and some others were using samples directly as liquid.
3. The amount of the sample number and the variance of the calibration method associated with it.
4. Differences in the samples used in the measurements like being blood, serum and plasma.
5. Our spectrum data was decreased to apply a Minitab PLS algorith, so some of information may be lost.
6. Minitab PLS algorithm may not be a good choice for better suited model.

In this study, our final goal is within one minute, in one microliter volume, under $ 1, and without any sample pretreatment to perform the determination of six components of blood. So the measurements were taken in the air background and applied any pretreatment. However; in the literature, even if the measurements were taken in the air background, the water spectra were subsequently subtracted as mathematically from all spectra or 0.9% NaCl background were taken[38, 40], and after that subsequently the water spectra were subtracted as mathematically from all spectra. As known, water gives wide

IR bands in the mid IR region. This can hide the existing spectral information. Although samples can be measured at aqueous solutions by the ATR technique, it may not sufficiently sensitive in low concentration studies. Therefore, mathematically extracting of water spectra from the entire spectra may be a logical test for our subsequent studies and may reduce our error rates. Also we decreased the data that we used in the calibration model. This may be caused the information lost especially for cholesterol and triglycerides.

Other issue was different type sample preperation. There were dried and liquid samples in previous researches. Drying is an extra time-consuming process and lack of reproducibility and it diverges us from our aim. However, drying process is evaporating the water from the liquid matrix so it remove interfering water absorptions and is quite simplified.[54]

Sensitivities of the devices also had an important influence on the measurements. We performed our measurements between at 4000-650cm^{-1} wavelengths with 20 scans and 4cm^{-1} resolution. Any cooling or air purging procedure was applied. The number of scans and noise reductions were shown at table 3.1. Brian C. Smith[36] suggests that; between 10-100 scans for a ATR-FTIR measurement, expected to give yield a spectrum with good signal to noise ratio(SNR) and for example, if 16 scans give a poor spectrum, by all means more scans should be tried. Table 3.6. shows relation between number of scans and SNR.

Table 3.10. Expected noise reduction by increasing number of scans

# of Scans	Noise Reduction
1	-
4	2
16	4
64	8
100	10
256	16
1000	31.6

Generally 20 scans were used in the literature[36] however; some studies had even more than 100 scans. This may lower the SNR and give more significant spectrums. However, our spectrometer needed too much time to take 100 or more scans. Furthermore, increasing the number of scans is not likely to be effective due to the device's detection

limits. In the previous section, we mentioned the detection limits of the PE spectrum II UATR.

Another important situation is the number of samples and variaty of concentration range of components. The PLS model forms a matrix from the spectra of the samples and solves them by separating to get maximum covariances. Therefore, increasing the number of samples and variaty of concentration range of components will help the model to work better in possible and unexpected scenarios. Therefore, it may have a good effect in reducing error rates, but after a point it may lose its effect.

CHAPTER 4

CONCLUSION AND FUTURE PERSPECTIVES

4.1. Conclusion

In this study, we tried to identify the limit of detection of the devices and we measured the artificial serum. In this preliminary study, we had gained insights into what we can do and what we should develop. We talked about the work to be done in the direction of the data obtained.

In chapter 2, we found that the detection limits of PE and Pyreos devices that were insufficient. The concentrations of the components in the serum were below the limit of detection of the devices. This was why we did not get insufficient data for a good data analysis. There was nothing we could do to improve the sensitivity of the commercial PE spectrum II instrument. However, sensitivity improvement studies can be done to increase the sensitivity of the handheld portable Pyreos ATR. We have the development kit of Pyreos PY712 ATR. The linear variable filters and line array sensors used by the device are state-of-the-art and are quite small. The light; that comes from ZnSe crystal, can be scanned and processed for a short time. So it can scan 200 times in as short as 45 seconds. In order to increase the sensitivity of the device, we have the opportunity to change the crystal, the light source, the detector and the filter in this development kit. With a proper microfludics crystals design and a stronger light source, the device limitations can be exceeded.

Another solution might change the detector or lower the noise level of the detector. We mentioned before, the noise level of the device is directly related to area of the detector. In line array sensor, the detector areas are splitted to pixel to pixel so it's already have small area. We cannot reduce the area any further with the technology we have. Changing the detector is of course possible solution. and it may need to be changed its filter and circuits as well. However, changing these parts can increase the size of the device under these conditions. We do not want to increase the size. We will try to decrease the size of the device. One of the importance is portability. For example, some IR spectrometers use MCT detector. Janatsch, Kruse-Jarres et al.[38] suggest that It is possible

to measure the ATR spectrum with a better signal-to-noise ratio making use of photon detectors like MTC detector, instead of the pyroelectric thermal detector. MCT detector needs to be cooled by liquid nitrogen so the spectrometers has to have nitrogen tank that is called as dewar. This increases the size of spectrometer and also increases the price of each measurement. Other importance is the low price measurements.

Also the environment can affact the signal to noise ratio. Air includes water vapour and CO_2 gases. They cause noise in the spectra as well. If the protection of the detector is improved, it may decrease the noise. Vacuum pump can be attached the spectrometers as an example for the isolation from the environment, however it will increase the size of the device.

In chapter 3, we calculated the root mean square for each component that was predicted by using Minitab PLS algorithm. RMSEP values for albumin and total protein were the second best values. RMSEP of glucose was average in the literature. However, RMSEP of triglycerides and cholesterol was too high unfortunately.

To lower the RMSEP values, one of the solution might be that to amplify peaks in the spectra, after taking the air or 0.9% NaCl background, the water spectrum measured in the same environment can be removed from all sample spectra.[46] This can help us to obtain spectra with clearer information. With these data we can build up more strong model. Other solution would be using spectra smooting process or spectra selection. In the literature, some studies were using these process in their work.[38-56, 77-80] Another solution would be to increase the number of samples. Increasing the number of samples will increase the number of equations solved together with the knowledge in the model. In this case, the model will have more robust bases and will corespond to broad concentration ranges. At the same time, the RMSEPs will also decrease. We can not comment on the maximum or minimum number of samples required within our current knowledge, but increasing the number of samples after a certain number will not be effective in reducing the RMSEPs. Another solution is to change the applied multiple calibration model. In the literature these studies are usually performed by the PLS and its combinations. This models have promising results in prediction of concentrations of the components in blood, plasma or serum samples, however; they are insufficient. If another model is used or developed, instead, an improvement might be seen in error rates.

4.2. Future Perspectives

The technology of biomedical instruments in the world is developing rapidly. In Turkey, biomedical instrument researches are increasing in recent years. Biomedical device research will become even more important in the future. For this purpose, a new biomedical device for blood tests can be developed by using our preliminary work. The devices used in the current system are not portable. Furthermore, the samples to be analyzed need pretreatment. This takes too much time. Separate sample is required for each test with around 5 ml of volume. Moreover, each test has a price and total test price for glucose, urea, albumin, total protein, cholesterol and triglycerides; is higher than 7TL. We might develop a device that was portability, low price for each test (1$ e.g.), low volume sample using(10µl) and less time consuming (tests for the six components in 1 minute). This compact device will help doctors. Because in Turkish healthcare system, the number of state hospital and doctor is not enough for population of Turkey; timely diagnosis has vital importance. Some hospitals or clinics do not even have basic analyzers. A doctor can use this device in his office. Blood test results of patient will be reported in a minute. He/she may direct the patient for more detailed tests if he/she deems it necessary. With this device, time and economic savings will be ensured and the rate of diagnosis at the time of illness will increase.

REFERENCES

1. Waldman, G., *Introduction to light: The physics of light, vision, and color*. Courier Corporation: 2002.

2. Young, H. D.; Freedman, R. A., *University physics with modern physics*. Addison-Wesley: 2015.

3. Corcoran, M., Quantum Physics: A Fundamental Approach to Modern Physics. *American Journal of Physics* **2011,** *79* (1), 143-144.

4. Pavia, D.; Lampman, G.; Kriz, G.; Vyvyan, J., *Introduction to spectroscopy*. Cengage Learning: 2008.

5. Skoog, D. A.; West, D. M., *Principles of instrumental analysis*. Saunders College Philadelphia: 1980; Vol. 158.

6. Settle, F., Handbook of instrumental techniques for analytical chemistry. **1997**.

7. Colthup, N., *Introduction to infrared and Raman spectroscopy*. Elsevier: 2012.

8. Bruce A. Averill , P. E. Principles of General Chemistry. http://2012books.lardbucket.org/pdfs/principles-of-general-chemistry-v1.0.pdf.

9. Marengo, E.; Liparota, M. C.; Robotti, E.; Bobba, M., Monitoring of paintings under exposure to UV light by ATR-FT-IR spectroscopy and multivariate control charts. *Vibrational Spectroscopy* **2006,** *40* (2), 225-234.

10. Friebe, A.; Siesler, H. W., In situ monitoring of an isocyanate reaction by fiber-optic FT-IR/ATR-spectroscopy. *Vibrational Spectroscopy* **2007,** *43* (1), 217-220.

11. Blum, M. M.; John, H., Historical perspective and modern applications of Attenuated Total Reflectance-Fourier Transform Infrared Spectroscopy (ATR-FTIR). *Drug Test Anal* **2012,** *4* (3-4), 298-302.

12. Karabudak, E.; Kas, R.; Ogieglo, W.; Rafieian, D.; Schlautmann, S.; Lammertink, R. G.; Gardeniers, H. J.; Mul, G., Disposable attenuated total reflection-infrared crystals from silicon wafer: a versatile approach to surface infrared spectroscopy. *Anal Chem* **2013,** *85* (1), 33-8.

13. Karabudak, E., Micromachined silicon attenuated total reflectance infrared spectroscopy: an emerging detection method in micro/nanofluidics. *Electrophoresis* **2014,** *35* (2-3), 236-44.

14. Karabudak, E.; Mojet, B. L.; Schlautmann, S.; Mul, G.; Gardeniers, H. J., Attenuated total reflection-infrared nanofluidic chip with 71 nL detection volume for in situ spectroscopic analysis of chemical reaction intermediates. *Anal Chem* **2012,** *84* (7), 3132-7.

15. Cocciardi, R. A.; Ismail, A. A.; Sedman, J., Investigation of the potential utility of single-bounce attenuated total reflectance Fourier transform infrared spectroscopy in the analysis of distilled liquors and wines. *Journal of agricultural and food chemistry* **2005,** *53* (8), 2803-2809.

16. Bass, M.; Freger, V., Facile evaluation of coating thickness on membranes using ATR-FTIR. *Journal of Membrane Science* **2015,** *492*, 348-354.

17. Dolamic, I.; Bürgi, T., In Situ ATR-IR Study on the Photocatalytic Decomposition of Amino Acids over Au/TiO2and TiO2. *The Journal of Physical Chemistry C* **2011,** *115* (5), 2228-2234.

18. Enders, D.; Nagao, T.; Pucci, A.; Nakayama, T., Reversible adsorption of Au nanoparticles on SiO2/Si: An in situ ATR-IR study. *Surface Science* **2006,** *600* (6), L71-L75.

19. Ewing, A. V.; Wray, P. S.; Clarke, G. S.; Kazarian, S. G., Evaluating drug delivery with salt formation: Drug disproportionation studied in situ by ATR-FTIR imaging and Raman mapping. *J Pharm Biomed Anal* **2015,** *111*, 248-56.

20. Fischer, D.; Sahre, K.; Abdelrhim, M.; Voit, B.; Sadhu, V. B.; Pionteck, J.; Komber, H.; Hutschenreuter, J., Process monitoring of polymers by in-line ATR-IR, NIR and Raman spectroscopy and ultrasonic measurements. *Comptes Rendus Chimie* **2006,** *9* (11-12), 1419-1424.

21. Kassis, A.; Bhawtankar, V. M.; Sowa, J. R., Jr., Attenuated total reflection infrared spectroscopy (ATR-IR) as an in situ technique for dissolution studies. *J Pharm Biomed Anal* **2010,** *53* (3), 269-73.

22. Kitadai, N.; Yokoyama, T.; Nakashima, S., In situ ATR-IR investigation of L-lysine adsorption on montmorillonite. *J Colloid Interface Sci* **2009,** *338* (2), 395-401.

23. Luengo, C.; Brigante, M.; Antelo, J.; Avena, M., Kinetics of phosphate adsorption on goethite: comparing batch adsorption and ATR-IR measurements. *J Colloid Interface Sci* **2006,** *300* (2), 511-8.

24. Marengo, E.; Liparota, M. C.; Robotti, E.; Bobba, M.; Gennaro, M. C., Monitoring of pigmented surfaces in accelerated ageing process by ATR-FT-IR spectroscopy and multivariate control charts. *Talanta* **2005,** *66* (5), 1158-67.

25. Orphanou, C. M., The detection and discrimination of human body fluids using ATR FT-IR spectroscopy. *Forensic Sci Int* **2015,** *252*, e10-6.

26. Pereira, A.; Lopes, M.; Timmer, J.; Keurentjes, J., Solvent sorption measurements in polymeric membranes with ATR-IR spectroscopy. *Journal of Membrane Science* **2005,** *260* (1-2), 174-180.

27. Popa, A. M.; Angeloni, S.; Burgi, T.; Hubbell, J. A.; Heinzelmann, H.; Pugin, R., Dynamic perspective on the function of thermoresponsive nanopores from in situ AFM and ATR-IR investigations. *Langmuir* **2010,** *26* (19), 15356-65.

28. Stepanyugin, A. V.; Samijlenko, S. P.; Martynenko, O. I.; Hovorun, D. M., ATR-IR spectroscopy as applied to nucleic acid films. *Spectrochim Acta A Mol Biomol Spectrosc* **2005,** *61* (9), 2267-9.

29. Vargas, A.; Ferri, D.; Baiker, A., DFT and ATR-IR insight into the conformational flexibility of cinchonidine adsorbed on platinum: Proton exchange with metal. *Journal of Catalysis* **2005,** *236* (1), 1-8.

30. Heise, H.; Bittner, A., Investigation of experimental errors in the quantitative analysis of glucose in human blood plasma by ATR-IR spectroscopy. *Journal of molecular structure* **1995,** *348*, 21-24.

31. Whitesides, G. M., The origins and the future of microfluidics. *Nature* **2006,** *442* (7101), 368-73.

32. Herzig-Marx, R.; Queeney, K.; Jackman, R. J.; Schmidt, M. A.; Jensen, K. F., Infrared spectroscopy for chemically specific sensing in silicon-based microreactors. *Analytical chemistry* **2004,** *76* (21), 6476-6483.

33. O'Brien, N. A.; Hulse, C. A.; Friedrich, D. M.; Van Milligen, F. J.; von Gunten, M. K.; Pfeifer, F.; Siesler, H. W. In *Miniature near-infrared (NIR) spectrometer engine for handheld applications*, Proc. SPIE, 2012; p 837404.

34. Solutions, P. S. Portable Pyreos ATR-IR. http://www.pyreos.com/line-array-components.

35. K.K., H. P. Micro-spectrometer. http://www.hamamatsu.com/jp/en/C12666MA.html (accessed 15 NOV).

36. Smith, B. C., *Fundamentals of Fourier transform infrared spectroscopy*. CRC press: 2011.

37. Odon, A., Modelling and simulation of the pyroelectric detector using MATLAB/Simulink. *Measurement Science Review* **2010,** *10* (6), 195-199.

38. Janatsch, G.; Kruse-Jarres, J.; Marbach, R.; Heise, H., Multivariate calibration for assays in clinical chemistry using attenuated total reflection infrared spectra of human blood plasma. *Analytical chemistry* **1989,** *61* (18), 2016-2023.

39. Stohr, E.; Bhandare, P.; Peura, R.; Mendelson, Y. In *Quantitative FTIR spectrophotometry of cholesterol and other blood constituents and their interference with the in-vitro measurement of blood glucose*, Bioengineering Conference, 1992., Proceedings of the 1992 Eighteenth IEEE Annual Northeast, IEEE: 1992; pp 105-106.

40. Bhandare, P.; Mendelson, Y.; Peura, R. A.; Janatsch, G.; Kruse-Jarres, J. D.; Marbach, R.; Heise, H. M., Multivariate determination of glucose in whole blood using partial least-squares and artificial neural networks based on mid-infrared spectroscopy. *Applied spectroscopy* **1993,** *47* (8), 1214-1221.

41. Bhandare, P.; Mendelson, Y.; Stohr, E.; Peura, R. A., Glucose determination in simulated blood serum solutions by Fourier transform infrared spectroscopy: investigation of spectral interferences. *Vibrational spectroscopy* **1994,** *6* (3), 363-378.

42. Heise, H.; Marbach, R.; Koschinsky, T.; Gries, F., Multicomponent assay for blood substrates in human plasma by mid-infrared spectroscopy and its evaluation for clinical analysis. *Applied Spectroscopy* **1994,** *48* (1), 85-95.

43. Heise, H.; Bittner, A., Multivariate calibration for near-infrared spectroscopic assays of blood substrates in human plasma based on variable selection using PLS-regression vector choices. *Fresenius' journal of analytical chemistry* **1998,** *362* (1), 141-147.

44. Shen, Y.; Davies, A.; Linfield, E.; Taday, P.; Arnone, D.; Elsey, T., Determination of glucose concentration in whole blood using Fourier-transform infrared spectroscopy. *Journal of biological physics* **2003,** *29* (2), 129-133.

45. Perez-Guaita, D.; Ventura-Gayete, J.; Pérez-Rambla, C.; Sancho-Andreu, M.; Garrigues, S.; de la Guardia, M., Evaluation of infrared spectroscopy as a screening tool for serum analysis. *Microchemical Journal* **2013,** *106*, 202-211.

46. Perez-Guaita, D.; Ventura-Gayete, J.; Pérez-Rambla, C.; Sancho-Andreu, M.; Garrigues, S.; de la Guardia, M., Protein determination in serum and whole blood by attenuated total reflectance infrared spectroscopy. *Analytical and bioanalytical chemistry* **2012,** *404* (3), 649-656.

47. Perez-Guaita, D.; Kuligowski, J.; Quintas, G.; Garrigues, S.; Guardia Mde, L., Modified locally weighted--partial least squares regression improving clinical predictions from infrared spectra of human serum samples. *Talanta* **2013,** *107*, 368-75.

48. Jessen, T. E.; Hoskuldsson, A. T.; Bjerrum, P. J.; Verder, H.; Sorensen, L.; Bratholm, P. S.; Christensen, B.; Jensen, L. S.; Jensen, M. A., Simultaneous determination of glucose, triglycerides, urea, cholesterol, albumin and total protein in human plasma by Fourier transform infrared spectroscopy: direct clinical biochemistry without reagents. *Clin Biochem* **2014,** *47* (13-14), 1306-12.

49. Li, Z.; Li, T.; Lv, H.; Wang, Q.; Si, G.; He, Z., Quantitative analysis of biofluids based on hybrid spectra space. *Chemometrics and Intelligent Laboratory Systems* **2017,** *165*, 22-28.

50. Li, Z.; Lv, H.; Li, T.; Si, G.; Wang, Q.; Lv, J.; Hu, X., Reagent-free simultaneous determination of glucose and cholesterol in whole blood by FTIR-ATR. *Spectrochim Acta A Mol Biomol Spectrosc* **2017,** *178*, 192-197.

51. Budinova, G.; Salva, J.; Volka, K., Application of molecular spectroscopy in the mid-infrared region to the determination of glucose and cholesterol in whole blood and in blood serum. *Applied Spectroscopy* **1997,** *51* (5), 631-635.

52. Werner, G. H.; Boecker, D.; Haar, H.-P.; Kuhr, H.-J.; Mischler, R., Multicomponent assay for blood substrates in human sera and haemolysed blood by mid-infrared spectroscopy. *Infrared Spectroscopy: New Tool in Medicine* **1998,** *3257*, 91-100.

53. Shaw, R. A.; Kotowich, S.; Leroux, M.; Mantsch, H. H., Multianalyte serum analysis using mid-infrared spectroscopy. *Annals of clinical biochemistry* **1998,** *35* (5), 624-632.

54. Low-Ying, S.; Shaw, R. A.; Leroux, M.; Mantsch, H. H., Quantitation of glucose and urea in whole blood by mid-infrared spectroscopy of dry films. *Vibrational spectroscopy* **2002,** *28* (1), 111-116.

55. Rohleder, D.; Kocherscheidt, G.; Gerber, K.; Kiefer, W.; Ko, W.; Mo, J.; Petrich, W., Comparison of mid-infrared and Raman spectroscopy in the quantitative analysis of serum. *Journal of biomedical optics* **2005,** *10* (3), 031108-03110810.

56. Perez-Guaita, D.; Sanchez-Illana, A.; Ventura-Gayete, J.; Garrigues, S.; de la Guardia, M., Chemometric determination of lipidic parameters in serum using ATR measurements of dry films of solvent extracts. *Analyst* **2014,** *139* (1), 170-8.

57. Brereton, R. G., *Chemometrics: data analysis for the laboratory and chemical plant*. John Wiley & Sons: 2003.

58. Mark, H.; Workman, J., *Chemometrics in spectroscopy*. Academic Press: 2010.

59. Beebe, K. R.; Pell, R. J.; Seasholtz, M. B., *Chemometrics: a practical guide*. Wiley-Interscience: 1998; Vol. 4.

60. Brereton, R. G., *Multivariate pattern recognition in chemometrics: illustrated by case studies*. Elsevier: 1992; Vol. 9.

61. Brereton, R. G., *Applied chemometrics for scientists*. John Wiley & Sons: 2007.

62. Caulcutt, R.; Boddy, R., *Statistics for analytical chemists*. Chapman & Hall: 1983
.

63. Cornell, J. A., *Experiments with mixtures: designs, models, and the analysis of mixture data*. John Wiley & Sons: 2011; Vol. 895.

64. Gans, P., Data fitting in the chemical sciences. *England: Wiley J. & Sons* **1992**, 59-87.

65. Geladi, P.; Kowalski, B. R., Partial least-squares regression: a tutorial. *Analytica chimica acta* **1986,** *185*, 1-17.

66. Jansson, P. A., *Deconvolution of images and spectra*. Courier Corporation: 2014.

67. Jolliffe, I. T., Principal component analysis: A beginner's guide—II. Pitfalls, myths and extensions. *Weather* **1993,** *48* (8), 246-253.

68. Kowalski, B. R., *Chemometrics: mathematics and statistics in chemistry*. Springer Science & Business Media: 2013; Vol. 138.

69. Martens, H.; Martens, M., Multivariate analysis of quality. **2000**.

70. Martens, H.; Naes, T., Multivariate Calibration John Wiley & Sons. *Chichester, UK* **1989**.

71. Massart, D. L.; Vandeginste, B. G.; Buydens, L.; Lewi, P.; Smeyers-Verbeke, J.; Jong, S. d., *Handbook of chemometrics and qualimetrics: Part A*. Elsevier Science Inc.: 1997.

72. Otto, M., *Chemometrics: statistics and computer application in analytical chemistry*. John Wiley & Sons: 2016.

73. Vandeginste, B. G.; Massart, D. L.; De_Jong, S.; Buydens, L.; Lewi, P.; Smeyers-Verbeke, J., *Handbook of chemometrics and qualimetrics*. Elsevier: 1998.

74. Massart, D. L.; Brereton, R.; Dessy, R.; Hopke, P.; Spiegelman, C.; Wegscheider, W., Chemometrics tutorials: Elsevier, Amsterdam, 1990 (ISBN 0-444-88837-3). viii+ 427 pp. Price Dfl. 130.00/US $66.75 (paperback). Elsevier: 1991.

75. Martens, H.; Martens, M., Multivariate analysis of quality. An introduction. IOP Publishing: 2001.

76. Kramer, R., *Chemometric techniques for quantitative analysis*. CRC Press: 1998.

77. Petrich, W., Mid-Infrared and Raman Spectroscopy for Medical Diagnostics. *Applied Spectroscopy Reviews* **2001,** *36* (2-3), 181-237.

78. Perez-Guaita, D.; Garrigues, S.; de la, M.; Guardia, Infrared-based quantification of clinical parameters. *TrAC Trends in Analytical Chemistry* **2014,** *62*, 93-105.

79. Bunaciu, A. A.; Fleschin, S.; Hoang, V. D.; Aboul-Enein, H. Y., Vibrational Spectroscopy in Body Fluids Analysis. *Crit Rev Anal Chem* **2017,** *47* (1), 67-75.

80. Soleymani, J.; Perez-Guaita, D.; Hasanzadeh, M.; Shadjou, N.; Jouyban, A., Materials and methods of signal enhancement for spectroscopic whole blood analysis: Novel research overview. *TrAC Trends in Analytical Chemistry* **2017,** *86*, 122-142.